THESIS FOR THE DEGREE OF DOCTOR OF PHILOSOPHY

Enzyme Immobilization in Mesoporous Silica

HANNA GUSTAFSSON

Department of Chemical and Biological Engineering
CHALMERS UNIVERSITY OF TECHNOLOGY
Göteborg, Sweden 2013

Enzyme Immobilization in Mesoporous Silica

Hanna Gustafsson

ISBN: 978-91-7385-882-3

Doktorsavhandlingar vid Chalmers tekniska högskola

Ny Serie Nr: 3563

ISSN 0346-718X

Department of Chemical and Biological Engineering

Chalmers University of Technology

SE-412 96 Göteborg

Sweden

Telephone +46 (0)31-772 1000

Cover: A graphical illustration of four types of enzymes immobilized in a support with hexagonally structured pores.

Printed by:

Chalmers Reproservice

Göteborg, Sweden 2013

Enzyme Immobilization in Mesoporous Silica

Hanna Gustafsson
Department of Chemical and Biological Engineering
Chalmers University of Technology

ABSTRACT

Enzymes are highly effective and versatile biological catalysts, with a high chemo-, stereo- and regioselectivity while operating under mild conditions, such as physiological temperature and pH and atmospheric pressure. Therefore, enzymes are a sustainable alternative to conventional catalysts in organic synthesis processes. They are also used in detergent formulations, in biosensors for analytical and diagnostic purposes, and in biofuel cells. However, the use of enzymes in their native form often results in high costs, low operational stability and difficulties in recovery and reuse. By immobilization of enzymes to a solid support these limitations can be minimized.

Mesoporous silica materials are a promising support for enzyme immobilization, offering a large surface area, a narrow pore size distribution and a high stability. Immobilization of enzymes in mesoporous silica has become a popular research topic, but despite the many techniques available, there is still a need for controlled strategies in order to adapt the support to the specific enzyme. It is crucial to better understand how the enzyme is affected by the microenvironment inside the pores and to gain more knowledge about the immobilization process.

A major part of this work has been focused on finding suitable mesoporous silica particles customized for an optimal performance of each individual type of enzyme investigated. Enzymes of different character were immobilized in mesoporous silica particles with varied pore size, particle size and particle morphology through physical adsorption. The influence of these parameters on the loading capacity, catalytic activity and reusability of the immobilized enzymes was evaluated.

A method to study the microenvironment inside mesoporous silica particles by covalently attaching a pH-probe (SNARF1) to proteins was developed. The results indicate that the immobilized proteins experience an environment inside the pores which is closer to neutral compared to the bulk solution. This approach can be used to characterize the pore environment without perturbing the properties of the material.

The immobilization process has been studied directly with quartz crystal microbalance with dissipation monitoring (QCM-D) by attaching silica particles to the sensor. We have demonstrated that QCM-D is a simple and robust measuring technique for real time study of enzyme immobilization into mesoporous silica particles and that it is a useful complement to conventional indirect measuring techniques. With QCM-D we were also able to follow the co-immobilization of glucose oxidase (GOD) and horseradish peroxidase (HRP), which was done by a combination of immobilization of GOD in mesoporous silica particles followed by adsorption of HRP covalently linked to a polycationic dendronized polymer. A cascade reaction was confirmed with enzymatic activity analysis.

Keywords: Mesoporous silica, pore size, particle morphology, immobilization, enzyme, biocatalysis, quartz crystal microbalance with dissipation monitoring, pH probe

List of papers

I. A comparison of lipase and trypsin encapsulated in mesoporous materials with varying pore sizes and pH conditions
Hanna Gustafsson, Christian Thörn and Krister Holmberg
Colloids and Surfaces B: Biointerfaces 87 (2011) 464– 471

II. Immobilization of lipase from *Mucor miehei* and *Rhizopus oryzae* into mesoporous silica -The effect of varied particle size and morphology
Hanna Gustafsson, Emma M. Johansson, Albert Barrabino, Magnus Odén and Krister Holmberg
Colloids and Surfaces B: Biointerfaces 100 (2012) 22– 30

III. Immobilization of feruloyl esterases in mesoporous materials leads to improved transesterification yield
Christian Thörn, Hanna Gustafsson and Lisbeth Olsson
Journal of Molecular Catalysis B: Enzymatic 72 (2011) 57– 64

IV. A method to measure pH inside mesoporous particles using protein-bound SNARF1 fluorescent probe
Christian Thörn, Nils Carlsson, Hanna Gustafsson, Krister Holmberg, Björn Åkerman and Lisbeth Olsson
Microporous and Mesoporous Materials 165 (2013) 240–246

V. QCM-D as a method for monitoring enzyme immobilization in mesoporous silica particles
Christian Thörn, Hanna Gustafsson and Lisbeth Olsson
Microporous and Mesoporous Materials 176 (2013) 71–77

VI. Co-immobilization of enzymes with the help of dendronized polymers and mesoporous silica
Hanna Gustafsson, Andreas Küchler, Krister Holmberg and Peter Walde
Manuscript

VII. Enzymes in mesoporous media: a physical-chemical perspective
Nils Carlsson, Hanna Gustafsson, Christian Thörn, Lisbeth Olsson, Krister Holmberg and Björn Åkerman
Advances in Colloid and Interface Science In press

Contribution Report

I. Responsible for experimental outline, experimental work and for writing the major part of the manuscript.

II. Responsible for experimental outline and experimental work except the synthesis of MPS-300 and MPS-40 silica particles. Responsible for writing the major part of the manuscript.

III. Performed synthesis and characterization of the mesoporous materials.

IV. Contributed with the synthesized particles and the corresponding TEM images.

V. Responsible for experimental outline, experimental work and for writing the manuscript. Christian Thörn and I have contributed equally. Responsible for submitting the manuscript.

VI. Responsible for experimental outline, experimental work and for writing the manuscript. Andreas Küchler and I have contributed equally.

VII. Responsible for writing the manuscript.
Christian Thörn, Nils Carlsson and I have contributed equally.

TABLE OF CONTENTS

Chapter 1

INTRODUCTION

Enzymatic catalysis has found widespread applications in the past decades, in organic synthesis as well as in the development of analytical devices and fuel cells [1-3]. Enzymes are biological catalysts found in all living organisms. They have high catalytic efficiency, substrate specificity and selectivity under mild reaction conditions with low energy requirements. Conventional synthetic catalysts used in organic synthesis often demand harsh conditions and multi-step processes, leading to excessive energy consumption and generation of much waste and toxic by-products. There is therefore a great need for more sustainable manufacturing and by replacing these catalysts with enzymes cleaner products and processes can be achieved [4, 5]. However, there are some limitations in using enzymes in large-scale production. They are for example much more expensive and have in general a quite low long-term operational stability. They are also difficult to separate from the reaction medium, which limits the recovery of the enzyme and may lead to contamination of the final product. A strategy to overcome these limitations is to immobilize the enzymes on a solid support [6, 7]. There are several immobilization methods available, including binding of the enzyme to a solid support, encapsulation inside a material or cross-linking the enzyme into large aggregates [6, 8].

A promising material as support for enzymes is mesoporous silica (silicon dioxide). The large surface area and the well-ordered and uniform pores with an adjustable pore size, typically in the size range of 2 to 15 nm, make them suitable for biomolecules, like enzymes [9, 10]. Compared to a non-porous support the porous structure enables a large quantity of enzyme to be immobilized. Moreover, mesoporous silica is a structurally robust material, chemically stable over a broad pH and temperature range. The materials are made by a templating procedure, using an organic template that is subsequently removed leaving a mesoporous end product [11]. The pore dimension can be tailored with high precision by the choice of templating molecule and by the synthesis conditions.

A considerable amount of research has been performed towards easy and efficient enzyme immobilization in porous materials, but despite the many techniques available, there is still a need for controlled strategies and for a rational design of the mesoporous material. A major limitation in the development of an optimal support is the gap of knowledge in the understanding of how the microenvironment and the material properties of the mesoporous particles affect the activity and selectivity of the immobilized enzymes [8]. Enzymes are a very diverse group of molecules

ranging from 12 kDa up to over 1000 kDa in size [12] and with specific surface characteristics, such as morphology, charge distribution and hydrophobicity, for each type of enzyme.

The main objective of this work was to find suitable mesoporous silica particles customized for an optimal performance for each individual type of enzyme investigated. The aim was also to gain knowledge of the immobilization process as it proceeds, how the immobilized enzymes are distributed in the porous particles, how they are affected by the environment in the pores, and how such effects relate to the enzymatic activity.

In order to achieve these objectives enzymes of different character were immobilized in mesoporous silica particles through physical adsorption. The influence of varying pore size, particle size and particle morphology on the loading capacity, catalytic activity and reusability of the immobilized enzymes has been evaluated (**Papers I-III**). The goal was to obtain a stable system, where the enzyme is properly retained inside the material with minimal leaching while maintaining a high and stable catalytic activity. Methods for studying the pore environment (**Paper IV**) and for studying the correlation between enzyme and support characteristics in real time (**Paper V**) were developed in order to obtain a deeper understanding of the immobilization process. Moreover, a method for co-immobilization of two types of enzymes, to create a cascade reaction, is described in **Paper VI**. **Paper VII** is a review describing and evaluating available methodologies that have been or may be utilized to gain knowledge of the immobilization process.

Chapter 2

MESOSTRUCTURED MATERIALS

Mesoporous materials are defined as inorganic solids with a pore size range of 2-50 nm. They have a large variety of properties with respect to composition, pore shape and particle morphology to name a few. Most mesoporous materials are oxides, such as SiO_2, Al_2O_3, TiO_2 and ZrO_2 and the structure is usually hexagonal or cubic [11, 13, 14]. This work has had a focus on mesoporous silica (MPS) and it is the only material described here. MPS was discovered in the early 90´s [9, 15, 16] and soon became the topic of much research. The material is obtained from organic-inorganic self-assembly between a surfactant and an inorganic species. When the reaction is finished the surfactant is removed, resulting in a porous framework. The robust and thermally stable structure together with a large surface area, tunable pore size, and well-ordered and uniform pores, make the material suitable as support in drug delivery [17, 18], separation [19], catalysis [20] and biocatalysis [21-24].

2.1 Surfactants and polymers in solution

Surfactants are amphiphilic molecules with a polar (hydrophilic) head group, which prefers water, and a hydrophobic tail group preferring a non-polar solvent. The polar head group can be either ionic or non-ionic. Due to the hydrophobic effect, surfactants in solution will form aggregates, called micelles, above a certain concentration, called the critical micelle concentration (CMC) [25]. In an aqueous solution the polar head groups in the micelles will face the solvent whereas the hydrophobic tail will be situated inside the micelle in order to minimize contact with water. The radius of the micelle core is mainly determined by the length of the hydrophobic chain. As the surfactant concentration is increased the separate micelles will eventually form liquid crystalline structures. A liquid crystal is characterized by a long-range order but with no order on the atomic scale. The aggregate structure primarily depends on the geometry of the surfactant and is determined by the critical packing parameter (CPP) (see Equation 1). The CMC also depends on the surfactant concentration and the solution conditions, such as temperature and salt concentration.

$$CPP = \frac{v}{l_{\max} \cdot a} \qquad (1)$$

In Equation 1 v is the volume of the hydrophobic group, l_{max} the length of the extended hydrocarbon chain, and a the cross sectional area of the head group. By varying the size of the hydrophilic and hydrophobic groups, micelles of different size and shape is obtained. Scheme 2.1 illustrates the relation between CPP and various aggregate structures.

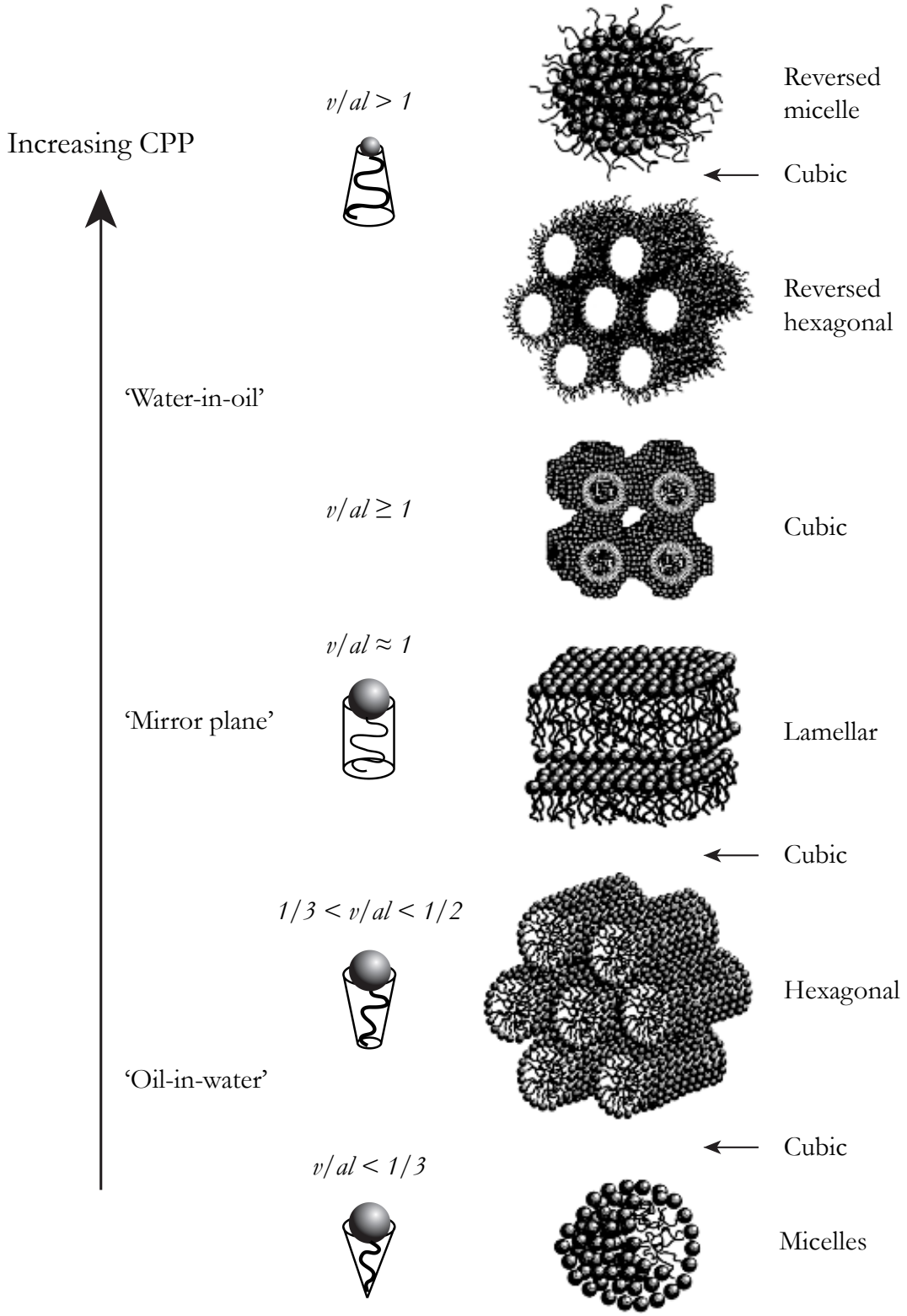

Scheme 2.1. Critical packing parameters and the corresponding aggregate structures. Redrawn from Holmberg et al., *Surfactants and Polymers in Aqueous Solution*: 2nd ed. [25].

In Scheme 2.2 the chemical structure of a cationic surfactant, a cationic gemini surfactant and a non-ionic surfactant is shown. All three are used in the synthesis of small mesoporous silica particles, discussed in this thesis (Section 5.1.2) [26].

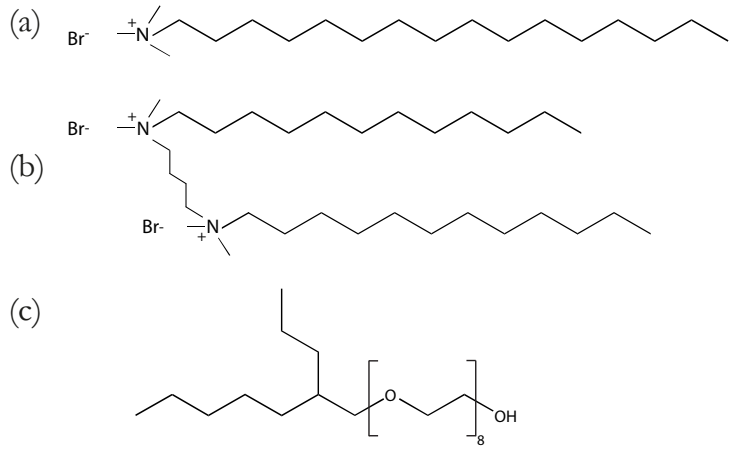

Scheme 2.2. Chemical structure of (a) the cationic surfactant cetyltrimethylammonium bromide (CTAB), (b) the cationic gemini surfactant, and (c) the non-ionic surfactant Ethylan 1008.

2.1.1 Block copolymers

A group of amphiphilic polymers are the block copolymers, consisting of two or more homopolymer subunits linked with covalent bonds. In solution block copolymers behave in many ways similar to surfactants. Above a certain concentration, the CMC, they self-assemble into well-defined structures, which depend on the relative lengths of the blocks and the interaction between the polymer chains. A special kind of block copolymers is the non-ionic triblock copolymer, often referred to as Pluronic after the BASF trade name. A Pluronic consists of two hydrophilic poly(ethylene oxide) chains (PEO) surrounding a hydrophobic poly(propylene oxide) chain (PPO) (Scheme 2.3). There are many different kinds of Pluronics as both the PEO/PPO ratio and the total molecular weight can be varied. When forming micelles in an aqueous solution the PPO groups will be localized in the core of the micelles whereas the PEO groups will be facing the aqueous solution in the micelle corona. The micelle formation is strongly dependent on the temperature. There also exist other copolymers based on PEO and PPO, for instance reverse Pluronics with a PPO-PEO-PPO structure. There are also random EO-PO copolymers on the market.

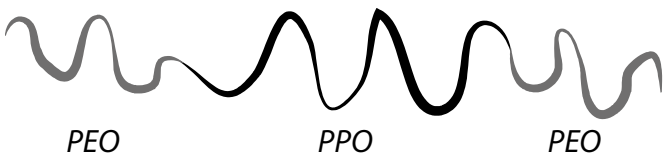

Scheme 2.3. Schematic illustration of a triblock copolymer of Pluronic type.

2.2 Mesoporous silica

A large number of studies have been focusing on the synthesis mechanism and formation pathway for ordered mesoporous silica (MPS). In the synthesis process, sol-gel chemistry [27] is combined with assembly of surfactant molecules as framework template. The material is obtained from the organic-inorganic self-assembly between the surfactant (template) and an inorganic species (precursor). The surfactant may be cationic, like CTAB [28], or non-ionic, usually a block copolymer [10], which is dissolved in an aqueous solution.

In the synthesis of MPS a silica precursor is added to the micellar solution. The precursor is either an alkoxide, for example tetraethyl orthosilicate (TEOS) (Scheme 2.4) or an inorganic salt such as sodium silicate. In this work, only TEOS has been used as precursor.

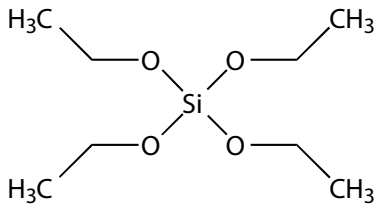

Scheme 2.4. Tetraethyl orthosilicate (TEOS).

An alkoxide hydrolyses and condensates in acidic or basic media, forming a silica network around the template. All reactions take place simultaneously. Acidic conditions promote the hydrolysis reaction whereas basic conditions result in fast condensation reactions [27].

Hydrolysis:

$$\equiv Si - OR + H_2O \leftrightarrow \equiv Si - OH + ROH$$

Condensation:

$$\equiv Si - OR + HO - Si \equiv \leftrightarrow \equiv Si - O - Si \equiv + ROH$$

$$\equiv Si - OH + OH - Si \equiv \leftrightarrow \equiv Si - O - Si \equiv + H_2O$$

Under basic conditions the hydrolysis of alkoxysilanes occurs by a nucleophilic mechanism. Water dissociates to produce nucleophilic hydroxyl anions (OH-) in a rapid first step, and then the hydroxyl anion attacks the silicon atom. When an alkoxide group (OR) is replaced by a hydroxyl group, the electron density of silicon is reduced, accelerating the hydrolysis rate of other alkoxide groups. Under acidic conditions H_3O^+ instead attacks the oxygen in the alkoxide in an electrophilic reaction [29]. The oxygen species in the remaining alkoxy groups then becomes less electrophilic promoting hydrolysis of new $Si(OCH_3)_4$ instead of further hydrolyzing the same alkoxysilane molecule.

The initial formation mechanism of ordered MPS materials, suggested by Beck et al., includes many possibilities where two of the main pathways are the "*liquid crystal templating*" (*LCT*) pathway and the "*cooperative templating mechanism*" (*CTM*) pathway [28]. Briefly, the *LCT* pathway includes an initial organization of surfactant molecules into a liquid crystalline structure followed by silica condensation around the aggregates [30]. The structure of the material can be designed *a priori* based on the phase diagram of the surfactant. The *CTM* pathway involves a lower surfactant concentration and the material formation is based on the interactions between the silica precursor and the surfactants to form inorganic-organic mesostructured composites [30]. The organic-inorganic self-assembly can be driven by either electrostatic interaction between charged surfactant molecules and the silica precursor or by a neutral pathway involving hydrogen bonding between precursor and template. The *CTM* is described in more detail in Section 2.2.1.

The particle growth is generally determined by electrostatic stabilization and by the concentration of reactants [31]. After the reaction is finished the formed material can be hydrothermally treated for further cross-linking, reorganization and particle growth [10]. In addition to hydrothermal treatment, there are several possibilities for controlling the particle growth and the final particle morphology. By varying parameters such as temperature and pH by including additives such as cosolvents, cosurfactants, inorganic salts etc., or by changing the type or amount of template surfactant, morphologies such as fibers, single rods, platelets, gyroids and spheres can be obtained [32-37].

The hydrophobic part of the surfactant molecule determines the pore size. In general, a large hydrophobic group generates a larger pore size. An additional way to tune the pore size of the mesoporous materials is to add an organic swelling agent that is solubilized in the hydrophobic core leading to swelling of the micelle [10, 38]. The pore size can also be adjusted by varying the temperature during the hydrothermal treatment (see Section 2.2.1) [10, 39]. After preparation of the organic-inorganic hybrid material, the template is removed by either calcination, which is the most common method, or extraction, resulting in a mesoporous material. During calcination the temperature is slowly elevated and kept constant for several hours to completely remove all organic material. During the calcination many of the silanol groups on the silica surface are converted into siloxane bridges, resulting in a more hydrophobic surface character [40, 41]. Calcination also leads to a slight pore shrinkage, possibly due to further framework condensation [42]. An alternative method for template removal is chemical extraction with for example ethanol [11] or hydrogen peroxide (H_2O_2) [43]. Using extraction pore shrinkage can be avoided and the silanol groups are preserved to a larger extent. Moreover, with ethanol extraction surfactant decomposition can be avoided, promoting surfactant recycling, but instead surfactant residues may remain inside the pores. This is typically a problem when block copolymers are used as template since they leave behind a microporous network inside the pore walls (see Section 2.2.1). Extraction with H_2O_2 completely removes the template and is equivalent to calcination with respect to template removal.

2.2.1 SBA-15

SBA-15 (Santa Barbara Amorphous) [11], first synthesized in 1998 by Zhao et al., is a hexagonally ordered mesoporous silica material with cylindrical pores and a rather large pore diameter (~5-18

nm) [10, 11, 44]. The material is synthesized under acidic conditions using a non-ionic triblock copolymer as template. Scheme 2.5 shows Pluronic P123, which is used as template in this study. The two PEO segments in P123 are each 20 units long and the central hydrophobic segment is 70 units long, giving a total molecular weight of 5750 g/mol. As mentioned in Section 2.1.1, when forming micelles in an aqueous solution the PPO groups will be localized in the core and the PEO groups will be in the corona. The PEO chains give rise to rather thick pore walls perforated with micropores after template removal (Scheme 2.7) [45].

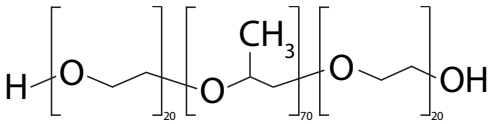

Scheme 2.5. The block copolymer surfactant Pluronic P123.

To achieve better understanding of the synthesis process studies on the initial formation mechanism have been performed using *in situ* small angle X-ray scattering (SAXS) [46, 47], small angle neutron scattering (SANS) [46, 48, 49] and also ^{1}HNMR and transmission electron microcopy (TEM) [50]. These studies have shed light on both the micelle structure and the development of the surfactant-silica composite during the synthesis (Scheme 2.6). Studies on the formation mechanism show that SBA-15 is formed by the *CTM* pathway with addition of the silica precursor to a micellar solution of the surfactant [46]. Hydrolysis of the silica precursor upon addition of TEOS is completed within a few minutes and condensation starts as soon as some TEOS is hydrolyzed. The formed silica oligomers interact with the PEO groups in the micelle corona. The adsorption of silica reduces the water content, changing the polarity in this region which leads to a lowering of the micelle curvature. This in turn initiates a sphere-to-rod transition of the micelles after the condensation has reached a critical value [46, 51, 52]. The ethanol molecules generated from hydrolysis of TEOS also affect the micelle structure as they migrate into the hydrophobic core causing swelling of the micelle. Furthermore, the silica polymerization gives rise to attractive interactions between the micelles which leads to micelle flocculation, rearrangement and precipitation of a hexagonally ordered mesophase [37, 50].

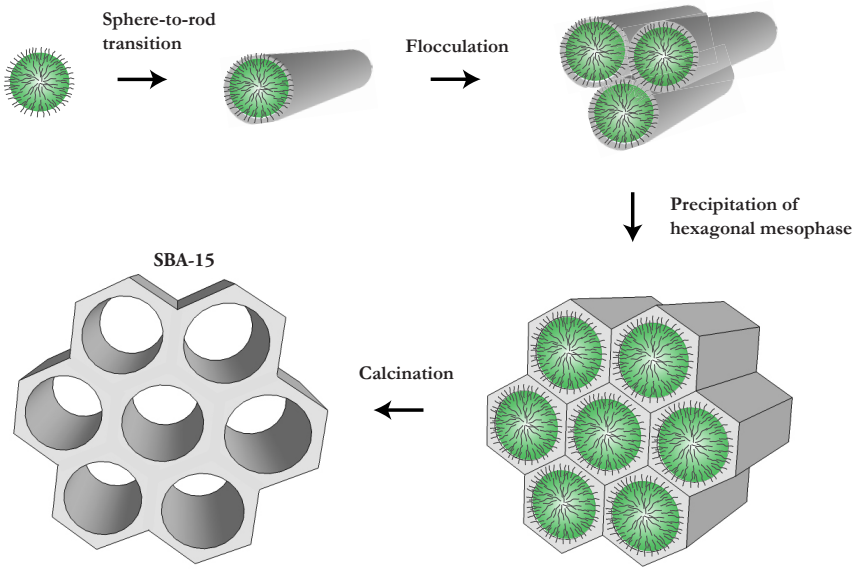

Scheme 2.6. Proposed formation mechanism of SBA-15 [46].

After formation of a hexagonally ordered structure a nucleation process is taking place leading to a progression of larger particles [37]. The material is further reorganized and cross-linked during an aging process. The process steps described are not isolated but will overlap in time throughout the synthesis. The morphology of mesoporous materials are developed after the phase separation stage. The particle morphology is dependent on the flocculation behavior which in turn is dependent on the micelle shape and the surface free energy. For elongated micelles with a low curvature the end caps of the rod shaped micelles have the largest surface energy. It has been shown that silica preferably adsorbs onto sections of the micelle with low surface energy and does not therefore attach to the ends of the elongated micelles [52]. This will result in an open pore structure after template removal. The high surface energy of the caps may also promote further particle aggregation, aligned end to end to minimize the number of ends and thereby also the surface free energy. The curvature and surface free energy are influenced by template, precursor, cosolvents, temperature, pH, salt addition, etc. By controlling these parameters SBA-15 particles formed as rods with varied length, fibers, doughnuts, gyroids and discs can be obtained [10, 32, 33, 53-55]. As an example, a low pH favors fiber morphology while a higher pH favors side by side anchoring of silicate micelles during the formation. This has been explained by variations of silicate protonation and electrical double-layer repulsion between colloidal particles when the pH is altered [56].

The pore size can be tuned by varying the temperature upon hydrothermal treatment or by adding a cosolvent [11]. When the temperature is increased the PEO groups are partially dehydrated and become more hydrophobic. The PEO groups are retracted from the silica network into the hydrophobic core, thereby increasing the pore size, reducing the microporosity and the wall thickness (Scheme 2.7) [39]. Finally, the block copolymer is removed resulting in a mesoporous material with hexagonally ordered pores.

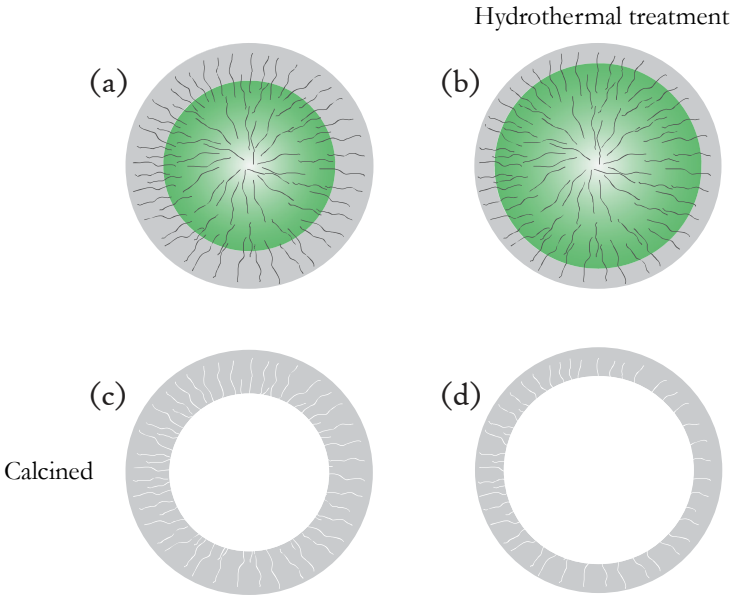

Scheme 2.7. The effect of hydrothermal treatment on the pore size. The micelle consisting of a block copolymer, with a PPO core and a PEO corona with condensed silica (a), obtains a larger core upon hydrothermal treatment due to retraction of dehydrated PEO segments (b). Removing the block copolymer by calcination causes minor pore shrinkage and the PEO segments leave micropores in the silica walls (c). Calcination of a swelled micelle results in less micropores in the pore walls (d).

The easily tunable pore size and the possibility to modify the particle morphology make SBA-15 a highly suitable support for enzymes. The material with its thick pore walls is also robust and stable in buffers in a wide range of pH. In **Paper I** and **Paper III** SBA-15 was synthesized with varying pore size and used as support for different enzymes. In **Paper II** the particle size and the morphology of SBA-15 have been investigated in regard to enzyme loading and specific activity.

2.2.2 HMM

Hiroshima mesoporous material (HMM) is a silica material consisting of small spherical particles with non-ordered mesopores [57]. They are synthesized by first forming an oil-in-water emulsion with a cationic surfactant, cetyltrimethylammonium bromide (CTAB) (Scheme 2.2a) and with styrene, octane and a silica precursor, such as tetraethylorthosilicate, constituting the oil phase. A basic amino acid, such as lysine, is added as a catalyst for the hydrolysis and the condensation of the silica precursor and a free radical initiator is added to promote polymerization of styrene. These reactions are assumed to take place simultaneously inside the drops. According to Yokoi et al. the amino acid limits the particle growth by covering the nanoparticles during the growth process, thus preventing agglomeration [34]. This mechanism may be due to electrostatic interactions between anionic silicate ($\equiv SiO^-$) and the protonated amino group of the amino acid in combination with hydrogen bonding between amino acid molecules. The pores obtained after removal of organic material have a non-uniform shape and therefore a much wider pore size distribution compared to SBA-15 and other ordered MPS materials. An attractive aspect of the HMM materials is that the synthesis yields unusually small particles. Spherical particles with a diameter of ~40 nm and with pores of a mean dimension of 10 nm can be obtained. Scheme 2.8 shows a schematic of the synthesis process, proposed by Nandiyanto et al. [57].

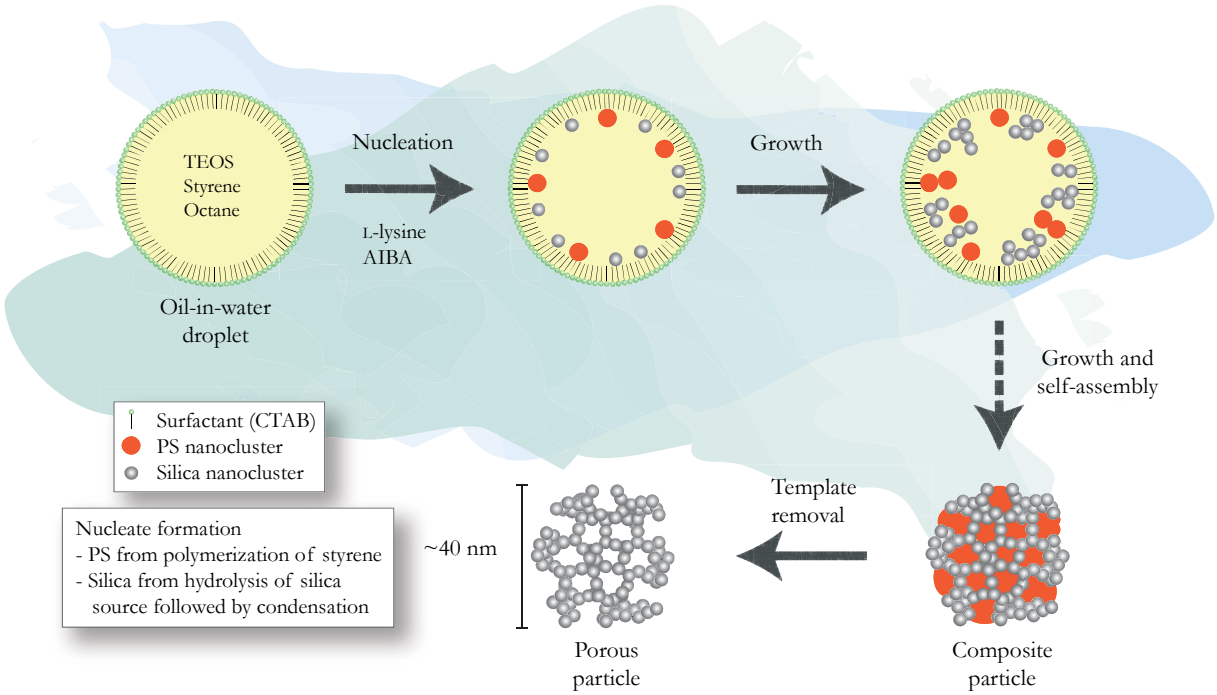

Scheme 2.8. Proposed synthesis route of HMM. Redrawn from Nandiyanto el al [57].

In **Paper II** HMM has been synthesized together with SBA-15 to study the influence of varying particle size and morphology on the enzyme immobilization. Because of the small particle size and the spherical morphology HMM particles were also used as support in **Paper V** and **Paper VI,** where QCM-D was used to study the immobilization process in real time. Moreover, special attention was given to the formation mechanism of these particles and the obtained experimental results (Section 5.1.2) [26] indicate a formation route different from the one proposed by Nandiyanto et al.

Chapter 3

IMMOBILIZATION OF ENZYMES

3.1 Short introduction to enzymes

A catalyst is a substance that increases the rate of a chemical reaction without itself being consumed or altered in the process. Enzymes are highly selective biological catalysts that accelerate and regulate the chemical processes in living matter. Without biocatalysis, chemical reactions involved in life-supporting processes such as digestion of food and synthesis of DNA could not occur on a useful time scale, and thus could not sustain life. In addition to the great catalytic power, enzymes operate in aqueous solutions under very mild conditions with respect to temperature and pH. Enzymes are proteins folded into a three dimensional structure which is crucial for the catalytic performance. The reaction takes place within a confined pocket in the enzyme (*E*) called the active site. Specific amino acid residues located in the active site bind the substrate molecule (*S*) to be catalyzed followed by a chemical transformation into a product (*P*). The many interactions between enzyme and substrate, including weak bonds (hydrogen bonds, hydrophobic interactions, ionic interactions) and strong covalent bonds, are responsible for the high substrate selectivity of enzymes. During the transformation, transient complexes (reaction intermediates) of the enzyme with the substrate and product are formed (*ES* and *EP*) (Scheme 3.1). A catalyst only affects the reaction rate, not the reaction equilibrium. The equilibrium represents the difference in free energy between the ground states of substrate and product.

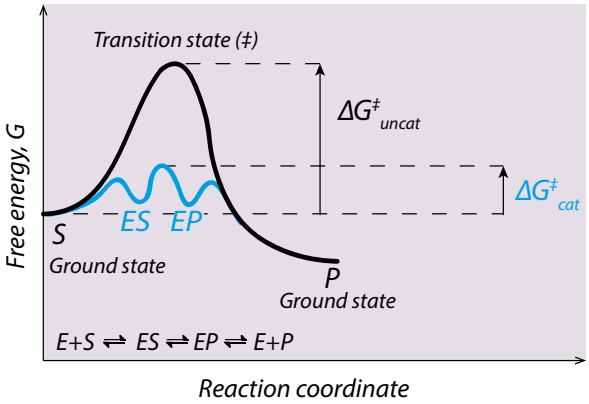

Scheme 3.1. Reaction coordinate diagram comparing an uncatalyzed and a catalyzed reaction. The free energy (G) is plotted against the progress of the reaction (reaction coordinate). Redrawn from Lehninger et al., *Principles of Biochemistry*: 5th ed. [12].

For a reaction to proceed the involved molecule(s) must be raised to a higher energy level and overcome an energy barrier. The difference between the energy levels of the *ground state* and the *transition state* is called the *activation energy*, $\Delta G^{\ddagger}$, where a higher activation energy corresponds to a slower reaction. Catalysts increase the reaction rate by lowering the activation energy. Enzymes have an optimum pH (or pH range) where the catalytic activity is at maximum. At higher or lower pH amino acids in the active site may gain a different ionization state leading to a loss of critical functions. Ionized amino acid side chains may also play an essential role for the overall protein conformation.

The use of enzymes as biocatalysts in industry is a field that is attracting considerable interest. The abovementioned qualities make them an environmentally friendly alternative to conventional synthetic catalysts that often demand harsh chemical conditions and multi-step processes, leading to excessive energy consumption and generation of much waste. Examples of applications for which enzymes have been and are being developed are in the manufacture of food (e.g. bread, cheese, butter, beer), fine chemicals (e.g. vitamins, amino acids), and pharmaceuticals [1]. They are also used in detergent formulations [1], in biosensors for analytical and diagnostic purposes [2], and in biofuel cells [3]. However, enzymes have in general a low long-term operational stability and they are difficult to recover from the reaction media, making the reuse very limited. A strategy to overcome these limitations is to immobilize the enzymes. The main driving forces for enzyme immobilization are:

- Improvement of enzyme stability
- Simplification of biocatalyst recycling and downstream processing
- Enhanced product recovery

There are numerous immobilization methods, including binding of the enzymes on a solid support or carrier, enzyme entrapment inside a material and enzyme cross-linking [6, 8, 21, 58].

3.2 Mesoporous silica as support for enzyme immobilization

Mesoporous silica (MPS) materials are attractive as support for enzymes from several points of view. As mentioned in Chapter 2, their pore size, pore structure and particle morphology can be tailored with a high degree of precision. They have a large surface area and pore volume, enabling a large quantity of enzymes to be immobilized and at the same time they provide a protective environment where the enzymes may tolerate more extreme pH, elevated temperature and higher salt concentrations [59, 60]. Immobilization can also generate a favorable microenvironment where the confinement of enzymes inside the pores may affect both the specific activity and the substrate selectivity. Moreover, the possibility of surface modifications allows for an optimized enzyme-support interaction and further control of the enzyme activity. There is no universal approach to immobilize a given enzyme for maintaining its maximum activity and stability. This has to be determined experimentally. The enzyme can be immobilized in the porous material by covalent binding, physical adsorption and electrostatic attraction. To optimize the enzyme performance, a deeper understanding of the immobilization procedure is desirable and the degree

of understanding of the molecular mechanisms needs to be improved. Scheme 3.2 shows an illustration of an enzyme immobilized in the pores of hexagonally ordered MPS.

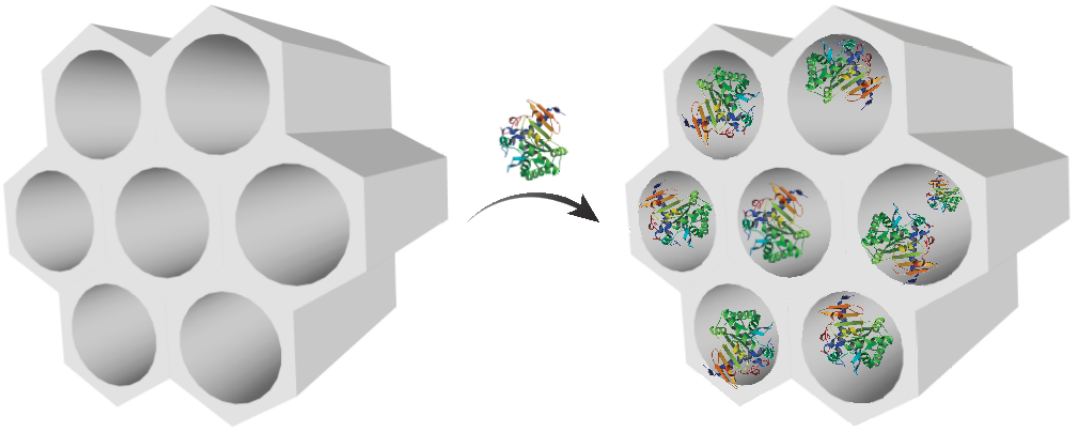

Scheme 3.2. Enzymes immobilized into the pores of hexagonally ordered MPS.

3.2.1 Immobilization strategies

Covalent binding

Covalent immobilization involves binding of reactive groups on the enzymes to a chemically active surface or molecule (Scheme 3.3a) [61]. The reactive groups may for example be amino, thiol or hydroxyl groups on amino acid side chains located on the enzyme surface. Amino groups in the side chain of lysine or other dibasic amino acids are usually the preferred groups because of their abundance. Thiol groups are very potent but are generally involved in disulfide bridges that affect the protein conformation [7]. The silica surface can be activated by functionalizing the silanol groups. Covalent binding of the enzyme to the silica carrier provides stable enzymes that can withstand elevated reaction temperatures and that can also be reused without leakage from the carrier. A major drawback with this approach is the risk of reduced enzymatic activity due to conformational changes upon attachment. If the covalent bond is involved in or close to any essential part of the catalytic site, the activity may be completely lost. Covalent binding of the enzyme to the silica may also contribute to clogging of the pore openings, thus preventing enzymes from reaching the interior of the pores.

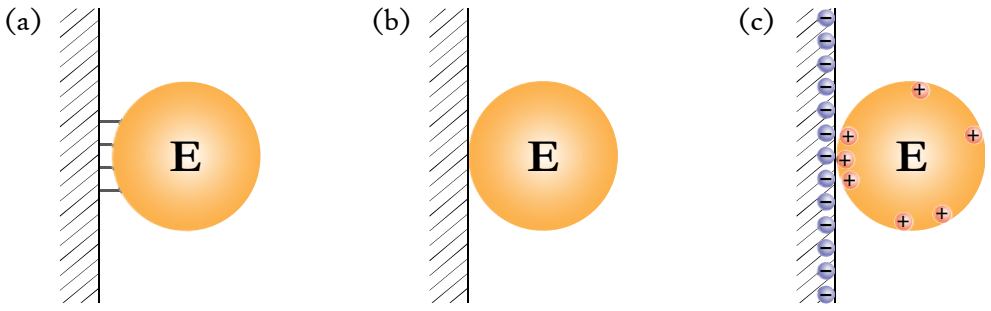

Scheme 3.3. Methods of enzyme immobilization to MPS. (a) Represents covalent binding, (b) adsorption due to hydrophobic interactions, (c) adsorption due to electrostatic interactions.

In **Paper VI** polymer mediated enzyme immobilization to a silica surface has been performed. Horseradish peroxidase is covalently attached to a polycationic dendronized polymer (denpol) (Scheme 3.4) through the bis-aryl hydrazone (BAH) linker (Scheme 3.5) [62]. The polycationic polymer can then adsorb onto negatively charged silica surfaces.

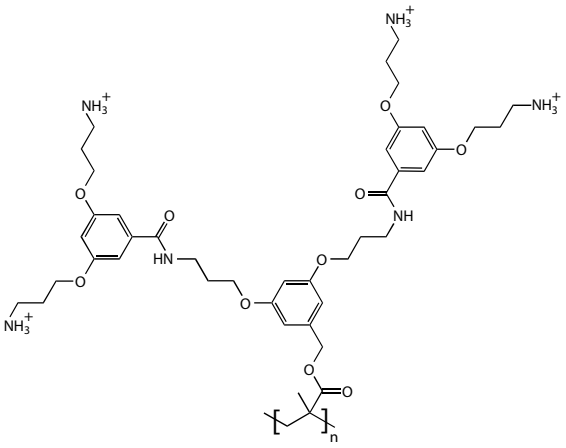

Scheme 3.4. Chemical structure of the second generation dendronized polymer *de*-PG2. The majority of the amino groups are protonated in aqueous solution below pH ≈ 9.

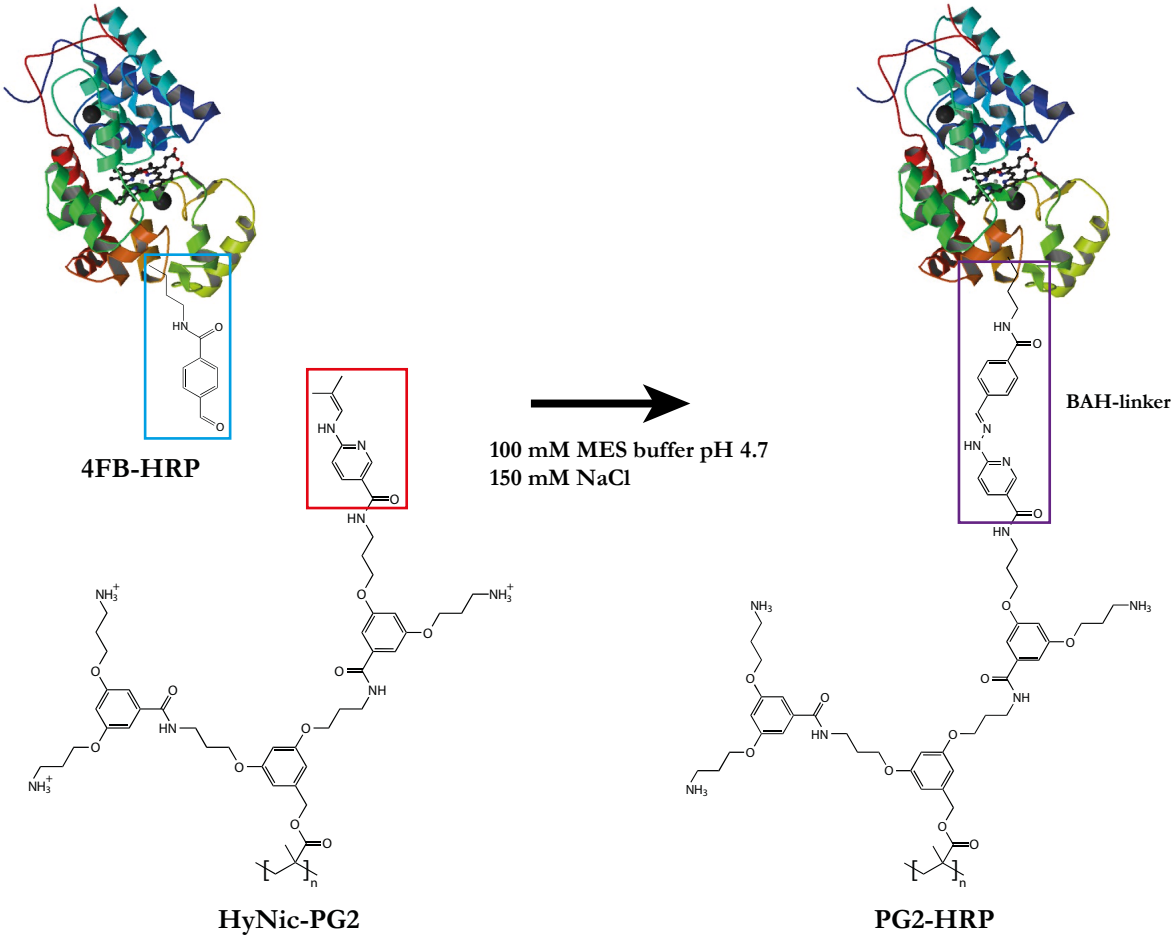

Scheme 3.5. Ligation of the modified denpol HyNic-PG2 and the functionalized enzyme (4FB-HRP) in aqueous solution via formation of a bis-aryl hydrazone (BAH) linker.

Physical adsorption

Physical adsorption comprises all weak interactions involved between enzyme and support, such as hydrogen bonding, van der Waals attraction and electrostatic interactions (Scheme 3.3b and c). With physical adsorption no activation of the support is needed and the method is therefore frequently used in large-scale production. Moreover, the risk of enzyme denaturation due to strong binding is minimized. A limitation with this method is that the interactions often are too weak to prevent the enzyme from leaking out of the material. To minimize leaking it is important to tailor-make the material with respect to pore size, etc. for a good fit of the enzyme in the pores and to find the optimal conditions for the specific enzyme. Ionic strength of the solution, pH and temperature are parameters that generally affect the enzyme adsorption.

The adsorption of enzymes to the silica surface can be improved and the leaking can be minimized if there are electrostatic interactions involved between oppositely charged residues on the enzyme molecules and the silica surface. The surface net charges on the enzyme and on the silica can be controlled by varying the pH of the solution. An attractive interaction between enzyme and silica is generally obtained at a pH somewhere in-between the point of zero charge (pzc) of silica (pzc ~2) and the isoelectric point (pI) of the specific enzyme [23]. The pI is the pH where a surface or a molecule has no net charge. At a pH below the pzc of silica or above the pI of the enzyme the two components will have the same net charge, which will lead to repulsive electrostatic forces. However, one has to keep in mind that the enzyme surface charge is generally not evenly distributed. Even though the overall charge above the pI of an enzyme is negative, positively charged regions may promote an electrostatic attraction between the enzyme and a negatively charged support [63]. As discussed in **Paper II**, enzymes are flexible and may adopt a conformation in the vicinity of a support surface such that they experience attractive electrostatic interactions even if their net charge is the same as that of the support. Adsorption through electrostatic interactions is a milder method compared to covalent binding so the degree of conformational changes and activity loss is generally lower. The immobilization procedure is also less complex and is therefore more suitable for large scale preparations.

In this thesis the focus was on enzyme immobilization in MPS through physical adsorption by intermolecular interactions. The pH of the immobilization solution has been studied in relation to enzyme-support interaction, loading and catalytic performance. An exception from the physical adsorption of enzymes to the support is the covalent attachment of horseradish peroxidase to a polycationic dendronized polymer (**Paper VI**). The polymer-enzyme conjugate was subsequently physically adsorbed to MPS particles (Section 3.2.1).

3.2.2 Support properties

During enzyme immobilization it is important to keep this in mind that enzymes can vary substantially in size, shape, isoelectric point, surface charge distribution, catalytic performance, etc. In addition to the immobilization methods discussed in Section 3.2.1, the support properties like pore size, particle size and particle morphology are crucial factors to consider where both enzyme loading and catalytic performance can be significantly improved with an optimized fit [23, 64, 65]. Moreover, depending on the physico-chemical properties of the support surface, like

charge density and hydrophobicity, the enzyme might experience a different environment inside the pores compared to the bulk phase. As an example, a change in the surface charge density influences the local proton concentration and as a result the local pH inside the pores. On a negatively charged surface the local proton concentration is increased due to electrostatic attraction of protons, leading to a shift to a more acidic pH. The adverse effect is observed in the case of positively charged surfaces [66].

Pore size

The size of the pore opening in relation to the enzyme determines whether the enzyme will fit inside the pores or not. Enzymes that are larger than the pore openings will obviously not fit inside the pore at all but may instead only adsorb on the outer surface of the particles [24]. If the pore and the enzyme are of similar size, or if the pore is slightly larger, the enzyme can diffuse into the pore and may be protected from the surroundings [67, 68]. However, the diffusion into the narrow pore may be slow. Enzymes can also get stuck in the pore opening and the immobilization may therefore not be optimal in terms of maximal loading. On the other hand, if the pore opening is much larger than the enzyme, a high loading can be obtained but leaking may be an issue and the enzyme will not be as protected from the surrounding medium as if the pore is of matching size [67, 69]. The optimal pore size is also influenced by the enzyme stability. An unstable enzyme may need a more narrow pore size compared to a relatively stable enzyme. Additionally, the confining effect in a narrow pore can enhance the specific activity due to a beneficial conformational change of the enzyme [70]. Another major factor concerning choice of pore size is mass transport limitations of the substrate to the active site of the enzyme. A narrow pore size can cause a hindered diffusion of the substrate, leading to a compromised product formation rate [69].

Particle size

The size of the MPS particles can also affect both the enzyme loading and the catalytic activity. The number of pore entrances increases with decreasing particle size. Smaller particles but with the same overall pore volume can improve the loading since shorter pores will decrease the enzyme diffusion distance and minimize empty space far down the pores [65]. Furthermore, shorter pores may give an improved availability of the enzyme towards the substrate. The substrate may be able to reach a larger relative amount of active sites within a certain time.

Microenvironment inside the pores

Physical effects, like the influence of substrate mass transfer are difficult to separate from biochemical effects inside the pores and it is consequently very difficult to make predictions of optimal immobilization conditions, as well as of intrinsic activity of the immobilized enzyme. Moreover, the environment inside the pores is not necessarily the same as in the bulk solution. Both the immobilization and the reaction conditions, like pH and substrate concentration, may differ significantly from the conditions in the bulk [71]. It is therefore important to characterize

the microenvironment inside the pores in order to improve the understanding of how material properties and solution composition can be used to control the enzymatic activity.

Enzymes are highly affected by the pH, both during immobilization and during the biocatalysis process. Changing the pH will alter the surface charge of both the enzyme and the silica surface, hence affecting the electrostatic interaction between enzyme and support. The pH also affects the enzyme conformation and immobilizing an enzyme at different pH values may lead to different enzyme conformations in the immobilized state which, in turn, may result in a change in enzymatic activity. This difference in enzymatic activity between free and immobilized enzyme may be due to an altered pH inside the pores of the support. In **Paper IV** fluorescence spectroscopy has been used to measure the pH sensed by proteins immobilized in MPS particles (SBA-15) by covalently attaching the pH probe SNARF1 to the proteins. In contrast to previous attempts where pH probes were attached to the pore surface [72], this approach allows the pH to be measured without altering the properties of the silica material.

3.3 Immobilization process

The by far most common method to monitor enzyme immobilization is to retrieve samples from the external solution at different times during the immobilization process and measure the remaining amount of enzyme [73]. With this indirect approach the enzyme loading in the support can be estimated but usually requires manual sampling which results in a low time resolution making the adsorption kinetics difficult to study. The location of the enzyme after immobilization is also a key issue. It is crucial to be able to determine whether the enzymes are mainly situated inside the porous structure or adsorbed at the external particle surface. Determination of the enzyme depletion (by standard protein concentration assays) from the continuous phase may show that the enzyme is bound to the porous particles but does not prove that the enzyme is actually inside the pores. In **Paper VII** other techniques commonly used for indirect monitoring of the enzyme immobilization are described, including N_2 adsorption, X-ray diffraction (XRD), Fourier transform infrared spectroscopy (FTIR) and thermogravimetric analysis (TGA).

To gain more knowledge about the immobilization process and kinetics we have developed, as described in **Paper V**, a direct technique for monitoring the enzyme immobilization in small silica particles attached to a surface using quartz crystal microbalance with dissipation monitoring (QCM-D) (see Section 4.7 for a description of the technique). The QCM-D technique measures the mass added to the mesoporous particles with a time resolution in the sub-second range, which can be easily compared to the mass added to non-porous paritcles. The stability of the immobilized enzyme-particle complex could also be studied with QCM-D by washing away the external protein and detect the rate of protein desorption from the particles as a mass loss.

Other techniques that, in a direct way, visualize enzyme molecules localized inside the material are fluorescence microscopy and transmission electron microscopy in combination with immunogold staining (TEM-IGS). These are described in **Paper VII**.

3.4 Co-immobilization

In nature, enzymatically catalyzed reactions are often incorporated into complex cascade reactions involving several enzymes. The efficiency of a cascade reaction is not only determined by the efficiency of the individual enzymes involved, but also by the transfer of reaction intermediates from one enzyme to the next. If the enzymes catalyzing subsequent steps of a cascade reaction are in close spatial proximity, substrate channeling may lead to an increased overall rate. This effect is exploited in nature by compartmentalization or co-immobilization in cells as well as in the formation of multi-enzyme complexes [74]. Controlling the spatial arrangement of different types of enzymes upon immobilization is therefore of high interest, if such cascades are targeted. As mentioned in the introduction of this chapter replacement of synthetic catalysts with more environmentally benign enzymes is an important strategy for establishing sustainable chemical processes. The multi-enzyme complex systems can be utilized in more advanced organic synthesis applications, involving a combination of several reactions [75]. Through co-immobilization it is possible to perform a one pot reaction instead of performing isolated steps where the reaction intermediates need to be separated in-between each reaction step. This results in a simplified process where undesired byproducts can be avoided and the cascade may proceed in a highly chemo- or stereoselective way compared to a conventional organic synthesis process [76]. Moreover, the loss of unstable intermediates can be reduced through *in situ* generation of substrates [77]. Immobilized multi-enzyme systems can also be utilized in biosensors for the quantification of molecules of biological interest, like D-glucose, lactose, choline, cholesterol, etc. In the detection of D-glucose, for example, the sensitivity can be increased by combining glucose oxidase (GOD) and a peroxidase (POD) together with an indicator dye in a co-immobilized system [78].

$$D-glu\cos e+O_2 \xrightarrow{GOD} gluconic\ acid+H_2O_2$$

$$H_2O_2+\underset{colorless}{reduced\ dye} \xrightarrow{POD} 2H_2O+\underset{colored}{oxidized\ dye}$$

In **Paper VI** co-immobilization of the two enzymes glucose oxidase and horseradish peroxidase together with the indicator dye o-phenylenediamine (OPD) has been used as a model system to detect glucose (see Section 4.5.2 for the cascade reaction). Here we combine polymer mediated enzyme immobilization with immobilization in MPS.

3.5 Enzymes used in the thesis

3.5.1 Lipase

Lipases (triacylglycerol acylhydrolases, E.C. 3.1.1.3) are a group of water-soluble enzymes that are the key enzymes in metabolism and fat digestion. They are recognized as one of the most important groups of enzymes in biotechnology, with applications in food, detergent,

pharmaceutical, leather, textile, cosmetic and paper industries [79]. Lipases are a sub group of esterases and are also called serine hydrolases. They catalyze the hydrolysis of triacylglycerol to glycerol and free fatty acids in aqueous media. In organic media they catalyze the reverse reaction, where esters are synthesized or transesterified.

Hydrolysis

$RCOOR' + H_2O \rightarrow RCOOH + R'OH$

Esterification

$RCOOH + R'OH \rightarrow RCOOR' + H_2O$

Transesterification

Interesterification

$RCOOR' + R''COOR^* \rightarrow RCOOR^* + R''COOR'$

Alcoholysis

$RCOOR' + R''OH \rightarrow RCOOR'' + R'OH$

Acidolysis

$RCOOR' + R''COOH \rightarrow R''COOR' + RCOOH$

In contrast to conventional esterases, lipases are surface active and the enzymatic activity is often greatly increased when the lipase is close to an interface. This behavior is due to the unique structural characteristics of lipases. The active site of most lipases is covered with a hydrophobic α-helical unit, called the "lid", which alters the conformation of the active site to an open state when interacting with an interface [80]. Thus, the active site is revealed. Immobilizing lipases on interfaces can therefore be very useful. The active site in lipases holds a catalytic triad, i.e., the three amino acids directly involved in the catalytic process. The triad is composed of the amino acids serine, histidine, and aspartate or glutamate. A similar triad is found in serine proteases. Close to the triad is an oxyanion hole that stabilizes the carbonyl group of the substrate during the hydrolysis. In **Paper I** lipase from *Mucor miehei* (MML) has been studied (Scheme 3.6a). The pI of MML is 3.8, the molecular weight is 32 kDa, and the hydrodynamic diameter is 4.5 nm [81]. In **Paper II** lipase from *Mucor miehei* was compared with lipase from *Rhizopus oryzae* (ROL) that has the same size (32 kDa) but a different pI (7.6) [82].

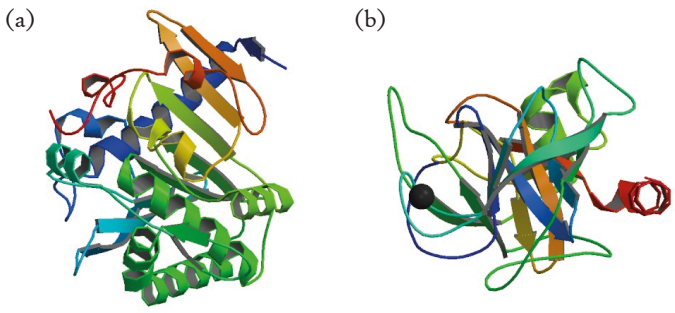

Scheme 3.6. Structure of (a) lipase from *Mucor miehei* [83] and (b) trypsin from *bovine pancreas* [84].

3.5.2 Trypsin

Trypsin (E.C. 3.4.21.4) is, like lipase, an important enzyme in the metabolic process where it degrades proteins. It is an enzyme with many applications in for example food, detergents, and waste management, as well as in the diagnostics and pharmaceutical industries [85]. More specifically, trypsin is a serine protease, also called peptidase that catalyzes the hydrolysis of peptide bonds at the carboxyl side of the amino acids lysine and arginine. Similar to lipases, see Section 3.5.1, the active site contains a catalytic triad and an oxyanion hole that stabilizes the intermediate molecule during the process. The triad consists of a serine, a histidine and an arginine, where serine acts as the nucleophilic amino acid interacting with positively charged amino acids [86]. Since trypsin is a protease it can degrade adjacent trypsin molecules (autolysis), as well as other enzymes in a solution. This can be a major problem since the stability of a trypsin solution is therefore very low in many industrial processes. Such degradation can to a large extent be overcome by immobilization because the trypsin molecules will be prevented from reaching each other.

In **Paper I** trypsin from *bovine pancreas* (BPT) (Scheme 3.6b) has been compared with lipase from *Mucor miehei*. The pI of this trypsin is 10.5, the molecular weight is 23 kDa, and the hydrodynamic diameter is 3.8 nm [24].

3.5.3 Feruloyl esterase

Feruloyl esterases (FAEs) (E.C. 3.1.1.73) are commonly found in fungi and participate in the cell wall degradation of plants. They are a subclass of carboxylic ester hydrolases that catalyze the hydrolysis of ester bonds between hemicelluloses and lignin, releasing hydroxycinnamic acids and sugars (polysaccharides) [87, 88].

The hydroxycinnamic acid derivative, ferulic acid (4-hydroxy-3-methoxycinnamic acid) (Scheme 3.7), is an interesting molecule with antioxidant and also possibly anticarcinogenic properties.

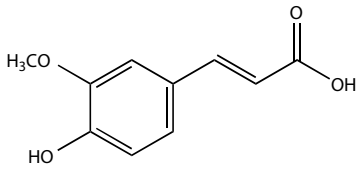

Scheme 3.7. Ferulic acid.

Possible applications for FAEs are numerous, including pulp and paper industry, production of fuel ethanol and farming industry [88]. Hydroxycinnamic acid derivatives have been shown to have both antioxidant and antitumor properties [89, 90]. It is therefore of interest to add these compounds to foods, cosmetics and therapeutics. However, it is often desirable to modify the properties of the hydroxycinnamic acids. For example, their hydrophobicity must be increased for use in oil-based products. It has been shown that if most of the water in the system is replaced by organic solvents FAEs catalyze the reverse reaction and can be used in the esterification of hydroxycinnamic acids [91]. Previous studies have shown that it is possible to promote the reverse reaction (esterification and transesterification) by confining the FAEs in the oil droplets of oil-in-water microemulsions [91, 92]. This may be due to a change of the FAE into a more favorable conformation, as well as a change in substrate access.

In **Paper III** immobilization of FAE into MPS has been studied and the degree of change of the activity by confining the enzymes into silica nanopores was assessed.

3.5.4 Horseradish peroxidase

Horseradish peroxidase (HRP) (EC 1.11.1.7) (Scheme 3.8a), found in the root of the horseradish plant (*Armoracia rusticana*), is an enzyme widely used as a reporter protein in biological and medical research in applications such as *immunohistochemistry* and *enzyme linked immunosorbent assay* (ELISA) [93]. It is also utilized as a reagent for organic synthesis and biotransformations [94]. HRP is an oxidoreductase acting on aromatic compounds using hydrogen peroxide as electron acceptor. Scheme 3.9 shows an example of the catalytic cycle of HRP C with ferulate as substrate. The heme-containing (iron(III) protoporphyrin IX) isoenzyme HRP C comprises a single polypeptide chain of 308 amino acid residues [95]. The enzyme also contains two calcium atoms which are, together with the heme group, essential for the structural and functional integrity. A reaction catalyzed by HRP includes a reducing substrate (AH_2) (typically aromatic phenols, phenolic acids, indoles, amines and sulfonates) and a radical product ($AH^{\bullet}$).

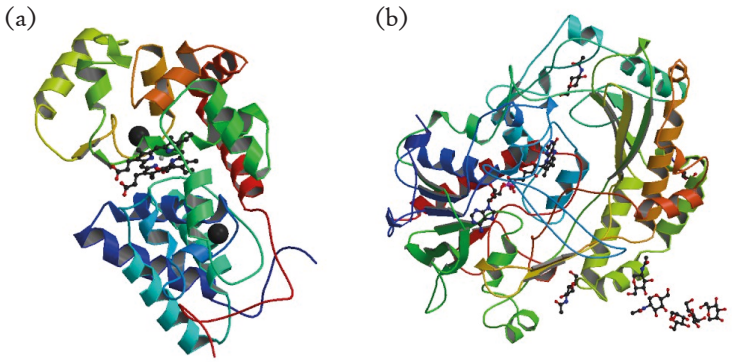

Scheme 3.8. Structure of (a) peroxidase from horseradish (*Armoracia rusticana*) [96] and (b) glucose oxidase from *Aspergillus niger* [97].

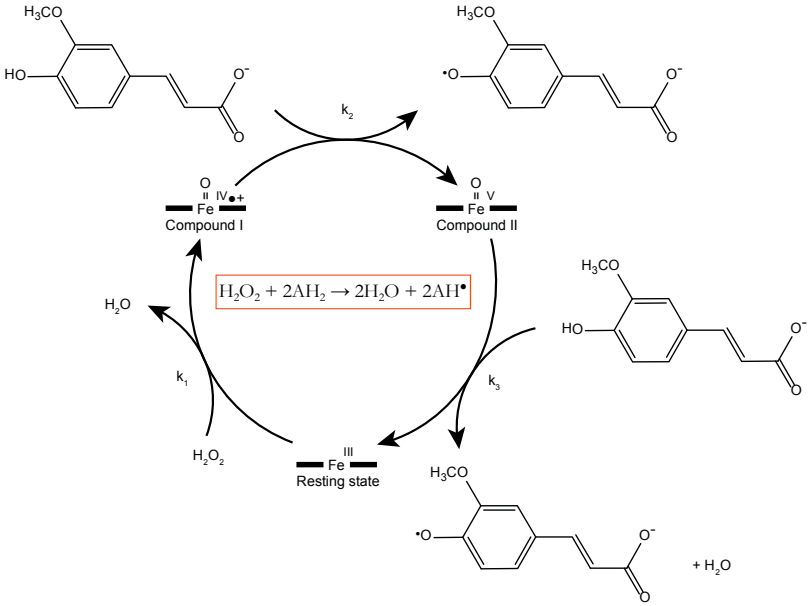

Scheme 3.9. The catalytic cycle of horseradish peroxidase (HRP C) with ferulate as reducing substrate, where k_1, k_2 and k_3 are the reaction rate constants.

3.5.5 Glucose oxidase

Glucose oxidase (GOD) (EC 1.1.3.4) (Scheme 3.8b) is found in some fungi and insects where its main function is to act as an antibacterial and antifungal agent through the production of hydrogen peroxide. The enzyme naturally catalyzes the oxidation of beta-D-glucose to D-gluconolactone and hydrogen peroxide using oxygen as an electron acceptor [98-100].

β-D-glucose + O_2 → D-gluconolactone + H_2O_2

Although both products break down spontaneously GOD is inactivated upon product accumulation. There are numerous commercial and industrial applications for GOD, including food processing as a preservative and stabilizer, gluconic acid production which is used as a acidity regulator, and biofuel cells where biochemical energy is converted into electrical energy using a biocatalyst, to name a few [100]. GOD is also utilized as a biosensor for blood glucose monitoring (Section 4.5.2) [78, 101].

Chapter 4

ANALYTICAL TECHNIQUES

Characterization of mesoporous materials demands a combination of analytical techniques. Small angle X-ray scattering (SAXS), transmission electron microscopy (TEM), scanning electron microscopy (SEM) and nitrogen physisorption are all used to determine the particle morphology, pore structure, pore size distribution, specific surface area and pore volume of the materials prepared in this work. The activity of the enzymes immobilized in the various materials and the enzyme concentrations have been evaluated with UV/Vis spectroscopy. Furthermore, the surface activity of lipase has been determined with optical tensiometry and enzyme immobilization was followed using quartz crystal microbalance with dissipation monitoring (QCM-D).

4.1 Small angle X-ray scattering

X-ray diffraction (XRD) is a method that utilizes the short wavelength of X-rays for analyzing the intermolecular structure of crystalline materials. However, the walls of mesoporous materials are amorphous with no long-range order and therefore only show X-ray diffraction patterns at small angles, if the material consists of ordered mesoporous channels [102]. For these materials small angle X-ray scattering (SAXS) can be used which is closely related to XRD. SAXS gives structural information in the region of 1-100 nm and is therefore specifically suited for mesostructured materials. The incoming X-rays are of the same order of magnitude as the distance between the lattice planes in the material. Scattered radiation, due to interference with the electron clouds around the atoms in the material, is detected and the intensity is plotted as a function of the scattering angle (2θ). The regular pattern in an ordered material gives rise to peaks in the plot due to constructively interfering scattered radiation characteristic for a specific structure. The distance between the peaks represents spacing of the lattice planes that can be calculated using Bragg´s law:

$$n\lambda = 2d_{hkl}\sin\theta \qquad (2)$$

where n is an integer, λ the wavelength of the incoming beam, d_{hkl} the spacing between the parallel crystal planes and θ the angle between the incoming beam and the crystal plane (Scheme 4.1). The path difference between two waves undergoing constructive interference is given by $2d\sin\theta$. The obtained spectrum indicates whether a hexagonal, cubic, lamellar, or disordered structure is present. For hexagonal structures with cylindrical assemblies crystallized in a two dimensional hexagonal lattice, $l = 0$.

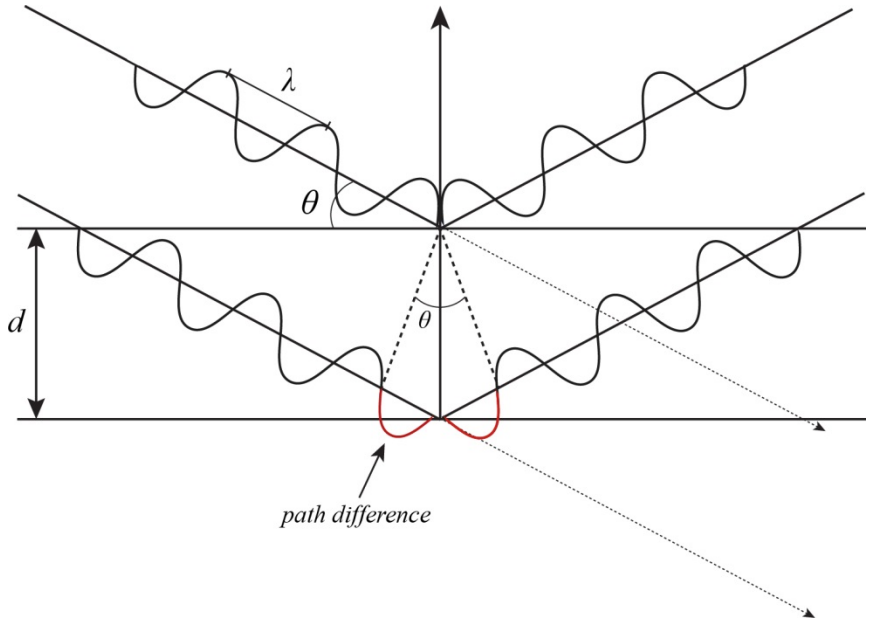

Scheme 4.1. Illustration of X-ray diffraction according to Bragg's law.

The structure can be determined from the relative distance between the Bragg peaks, denoted q_{hk}. The spacing is defined as

$$d_{hk} = \left[\frac{4}{3a^2} \left(h^2 + k^2 + hk \right) \right]^{-1/2} \quad (3)$$

and

$$q_{hk} = \frac{2\pi}{d_{hk}} = \frac{4\pi}{\sqrt{3}a} \sqrt{h^2 + k^2 + hk} \quad (4)$$

where a is the unit cell length.

Typical for mesoporous silica (MPS) with hexagonally structured pores are three to five Bragg reflection peaks at 2θ angles below 3°. According to Equation 4 the relative distance between the Bragg peaks for a hexagonal structure are q_{10}:q_{11}:q_{20}:q_{21}:q_{30}:q_{22} = 1:√3:2:√7:3:√12. A typical plot for a hexagonal pattern is shown in Scheme 4.2. SAXS is a very good technique for determining the structure of a material but is not suitable for quantifying the degree of order.

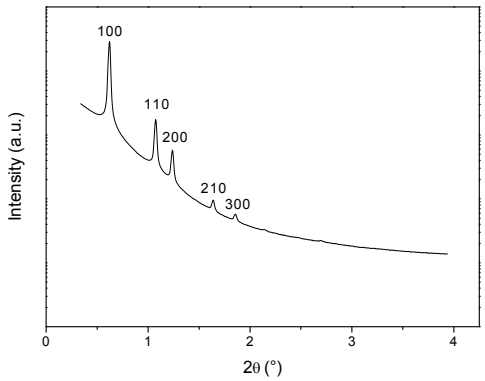

Scheme 4.2. Typical SAXS pattern for a hexagonally ordered silica material.

Atoms with high electron density, like silica, scatter X-rays with a relatively high intensity, but the intensity can be further increased by using a synchrotron with a high flux of radiation. The photons emitted by electrons circulating in a magnetic field are used to irradiate the sample. In this work SAXS measurements have been performed on the I711 and I911 beam lines at the MAX-lab synchrotron facility (Lund, Sweden).

4.2 Transmission electron microscopy

Transmission electron microscopy (TEM) is a microscope technique that utilizes electrons to visualize specimens with a magnification up to 10^6. Due to the short wavelength of electrons it is possible to obtain a resolution in the range of 1 Å. An electron beam is accelerated in vacuum at high voltages through a thin sample. The image is obtained by focusing the electron beam onto the specimen (Scheme 4.3). The objective lens situated below the sample together with several intermediate lenses forms the image from the transmitted electrons. Finally, the projector lens enlarges the image and projects it onto a fluorescent screen. Thicker regions in the sample scatter more electrons compared to thinner regions. Therefore, thicker regions with high scattering will appear darker on the screen than thinner regions.

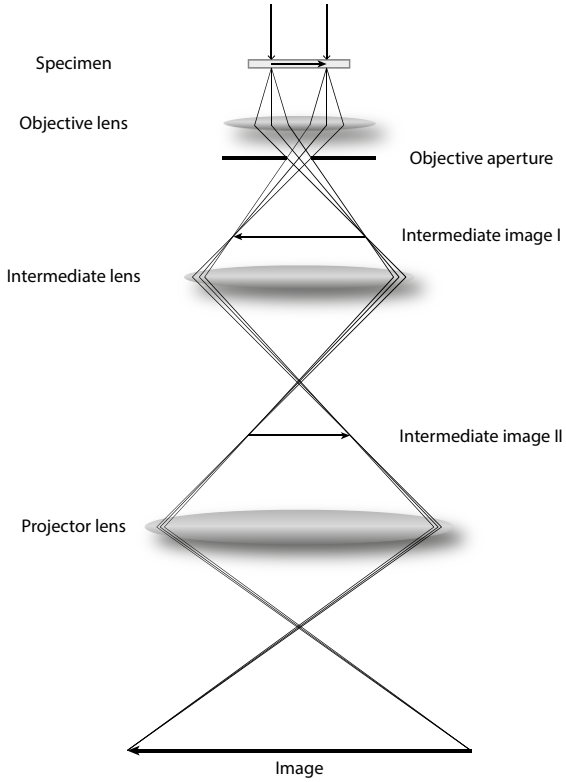

Scheme 4.3. Schematic illustration of the ray-path in TEM imaging.

In this work, a JEM-1200 EX II TEM (Jeol, Tokyo, Japan) operated at 120 kV has been used for determining the local pore structure and order of MPS and also for estimating the size of small silica particles. Thin specimens were prepared by grinding silica particles followed by dispersion in ethanol, sonication for 10 minutes and finally dripped onto holey carbon copper grids. Complementary techniques were needed to confirm the results since TEM only displays a limited part of the sample.

4.3 Scanning electron microscopy

Scanning electron microscopy (SEM) is like TEM a non-destructive electron microscopy technique. But, unlike TEM, the electrons emitted from the specimen are collected. The electron beam is scanned over the specimen, creating signals when the electrons interact with the sample. Secondary electrons emitted from the specimen surface and backscattered electrons are detected

and utilized to visualize a three-dimensional topology, surface morphology and surface composition of materials with a resolution in the nanometer range.

In this work, a Leo Ultra 55 FEG SEM (Leo Electron Microscopy, Cambridge, UK) has been used to study the particle size and morphology of the MPS materials and also to some extent the mesoporous structure. In order to prevent charging of the material it is common to coat the surface with a metal. However, the metal coating aggravates a detailed observation of the pore structure. By instead using a low accelerating voltage (2.0 kV in this case) the surface charging can be minimized. Prior to use, silica particles were dispersed in ethanol and sonicated for 10 minutes. The secondary electrons were collected with an in-lens detector.

4.4 Nitrogen physisorption

Physisorption is a method to characterize the specific surface area, pore volume and pore size distribution (PSD) of solid porous materials. The method utilizes attraction between gas molecules and the atoms on the surface of the porous material. The most common gas in this technique is nitrogen, but helium and argon are also used for characterizing materials. The sample is first degassed in a vacuum oven to remove any adsorbed contaminants followed by cooling to 77 K and then exposure of nitrogen gas under controlled pressure. The surface area is quantified by creating a monolayer of nitrogen molecules at the solid surface with an increasing pressure. Using the universal gas law and the Brunauer-Emmett-Teller (BET) gas adsorption method [103] the adsorbed amount can be calculated. Information about the pore volume, pore size and shape of the pores is obtained by further saturating the pores with nitrogen gas. The partial pressure (p/p_0), is stepwise increased until the point of condensation is reached followed by a pressure reduction resulting in gas evaporation. There are several methods, such as the BJH [104], BdB [105-107] or KJS [108] methods used to determine the pore size distribution (PSD) from nitrogen sorption isotherms. Different methods are suitable for different pore shapes and sizes. In this work, only the Barrett-Joyner-Halenda (BJH) method has been used. This method is based on the assumption that all pores are of cylindrical shape.

The data is presented as adsorption/desorption isotherms, which can be grouped into six types (I-VI), shown in Scheme 4.4. The shape of the isotherm can be used to provide details of the structure of the material being analyzed. Typical for a mesoporous material is a well-defined hysteresis loop (type IV), due to the capillary condensation inside the mesopores. The first part of the curve represents the monolayer condensation where point B, in the beginning of the almost linear middle section of the isotherm, indicates the stage at which monolayer coverage is complete and multilayer adsorption begins. There are four types of hysteresis loops (H1-H4), shown in Scheme 4.5, where the shape depends on the type of pore structure. Mesoporous materials with a uniform pore structure and narrow pore size distribution typically result in adsorption and desorption isotherms almost vertical and parallel to each other (H1). A H2 loop indicates occurrence of non-uniform pores whereas slit-shaped pores often result in a H3 loop. Slit-shaped pores are also associated with a H4 loop but the almost horizontal plateau indicates microporosity.

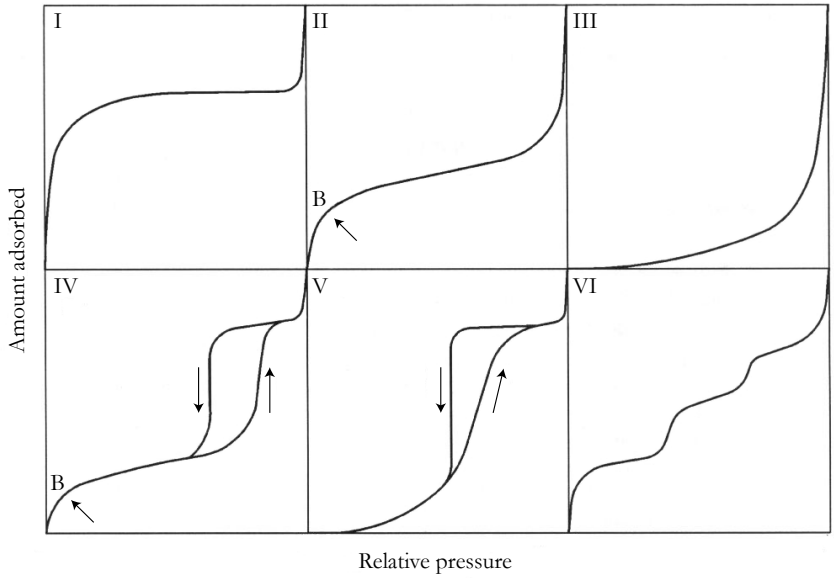

Scheme 4.4. Types of physisorption isotherms according to the IUPAC classification [109].

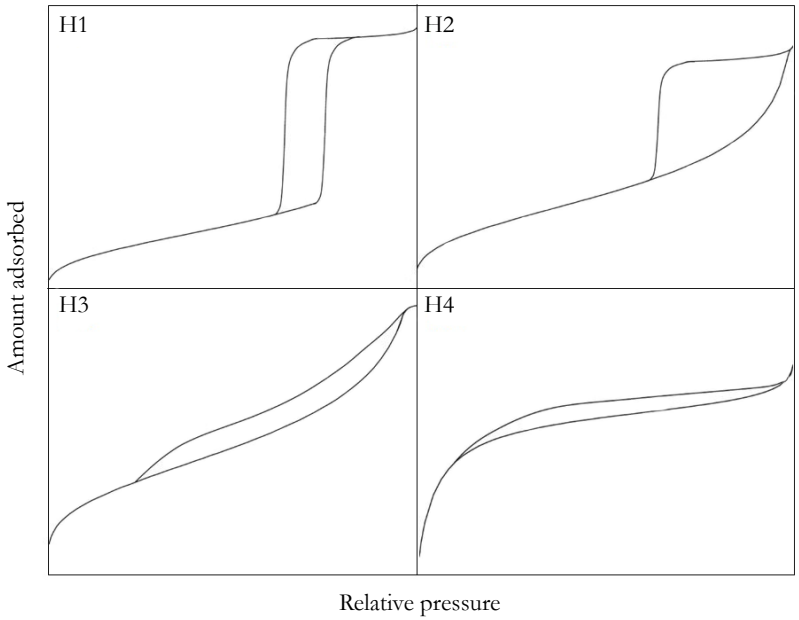

Scheme 4.5. Types of hysteresis loops according to the IUPAC classification [109].

In this thesis, MPS particles were analyzed in a Micromeritics ASAP 2010 instrument after degassing the samples in a vacuum oven at 225 °C for 2 h.

4.5 UV/Vis spectroscopy

UV/Vis spectroscopy is an analytical tool for quantitative determination of analytes. It is based on measurement of the absorbance in the ultraviolet and visible spectral region when a beam of parallel radiation passes through a solution of a compound. Electromagnetic energy from the beam is transferred to the atoms or molecules in the sample solution. This absorption of energy

causes excitation of the electrons to a higher energy state if the photons, with a specific wavelength, exactly match the energy difference between the ground state and one of the excited states of the compound. The electrons in a molecule are bound in a specific way, and therefore all compounds have a unique absorption spectrum. The amount of light absorbed is directly proportional to the path length through the solution and the concentration of the absorbing species is expressed by the Lambert-Beer law:

$$A = \log\left(I_0 / I\right) = \varepsilon c l \qquad (5)$$

where A is the absorbance or extinction, I_0 and I the intensities of the monochromatic light before and after passing through the sample, ε the molar absorptivity or extinction coefficient, c the concentration of the compound and l the path length. The molar absorptivity is a substance-specific constant, describing the light absorbing ability at a given wavelength under specified conditions regarding solvent, pH, temperature, etc. From this relation the concentration can be plotted as a linear function of the absorbance. UV/Vis absorption spectroscopy is normally sensitive to electrons participating in the formation of multiple bonds or aromatic groups within organic molecules.

4.5.1 Protein concentration

The amount of immobilized enzyme per amount of porous support (pore loading, P_{LD})is a key property of an enzyme/particle system and is usually reported as the weight of immobilized enzyme per particle weight [110]. The common way to measure protein loading is by an indirect approach where the amount of immobilized enzyme is calculated from the decrease in enzyme concentration in the solution surrounding the particles. The particles are removed by centrifugation and the enzyme concentration in the supernatant is determined by native protein absorbance at 280 nm or by some standard assay such as Lowry, BCA or Bradford. In this thesis the BCA assay, the Bradford assay and the native protein absorbance have been used to estimate the pore loading.

Ultraviolet light absorption

UV/Vis spectroscopy is a widely used method for concentration measurements of proteins. Proteins have characteristic absorption peaks at 200 nm and 280 nm. The absorbance at 200 nm is mainly due to the many peptide bonds in a protein. However, many other substances also absorb light in this area and 200 nm is therefore not a suitable wavelength for estimating the concentration of proteins. Therefore measurements are normally performed at 280 nm, which is the region where the aromatic amino acids tryptophan and tyrosine absorb UV light. This spectrophotometric method, used in **Paper II**, is straightforward and rapid and demands no preparation of the samples. However, one should be aware of the possible interference by contaminating nucleic acids (and possibly other substances) that absorb strongly in the same wavelength region.

Horseradish peroxidase can be quantified (**Paper VI**) by detecting the Soret peak at 403 nm which is observed for molecules containing a porphyrin, in this case a heme group (Section 3.5.4). The Reinheitzahl (RZ) ratio (A403/A280) can be used to determine the purity of a HRP [111].

Colorimetric assays

Colorimetric assays are also used for determination of protein concentration. Well-known examples are the Lowry assay [112], the BCA assay [113] and the Bradford assay [114]. These assays are all based on a color shift of an extrinsic molecule in the presence of a protein. The BCA assay has been used in **Paper I** and is based on reduction of Cu^{2+} to Cu^{+} by proteins under alkaline conditions followed by detection of the generated Cu^{+} with a reagent containing bicinchoninic acid (BCA) (Scheme 4.6a). The cuprous ion chelates two BCA molecules and the complex absorbs visible light at 562 nm. According to Wiechelman et al. the reduction of copper is performed by the amino acids cysteine, cystine, tryptophan and tyrosine together with peptide bonds in protein backbone structure [115].

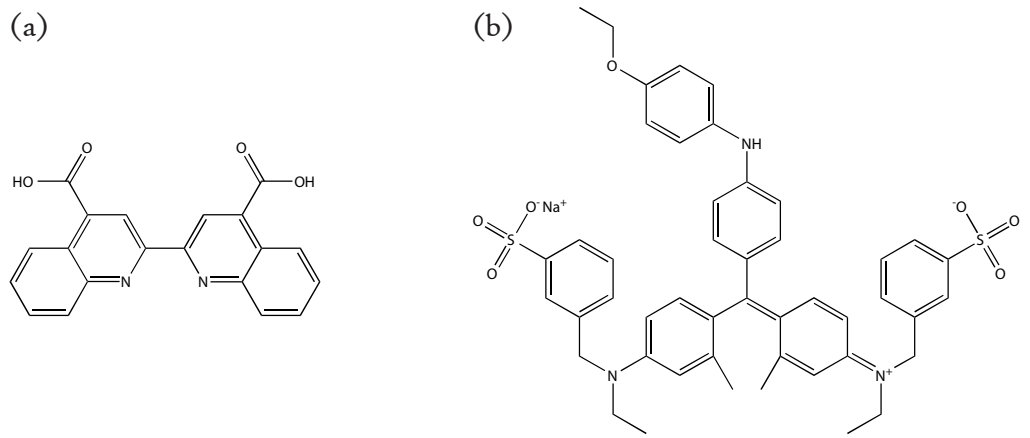

Scheme 4.6. (a) Bicinchoninic acid, (b) Coomassie brilliant blue G-250.

In the Bradford assay, used in **Paper III**, the binding of the dye Coomassie brilliant blue G-250 (CB) (Scheme 4.6b) to proteins is utilized for determining protein concentration. The dye is converted from a red form to blue upon protein binding under acidic conditions. The mechanism is not fully understood but CB probably binds mainly to the charged amino acids residues arginine and lysine. The protein bound dye has an absorption maximum at 595 nm.

4.5.2 Enzyme activity assays

As mentioned in the introduction and throughout the thesis the main purpose of enzyme immobilization is to facilitate separation of the enzyme from the reaction medium to enable enzyme recycling and to protect the enzyme from the surrounding environment. However, the immobilization loses its purpose if the catalytic performance is lost due to for example compromised substrate diffusion or enzyme denaturation upon binding to the support. It is

therefore essential to evaluate whether the immobilization of the specific enzyme is more advantageous compared to keeping the enzyme free in solution. In order to evaluate how the catalytic performance is affected by the confinement inside the pores the enzyme activity must be monitored. It has been shown that immobilization can either increase or decrease the specific activity (enzyme activity per weight of total enzyme) [116, 117], which illustrates the need of comparing the specific activity of the immobilized enzymes with that of the free enzyme in solution.

Lipase activity assay

The activity of native and immobilized lipase has been assayed (**Paper I** and **Paper II**) by monitoring the catalytic hydrolysis of 4-nitrophenyl acetate (pNPA) into 4-nitrophenol (pNP) and acetic acid (Scheme 4.7). Under alkaline conditions pNP is deprotonated to 4-nitrophenolate, which is bright yellow. The absorbance is detected at 400 nm (ε_{400} = 14,200 M^{-1} cm^{-1}). The measurements were carried out using a Agilent HP8453 spectrophotometer.

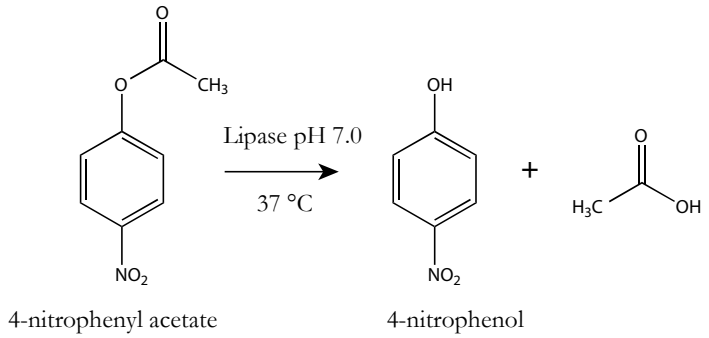

Scheme 4.7. Lipase-catalyzed hydrolysis of 4-nitrophenyl acetate (pNPA).

Trypsin activity assay

The activity of native and immobilized trypsin was assessed (**Paper I**) by monitoring the catalytic hydrolysis of N-α-benzoyl-DL-arginine-4-nitroanilide (BAPNA) into 4-nitroaniline (Scheme 4.8). The absorbance can be detected at 405 nm (ε_{405} = 10,500 M^{-1} cm^{-1}). The measurements were carried out using a Agilent HP8453 spectrophotometer.

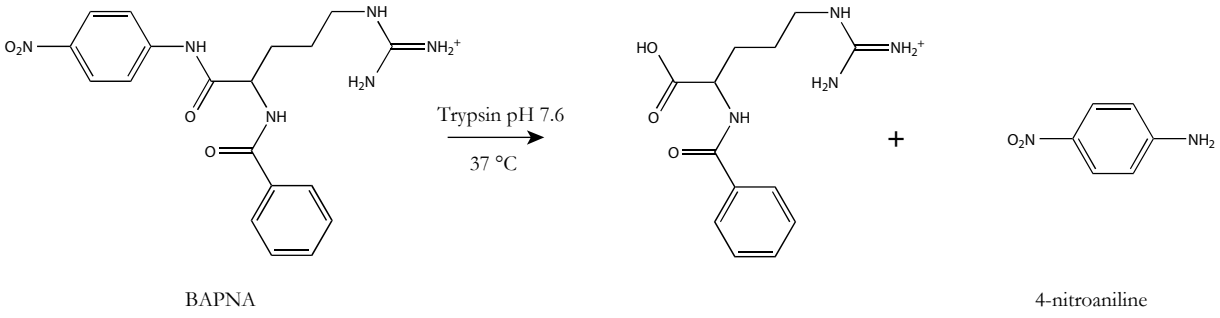

Scheme 4.8. Trypsin-catalyzed hydrolysis of N-α-benzoyl-DL-arginine-4-nitroanilide (BAPNA).

Horseradish peroxidase activity assay

Enzymatic activity of horseradish peroxidase (HRP) was quantified in **Paper VI** using 2,2'-azino-bis(3-ethylbenzothiazoline-6-sulfonic acid) diammonium salt (ABTS) as a chromogenic substrate and hydrogen peroxide as electron acceptor (Scheme 4.9) [118]. The product formation was monitored with a spectrophotometer and quantified using the absorption band at 414 nm (ε_{414nm}= 36000 M^{-1} cm^{-1}).

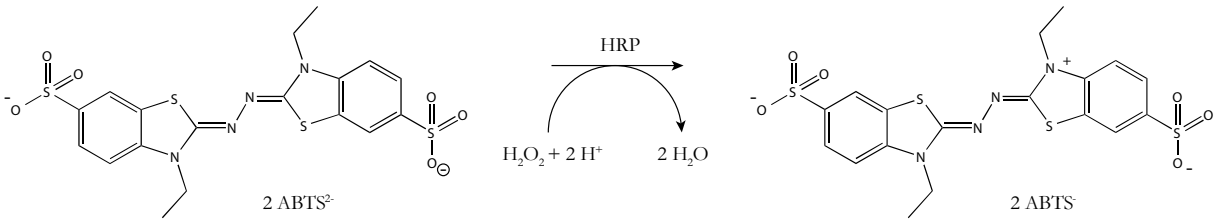

Scheme 4.9. HRP quantification using $ABTS^{2-}$ and H_2O_2 as substrates.

Glucose oxidase activity assay

GOD activity was quantified in **Paper VI** using a combined assay including D-glucose and oxygen (as available in non-degassed buffer) as substrates together with HRP and *o*-phenylenediamine (OPD) for *in situ* detection of the hydrogen peroxide formed (Scheme 4.10) [119]. The concentration of active GOD was determined based on the generated amount of the reaction product 2,3-diaminophenazine (DAP), with a maximum absorbance at 418 nm. This system can also be applied for quantification of D-glucose to evaluate the efficiency of the GOD/HRP cascade reaction.

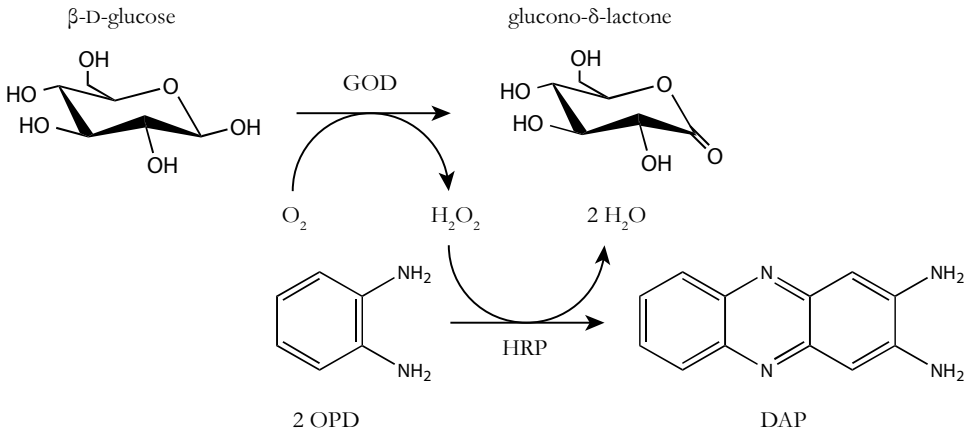

Scheme 4.10. Quantification of GOD in a cascade reaction together with HRP, using D-glucose and *o*-phenylenediamine (OPD) as substrates.

4.6 Optical tensiometry

Surface and interfacial tension of liquids can be measured with pendant drop shape analysis using an optical tensiometer. A drop of the liquid is hanging from a syringe tip and the shape of the

drop is determined by the balance between surface forces and gravity (Scheme 4.11). The surface tension, γ_{LF}, is determined by fitting the drop shape (in a captured video image) to the Young-Laplace equation (Equation 6) which relates interfacial tension to drop shape [120, 121]. The shape factor, β, is obtained from the coupled first order differential equations 7-9.

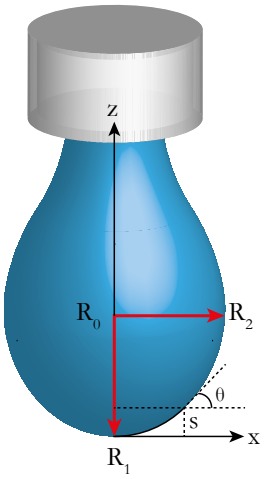

Scheme 4.11. Illustration of a pendant drop.

$$\gamma_{LF}\left(\frac{1}{R_1}+\frac{1}{R_2}\right)=\frac{2\gamma_{LF}}{R_0}+\Delta\rho g z \qquad (6)$$

$$dx/ds = \cos\theta \qquad (7)$$

$$dz/ds = \sin\theta \qquad (8)$$

$$d\theta/ds = 2+\beta z-\frac{\sin\theta}{x} \qquad (9)$$

where R_0 is the radius at the drop apex, R_1 and R_2 the radii of curvature, $\Delta\rho$ the density difference between the drop and the surrounding media, g the gravitational constant, and β the shape factor. After finding the best corresponding β value the surface tension can be deduced (Equation 10).

$$\gamma_{LF}=\Delta\rho g\frac{R_0^2}{\beta} \qquad (10)$$

Surface tension measurements of lipase solutions are described in **Paper II** as a way to determine the difference in surface activity between lipase from *Mucor miehei* and lipase from *Rhizopus oryzae* (ROL). An optical tensiometer, Attension, Theta Lite, KSV Instruments for pendant drop shape analysis was used in the study.

4.7 Quartz crystal microbalance with dissipation monitoring

Quartz crystal microbalance with dissipation monitoring (QCM-D) is a surface sensitive technique, capable of measuring mass changes at the sensor surface in the nanogram range (<10 ng/cm^2) in real time and at the same time monitor the elastic and viscoelastic properties of the adsorbed layer [122-125]. A QCM sensor consists of a thin, disc shaped, quartz crystal with metal electrodes deposited on both sides (Scheme 4.12).

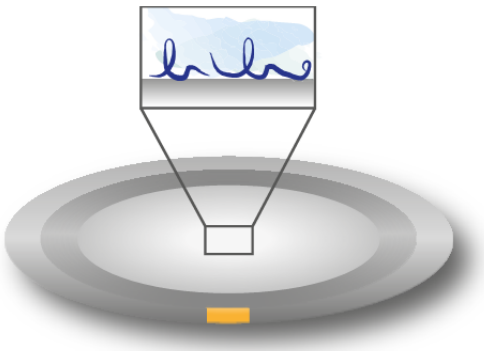

Scheme 4.12. Illustration of a silica covered quartz crystal with a polymer adsorbed on the surface.

Due to the piezoelectric properties of quartz, the crystal oscillates at a characteristic resonance frequency when subjected to an alternating electrical potential. Adsorption of a small mass to the sensor, including coupled solvent, induces a decrease in oscillation frequency. For a thin and rigid film, evenly adsorbed over the sensor surface the mass change is linearly proportional to the shift in frequency and can be determined with the *Sauerbrey equation* (Equation 11) [126],

$$\Delta m = \frac{-C\Delta f_n}{n} \tag{11}$$

where Δm is the adsorbed mass per unit area, Δf_n is the frequency shift for a given overtone (harmonic) number n(=1, 3, 5, 7…) and C is the mass sensitivity constant, typically 17.7 ng/(cm^2*Hz) for a sensor with f_1=5 MHz.

A soft viscoelastic film induces frictional (viscous) losses of the sensor oscillation leading to an underestimation of the adsorbed mass with the *Sauerbrey equation*. The viscoelasticity can be due to solvent that is coupled to the dry mass via direct hydration, as a viscous drag, or entrapped in cavities in the adsorbed film. The damping or energy *dissipation* (D) can be detected by switching on and off the driving voltage and observing the decay time (τ) of the oscillation amplitude (A) [122-124], as expressed by Equations 12 and 13.

$$A \propto \exp(-t/\tau) \tag{12}$$

$$D = \frac{1}{\pi \int \tau} = \frac{E_D}{2\pi E_S} \tag{13}$$

where E_D is the energy that is lost and E_S is the energy stored during one period of oscillation.

To estimate the adsorbed mass of a soft film where the dissipation is large and the Sauerbrey equation does not hold a viscoelastic model can be applied. By using multiple frequency measurements, an adhering soft film can be characterized in detail with the Voigt viscoelastic model [123]. It describes the propagation and damping of shear bulk acoustic waves in a single uniform viscoelastic adsorbed film in contact with a semi-infinite bulk Newtonian liquid with no slip. The film is defined by an effective thickness (d_{eff}), density (ϱ_{eff}) and complex shear modulus ($\mu + i\omega\eta$) (stiffness), where μ is the effective shear elasticity, $\omega=2\pi f$ the oscillation frequency and η the shear viscosity. The total mass of the film is estimated by the effective thickness multiplied by effective density and includes adsorbed dry material together with coupled water, see Equation 14:

$$\Delta m = d_{eff} \cdot \rho_{eff} \tag{14}$$

The film density is approximated somewhere between the density of the dry material and that of water.

QCM-D has been used in **Paper V** and **Paper VI** to study the enzyme immobilization process into (MPS) particles in real time. A schematic illustration of the procedure in **Paper V** is illustrated in Scheme 4.13. Small (40 nm) MPS particles (HMM) were adsorbed onto silica coated

sensors modified with amine linkers and the particle-coated surface was subsequently used for immobilization of either lipase from *Rhizopus oryzae* (ROL) or feruloyl esterase from *Fusarium oxysporum* (FoFAEC). The stability of both particle adsorption and enzyme immobilization was evaluated by rinsing procedures. The influence of pH on the immobilization efficiency was studied for both enzymes.

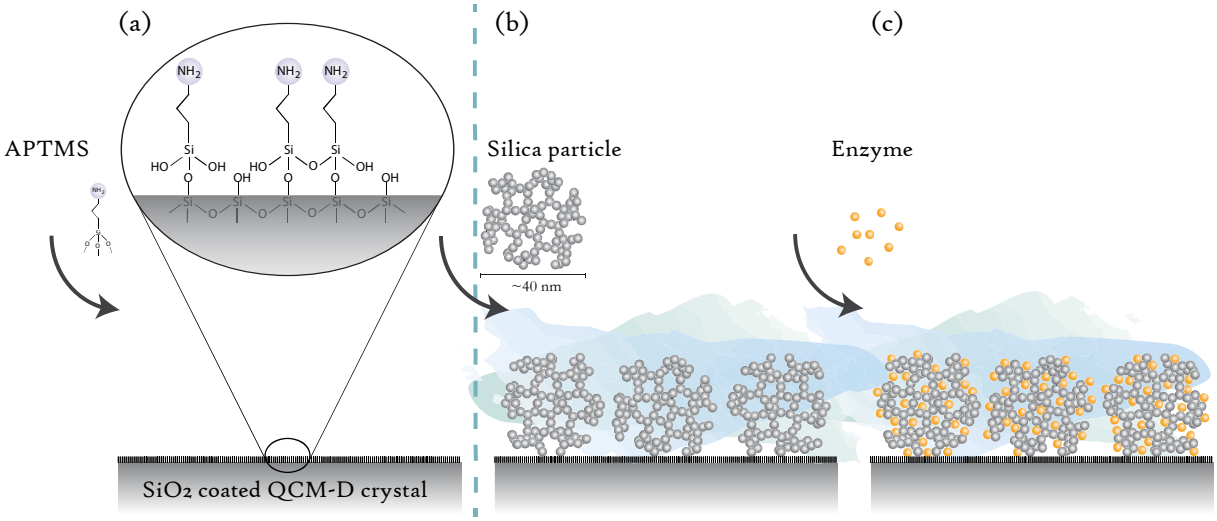

Scheme 4.13. Schematic illustration of attachment of silica particles to the QCM-D sensor followed by enzyme immobilization: (a) Sensor functionalization with APTMS (performed outside the QCM-D chamber), (b) attachment of particles, and (c) enzyme immobilization. The schematic illustrates the results from **Paper V**.

In **Paper VI** co-immobilization of glucose oxidase (GOD) and horseradish peroxidase (HRP) was studied with QCM-D by combining immobilization in MPS with polymer mediated enzyme immobilization (Scheme 4.14).

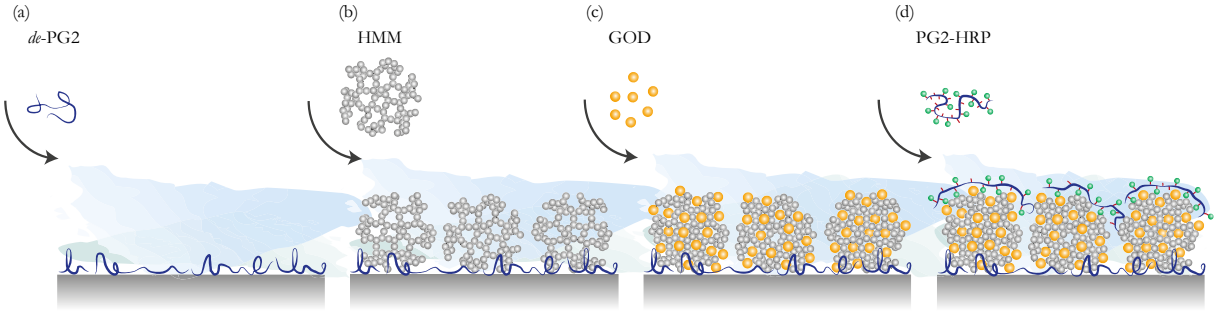

Scheme 4.14. Schematic illustration of co-immobilization of glucose oxidase (GOD) and horseradish peroxidase (HRP) through immobilization in mesoporous HMM particles and dendronized polymer (de-PG2) mediated immobilization: (a) Adsorption of the polycationic de-PG2 to a silica coated sensor, (b) attachment of HMM particles onto the polymer, (c) immobilization of GOD, and (d) attachment of HRP covalently linked to a dendronized polymer. The schematic illustrates the results from **Paper VI**.

Chapter 5

RESULTS AND DISCUSSION

In this work mesoporous silica (MPS) particles have been synthesized and used as support for biocatalysts with the intention to improve the catalytic stability and enable enzyme recycling. The large surface area of mesoporous materials facilitate a larger quantity of immobilized enzymes compared to corresponding non-porous materials and provides a protected environment inside the pores. In order to achieve the most optimally operating biocatalyst the support must be adapted towards the particular enzyme with respect to size and morphology. The pore microenvironment is a crucial factor to take into account and it is important to understand the immobilization process as well as the interactions between support and enzyme. In this thesis the obtained results are divided into two parts, where the first part is focused on the silica support and the second part on the immobilization process and the catalytic performance of the immobilized enzymes.

5.1 Synthesis and characterization of mesoporous silica

In the following sections, the synthesis of different types of mesoporous silica (MPS) with varying pore size, particle size, pore structure and particle morphology is summarized. Characterization of the particles was performed by the combined use of SEM, TEM, nitrogen physisorption and SAXS. See attached papers (**Papers I and II**) for detailed descriptions of the preparation protocols. All the material properties analyzed with nitrogen physisorption are summarized in Table 5.1.

Table 5.1. Material properties of MPS particles, analyzed by nitrogen adsorption.

Material	Synthesis temp. (°C)	BJH pore width (nm)	BET surface area (m^2/g)	Total pore volume (cm^3/g)
MPS-5P	80	5.0	860	0.70
MPS-6P	100	6.0	986	1.08
MPS-9P	140	8.9	554	1.17
MPS-1000	n.r.[a]	9.3	502	1.18
MPS-300	n.r.	9.4	606	1.03
MPS-40	n.r.	9.1	463	0.91

[a] Not relevant

5.1.1 SBA-15

Pore size

SBA-15 was synthesized with three different pore sizes in **Paper I** and with two different pore sizes in **Paper III**, using the standard protocol developed by Zhao et al. with only minor modifications [11]. Only the results from **Paper I** are shown here as nothing new regarding the materials was presented in **Paper III**. The obtained particles all had a rod-like shape, about 2 μm in length and 1 μm in diameter (Figure 5.1). The particles were agglomerated, both side by side and end by end, into clusters. Typical TEM micrographs of calcined SBA-15 displayed hexagonal patterns (Figure 5.2a) with long range order (Figure 5.2b) and uniform pores.

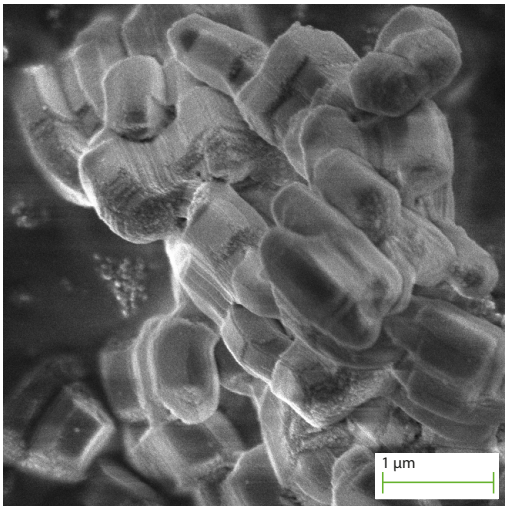

Figure 5.1. Typical SEM micrograph of SBA-15 synthesized with the standard protocol [11].

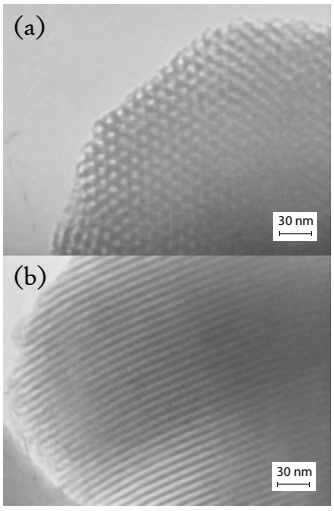

Figure 5.2. Typical TEM micrographs of SBA-15, where (a) displays the hexagonal pore structure and (b) displays the long-range order.

The pore size was tuned by varying the hydrothermal temperature during the aging process. The synthesis temperatures 80 °C, 100 °C and 140 °C resulted in mesoporous materials with a pore diameter of 5 nm, 6 nm and 9 nm, respectively, calculated with the BJH method (Table 5.1). They are here denoted MPS-5P, MPS-6P and MPS-9P, according to their pore diameter. It was observed that the surface area decreased from about 1000 m^2/g to about 500 m^2/g when increasing the temperature from 100 °C to 140 °C. This is, as discussed in Section 2.2.1, a consequence of the reduced microporosity at high temperatures. Since micropores are too small (< 2 nm) to fit enzymes the lower surface area does not affect the available surface area significantly. The lower abundance of micropores was also confirmed by the isotherm plot (Figure 5.3) and by the pore size distribution plot (Figure 5.4). The sorption isotherm shows a lower volume of adsorbed nitrogen at low relative pressure for the largest pore size together with a flat line in the micropore region in the pore size distribution plot.

The N_2-sorption isotherms of calcined SBA-15, shown in Figure 5.3, also confirm the mesopore structure observed in the TEM micrographs. All materials exhibit a sorption isotherm type IV with HI hysteresis, characteristic of SBA-15 materials with cylindrical and hexagonally ordered mesopores. The pore-filling step in the adsorption and desorption curves is sharp for the SBA-15

materials, corresponding to a narrow pore size distribution, also shown in Figure 5.4. Figure 5.5 shows the SAXS patterns of SBA-15 with varied pore size. At least three well-resolved peaks can be observed for all the materials. These are indexed (100), (110) and (200), characteristic of a two dimensional hexagonal structure.

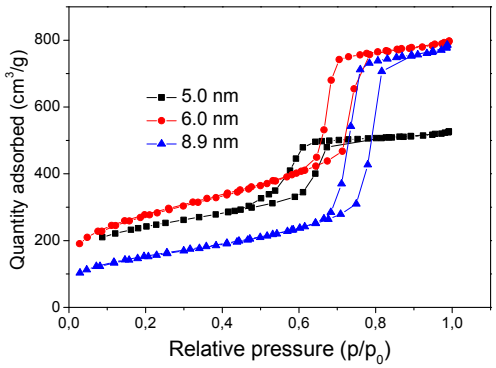

Figure 5.3. Nitrogen sorption isotherms of SBA-15 with varied pore size.

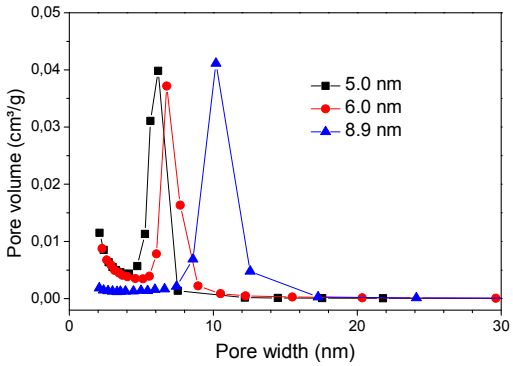

Figure 5.4. Pore size distribution of SBA-15 with varied pore size.

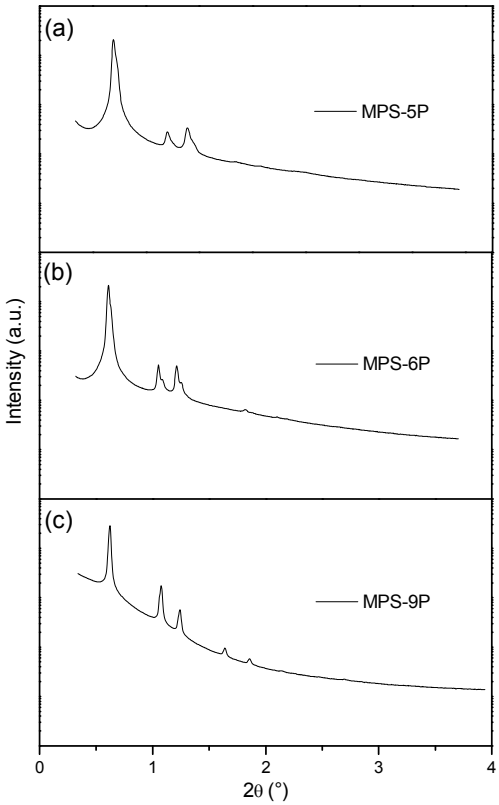

Figure 5.5. SAXS patterns of hexagonal mesoporous material with (a) 5 nm, (b) 6 nm, and (c) 9 nm pores.

Particle morphology

In addition to SBA-15 synthesized using the standard protocol, two materials with different morphologies but similar pore size (~9 nm) were prepared, here denoted MPS-1000 and MPS-300 (Table 5.1) (**Paper II**). For comparison, MPS-9P from the previous section is also displayed in the graphs in this section.

Addition of potassium salt to the standard synthesis protocol together with the use of static conditions during the aging process resulted in shorter particles, about 1000 nm (MPS-1000), and with a broader base (Figure 5.6a). The particles were less agglomerated compared to the conventional SBA-15 particles. As mentioned in Section 2.2.1, inorganic salts can enhance the interaction between silica species and the polyoxyethylene segments of the non-ionic block copolymer, thereby affecting the morphology of the silica particles. The particle agglomeration was reduced by decreasing the stirring time during the condensation step. A slower rate of precipitation and absence of shear flow are possible factors that may contribute to reduced particle aggregation under static conditions [127].

By using a low temperature synthesis with addition of heptane and NH_4F, smaller particles, about 300 nm (MPS-300) with a rod-shaped morphology, were obtained (Figure 5.6b). A decrease in stirring time and an increase in HCl concentration yielded discrete, non-agglomerated particles. The particle elongation is believed to be related to the hydrolysis rate of the silica precursor which is dependent on the HCl concentration and on the presence of NH_4F. The fluoride ion, F^-, functions as a catalyst for hydrolysis and condensation of TEOS. With F^- present silica networks are formed that cannot penetrate deep into the poly(ethylene oxide) (PEO) shell [128]. This results in less flexibility of the micelles; the walls will become denser at an earlier stage and the structure will become freezed. An increased HCl concentration will cause formation of HF leading to a lower concentration of the catalyst, F^-. Smaller oligomers will form more flexible micelles that can become elongated. Furthermore, a decreased pH increases the hydrolysis and condensation rates of the silica precursor, which increases the formation rate of the particles. [127].

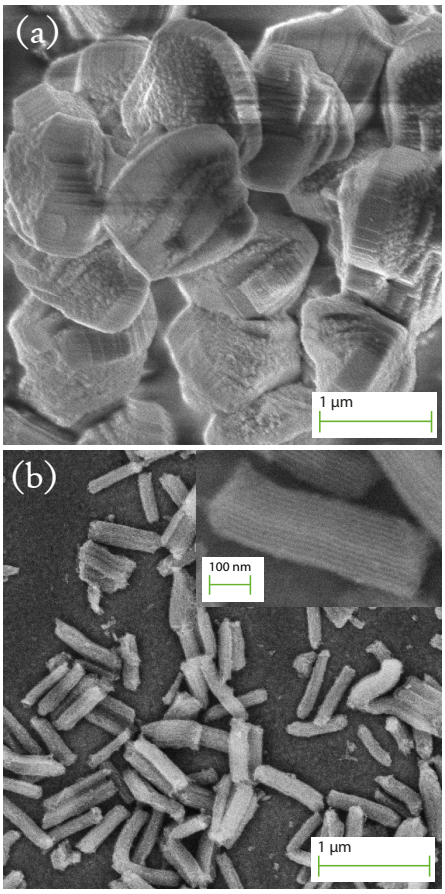

Figure 5.6. SEM micrographs of (a) MPS-1000 and (b) MPS-300.

The N_2-sorption isotherms (Figure 5.7) as well as the pore size distribution (Figure 5.8) of MPS-1000 and MPS-300 were similar to MPS-9P.

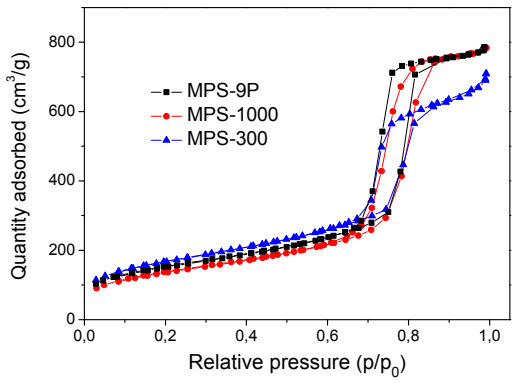

Figure 5.7. Nitrogen sorption isotherms of SBA-15 with varied morphology.

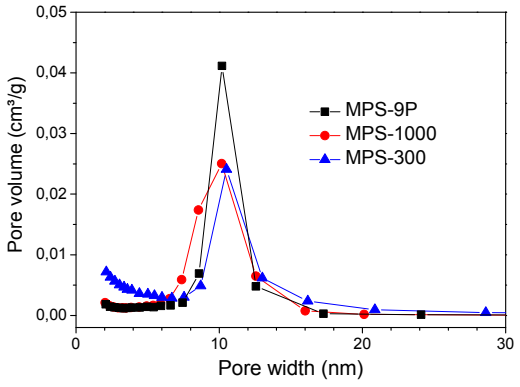

Figure 5.8. Pore size distribution of SBA-15 with varied particle morphology.

5.1.2 HMM

The preparation of HMM particles is very different from the synthesis of SBA-15. In the standard protocol developed by Nandiyanto et al. [57] an oil-in-water emulsion is formed with a cationic surfactant and with octane constituting the organic phase (described in Section 2.2.2). At first our focus was to synthesize small, spherical particles with pores around 9 nm (MPS-40, Table 5.1) and utilize them as support for enzymes (**Papers II**, **V** and **VI**). However, during the attempts to control the particle and pore size, efforts were also put on the understanding of the formation mechanism. This work is still in progress but the results so far indicate a different type of mechanism than the one proposed by Nandiyanto et al.

After removal of the organic components by calcination spherical MPS particles around 40 nm in diameter (MPS-40) were obtained. The TEM and SEM micrographs (Figure 5.9), show quite monodisperse particles but with a non-ordered pore structure. Instead of cylindrical uniform pores, as for SBA-15, the pores were more varied with respect to both size and shape. A particle size around 40 nm was confirmed.

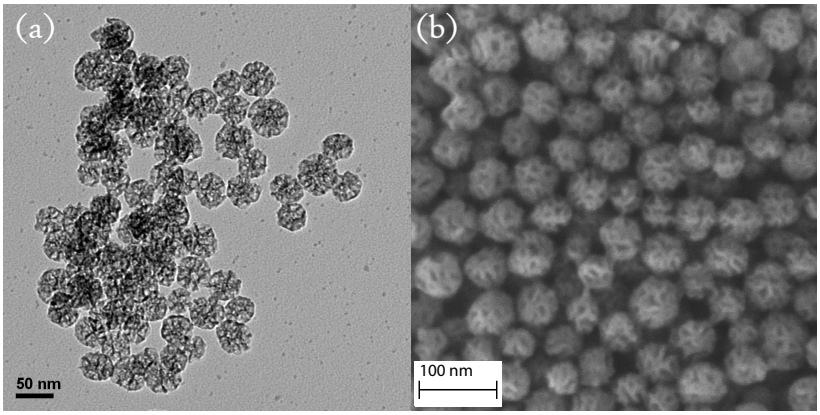

Figure 5.9. (a) SEM micrograph and (b) TEM micrograph of HMM particles (MPS-40).

MPS-40 displays a type IV sorption isotherm with H3 hysteresis (Figure 5.10), which is characteristic of mesoporous materials with slit-shaped or irregular pores. The pore size distribution was wide (Figure 5.11) compared to SBA-15 materials and no pore order could be detected with SAXS (Figure 5.12). One should note that the BJH method used for calculating the pore size assumes cylindrical pores which is not the case for MPS-40. The pore size may therefore not be as precise as for SBA-15.

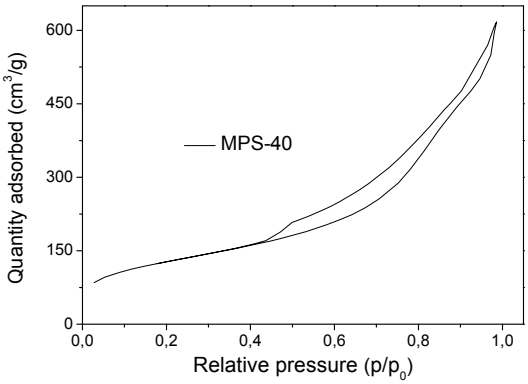

Figure 5.10. Nitrogen sorption isotherms of MPS-40.

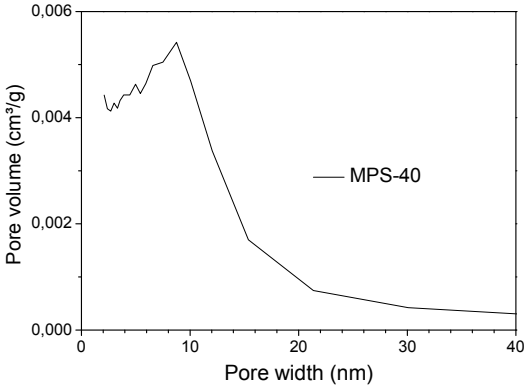

Figure 5.11. Pore size distribution of MPS-40.

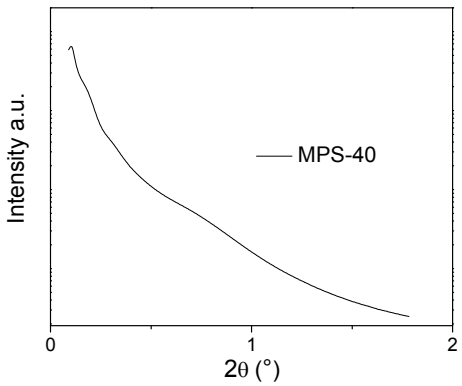

Figure 5.12. SAXS patterns of MPS-40.

Formation mechanism

In this part the focus was on controlling and understanding the synthesis process [26]. The work is still ongoing and at the time of writing this thesis no SEM and TEM images with a quality sufficiently good for publishing have yet been acquired. Therefore the obtained particles will be presented with a schematic illustration based on the electron microscopy images (Scheme 5.1).

According to Nandiyanto et al. a composite material with silica and polystyrene clusters are formed simultaneously inside the oil droplets stabilized with CTAB (Scheme 2.2a) and with lysine added as a combined catalyst and particle size constrainer. To test this hypothesis we varied the emulsion composition by removing or exchanging components in the formulation. Throughout the synthesis series we used a ten times larger amount of surfactant compared to the standard protocol. SEM analysis indicated that this change resulted in less of non-spherical material (Scheme 5.1a). To test the significance of lysine as a particle size constrainer we replaced lysine with ethanolamine as a catalyst. No difference in particle size could be observed. Use of methyl methacrylate as a polymer precursor for poly(methyl methacrylate) instead of using styrene as a precursor for polystyrene also did not affect the appearance of the obtained particles in a noticeable way. The synthesis was then performed without any polymer precursor and surprisingly MPS particles of similar size and shape were formed. Taken together, this is a strong indication that the mechanism proposed by Nandiyanto et al., involving formation of organic-inorganic composite particles from which the porous silica particles were obtained after calcination is not correct. Most likely, the polymerizable monomer, styrene or methyl methacrylate, is just an inert component in the oil droplets of the emulsion. Under the reaction conditions used, the only reactive species in the droplets is TEOS.

Furthermore, the role of the surfactant for the final particle morphology was investigated. First, the cationic single tail surfactant CTAB was replaced with a cationic gemini surfactant (Scheme 2.2b). This resulted in particles twice the size of the particles obtained with the standard protocol (Scheme 5.1b). The gemini surfactant, with its two C_{12} tails and C_4 as a linker, can be assumed to pack in a different way compared to CTAB. If the size of the final particles is affected by the size of the emulsion drops, this could be the reason for the larger particle size. With the gemini surfactant a smaller pore size was also observed, which means that the choice of surfactant affects both the particle morphology and the pore character. A non-ionic surfactant of fatty alcohol ethoxylate type, a branched C_{10} alcohol with 8 moles of ethylene oxide added (Ethylan

1008) (Scheme 2.2c) was also tested as surfactant. This resulted in a similar particle size as for CTAB and a mesoporous structure was confirmed. In many of the particles a large cavity, like a partly collapsed core-shell structure, was observed. Again, the surfactant packing could be the reason for this difference in particle morphology. Obviously, a broader range of surfactants needs to be investigated in order to be able to put forward a hypothesis of how the surfactant influences the size of the particles and the diameter of the pores. Such studies are underway.

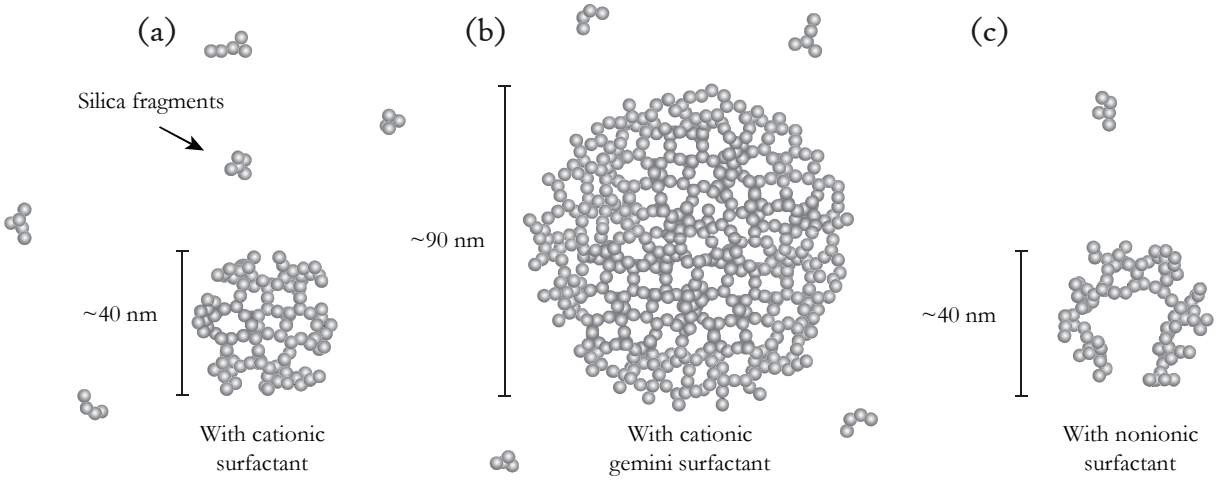

Scheme 5.1. Schematic illustration of HMM particles synthesized with (a) a cationic single tail surfactant (CTAB), (b) a cationic gemini surfactant, and (c) a non-ionic surfactant.

To conclude, we do not believe that there are two polymerization processes occurring simultaneously, as proposed by Nandiyanto et al. As discussed in Section 2.2 the initial silica condensation is a rather fast process, while it can be assumed that the polymerization rate of styrene under the synthesis conditions used is much slower. We have shown that the surfactant plays an important role both for the particle morphology and for the pore structure and seems to act as template during the silica condensation. We are, however, aware of the difference in surfactant concentration between our protocol and the one developed by Nandiyanto et al. Our intention is to repeat the synthesis without polymer precursor and with the lower concentration of surfactant in order to conclusively be able to rule out the formation mechanism proposed by Nandiyanto et al.

We believe that the reason why the emulsion-based synthesis process results in porous and not solid silica particles is that the dispersed phase is not a plain oil phase but a water-in-oil (W/O) microemulsion. It is well-known that surfactants solubilize water into oil forming a W/O microemulsion, also sometimes called a reversed micellar system. This means that the droplets of an O/W emulsion usually contain very small water droplets [129, 130]. Also the continuous water phase of an O/W emulsion is not pure water. The water phase is a micellar solution of the surfactant and oil is usually solubilized into the micelles. Thus, strictly speaking an O/W emulsion is a water-in-oil microemulsion dispersed in an oil-in-water microemulsion, as is illustrated in Scheme 5.2.

We now propose the following alternative formation mechanism. The hydrolysis of TEOS, which is solubilized in the oil droplets, starts at the interface between oil and water and that interface is very large due to the many small water droplets present in the oil. Silica migrates into the interior of the microemulsion droplets where the condensation continues. The water droplets (reversed micelles) start to coalesce and a network is formed, which in the end gives rise to the irregular pore structure obtained when the organic material is removed. The swollen micelles in the water phase may give rise to the non-spherical silica fragments that are also observed in the samples.

Scheme 5.2. Proposed emulsion system prior to addition of silica precursor and with an excess of surfactant. An O/W emulsion is formed stabilized by the surfactant, with the oil droplets constituting a W/O microemulsion. The droplets are surrounded by oil-swollen micelles; thus, the continuous water phase is in reality an O/W microemulsion.

5.2 Immobilization of enzymes in mesoporous silica

This section is divided into three subchapters which represent how the focus evolved during this doctoral project. In Section 5.2.1 the focus is on investigating how the silica support can be optimized in order to attain a support with a high enzyme loading, holding enzymes that are properly retained inside the support giving a high and stable catalytic activity. The results from **Papers I-III** are summarized. Section 5.2.2 presents the methods that were developed in order to better understand the immobilization process (**Papers IV and V**). The last subchapter (Section 5.2.3) summarizes the results from the co-immobilization of two enzymes using a dendronized polymer and mesoporous silica as support (**Paper VI**).

5.2.1 Finding the most optimal support

In **Papers I, II** and **III** immobilization through physical adsorption of *bovine pancreatic* trypsin (BPT), *Mucor miehei* lipase (MML), *Rhizopus oryzae* lipase (ROL) and a crude enzyme preparation (Depol740L), shown to have feruloyl esterase (FAE) activity, was performed. In **Papers I** and **III** the mesoporous silica SBA-15 with varied pore size was evaluated as support.

BPT and MML were compared in **Paper I** and FAE was studied in **Paper III**. In **Paper II** the role of the particle size and morphology of MPS for the immobilization of MML and ROL was investigated. The physical properties of the enzymes are summarized in Table 5.2.

Table 5.2. Isoelectric point (pI), diameter (∅), and molecular weight (M_W) of the enzymes.

Enzyme	pI	∅ (nm)	M_W (kDa)
BPT	10.5	3.8	23
MML	3.8	4.5	32
ROL	7.6	-	32
FAE	6.8	-	62

Enzyme loading

The immobilization was followed over time indirectly by measuring the residual total protein concentration of the supernatant. The time resolution with the indirect methods is low but fulfills the purpose of estimating the final amount of immobilized enzyme and the time frame required to reach the loading equilibrium for each enzyme; i.e., the time at which no more protein is adsorbed.

In **Paper I** SBA-15 with three different pore sizes was evaluated as support for BPT and MML. For BPT it took about 24 hours to reach loading equilibrium when immobilized in MPS-5P (5 nm pore diameter), while equilibrium was reached within one hour in MPS-6P (6 nm) and MPS-9P (9 nm) (Figure 5.13a). These results indicate a somewhat hindered diffusion of BPT (∅ 3.8 nm) into the 5 nm pores. It is important to note that some enzyme also adsorbs on the outer particle surface (see Section 5.2.2). The immobilization of MML (∅ 4.5 nm) was very different from that of BPT, both in rate and in loading (Figure 5.13b). After the initial uptake a very slow immobilization rate was observed which did not level off until after about 48 hours. The loading capacity of MML in SBA-15 clearly increased with increasing pore size but the final loading was found to be significantly lower than for BPT.

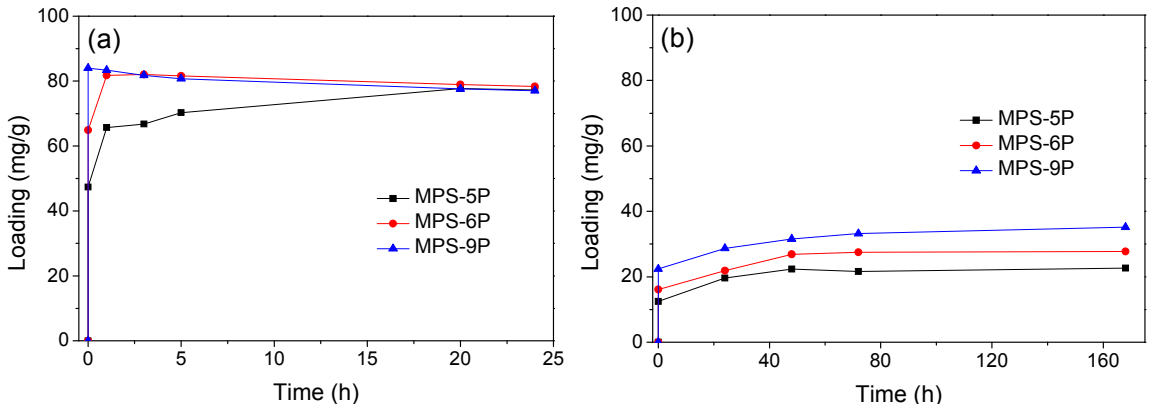

Figure 5.13. Immobilization rate of (a) BPT and (b) MML into SBA-15 with 5 nm, 6 nm and 9 nm pores in Tris-buffer of pH 7.6.

The large difference in loading of BPT and MML in SBA-15 may be related to the molecule size as well as the surface charge (see Table 5.2). The isoelectric point (pI) of BPT is 10.5, and the point of zero charge (pzc) of the porous particles is 2-3 [131], which means that at pH 7.6 there is an overall electrostatic attraction between the positively charged enzyme and the negatively charged support. For MML (pI = 3.8), with a net negative charge at pH 7.6, repulsive forces are likely to dominate. However, positively charged areas on the enzyme surface can exist even though the overall charge is negative. Moreover, other contributing interactions, such as hydrophobic interactions and hydrogen bonding between enzyme and uncharged silanol groups on the pore walls, may also be involved in the binding.

The immobilization of protein in **Paper III** was rapid with the majority being immobilized during the first 10 minutes (see **Paper III**, Figure 2). Since Depol740L contains a mixture of proteins, FAE immobilization was confirmed by comparing FAE activity before and after

immobilization. For MPS-9P 83 % of the proteins from the solution was immobilized whereas almost no FAE activity could be detected in the solution after immobilization (see **Paper III**, Section 3.1). This indicates that the immobilization of FAE was quite selective. For MPS-5P 39 % of the proteins were immobilized and no selectivity towards FAE was detected. It is likely that the pore size is the limiting factor for immobilization in MPS-5P.

In **Paper II** MPS-1000, MPS-300 and MPS-40 were used as support for MML and ROL. As shown in Section 5.1, the materials have varying particle size and morphology but they all have a pore size around 9 nm. The two lipases have the same molecular weight but widely different isoelectric points (Table 5.2). As can be seen in Figure 5.14a, the amount of immobilized MML and ROL for the three materials was very similar. This is counter to what one would anticipate considering that smaller particles mean a larger surface area, i.e., more pores exposed to the surrounding water phase, where the enzyme is present. Thus, it seems that the particle size is not an important parameter for the loading capacity within the particle size range investigated.

The immobilization was also carried out in buffers at varying pH values (pH 5-8) to investigate whether the immobilization of MML and ROL could be further improved. Under these conditions both the silica pore walls and MML carries a negative net charge whereas ROL (pI 7.6) has a positive net charge at pH 5, 6 and 7 and is slightly negatively charged at pH 8. For MML the loading increased with decreasing pH, most likely because the electrostatic repulsion between MML and silica, as well as between MML molecules, was quite weak closest to the pI. The loading of ROL did not vary much with the pH. For ROL the lower the pH within the interval 5-7, the more pronounced is the positive net charge of ROL but the less pronounced is the negative surface charge of silica. In the paper we reasoned that it is therefore not obvious how the Columbic attraction between the enzyme and the silica surface will vary with pH. We also discussed that at pH 8 the net charge of ROL is slightly negative but the enzyme may adopt a conformation such that it exposes positively charged groups toward the silica surface or other interactions may be dominating. More recent results, presented in **Paper V** (see Section 5.2.2), demonstrate that the immobilized amount of ROL increased with a decrease in pH within the pH interval 5–8. Therefore, we have the reason to believe that the lack of variation in ROL loading in **Paper II** is due to high concentrations of salt in the enzyme solution, transferred from the lyophilizate, which can affect the immobilization. To minimize the salt content in **Paper V** the enzyme solutions were washed with buffer, using spinfilters, prior to the immobilization. Using the same procedure in **Paper II** may have resulted in a more varied ROL loading. (This was not a concern for MML since the enzyme solution was prepared from a much more pure lyophilizate.) For BPT (pI 10.5) the loading increased with increasing pH (from pH 6.0 to pH 7.6). However, the difference was not as pronounced as for MML (see the results in **Paper I**, Table 4). As stated above, it is important to recall that the distribution of the enzyme surface charge, and not just the net charge, may influence the interaction between enzyme and silica. Furthermore, negatively charged enzymes, like MML, may diffuse into the pores without adsorbing to the likewise negatively charged walls, whereas positively charged enzymes are likely to adsorb more readily to the pore walls and thus may never reach as far into the channels.

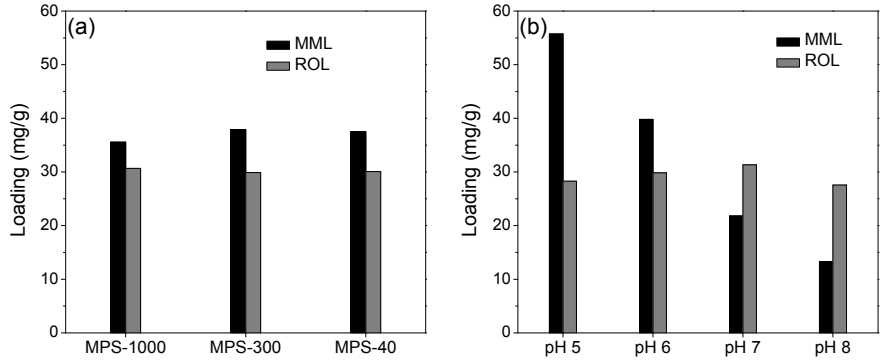

Figure 5.14. Immobilization of MML and ROL into (a) MPS-1000, MPS-300 and MPS-40 in phosphate buffer of pH 6 and (b) MPS-300 in phosphate buffers of pH 5, 6, 7 and 8.

Enzyme leakage

Figure 5.15 shows the leakage of MML and ROL after 24 hours at varying pH (**Paper II**). For MML, where both the enzyme and the pore walls are negatively charged, there is considerable leakage, particularly at the lower pH values (Figure 5.15a). For ROL, where one can assume attractive interactions to be dominating in this pH range, there is virtually no leakage during the first 24 hours (Figure 5.15b). Extending the time further gave no leakage of any of the lipases.

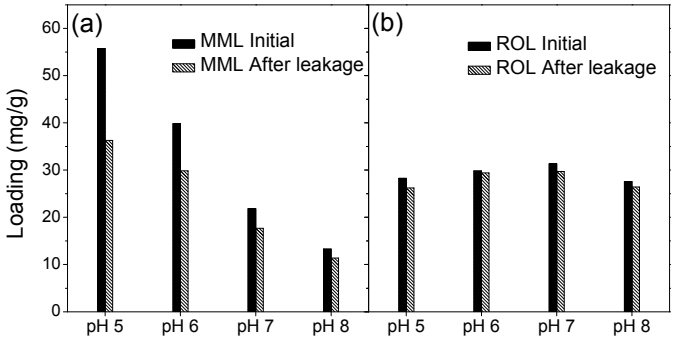

Figure 5.15. Amount of (a) MML and (b) ROL in MPS-300 initially and after 24 h exposure to water.

For BPT, in **Paper I**, around 30 % of the amount of initially loaded enzyme leaked out from the MPS-5P particles and the leakage was somewhat higher from both MPS-6P and MPS-9P. For MML 32 % leaked from MPS-5P, 23 % from MPS-6P and 16 % from MPS-9P. For both enzymes the leakage mainly took place within the first 30 minutes. The relatively large leakage of BPT may be explained by the large initial loading compared to MML (Figure 5.13). A large loading may result in a larger amount of loosely bound enzymes which are more prone to leach out from the pores. No leakage of FAE was detected (see Section 5.3, **Paper III**).

Catalytic activity of immobilized enzymes

In **Paper I** hydrolysis of N-α-benzoyl-DL-arginine-4-nitroanilide (BAPNA) into 4-nitroaniline was used as model reaction to test the activity of BPT (Scheme 4.8, Section 4.5.2). To get comparable results the immobilization time was chosen to be five hours, which was close to

equilibrium for all pore sizes (see Figure 5.13a). Figure 5.16 shows the decline in product yield over time, which was attributed to deactivation of BPT. However, the initial rapid decrease is also due to leakage during the first 30 minutes. The activity was significantly affected by the pore size. MPS-6P gave both the highest yield of product and the best retention of the activity. However, the specific activity for MPS-6P was very similar to the specific activity for MPS-5P (Figure 5.17) which means that BPT is initially equally active in the two materials. A tentative explanation to the lower activity in MPS-9P is that the pores are too large to provide the enzyme with a protected environment that retards the autocatalytic degradation during the immobilization. This assumption is supported by the lower specific activity. The low product yield of immobilized BPT compared to BPT free in solution (Figure 5.16b) was most probably mostly due to a deactivation during the immobilization. However, limitations in substrate access inside the pores and unfavorable enzyme conformation may also be contributing factors.

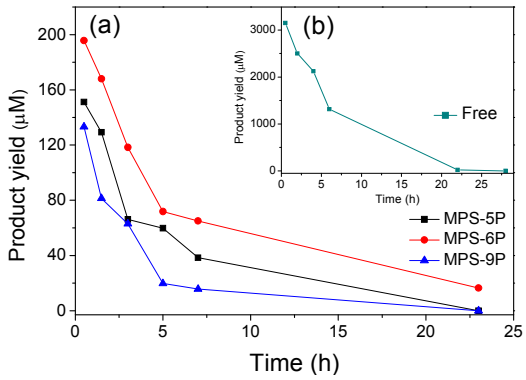

Figure 5.16. Concentration of produced 4-nitro-aniline by a) BPT immobilized in MPS-5P, MPS-6P and MPS-9P and b) BPT free in solution. (Amount of free enzyme corresponds to the amount incorporated into MPS-9P at pH 7.6.)

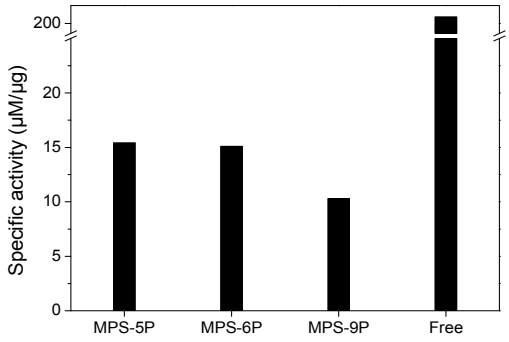

Figure 5.17. Comparison of the initial specific activity (amount of product/mass of enzyme) for BPT in SBA-15 and free in solution. The graph is based on data from **Paper I**.

Hydrolysis of 4-nitrophenyl acetate (pNPA) into 4-nitrophenol (pNP) was used as model reaction to test the activity of the immobilized lipase (Scheme 4.7, Section 4.5.2). The effect of the pore size was even more apparent than for BTP (Figure 5.18). The product yield, as well as the specific activity (Figure 5.19), was by far the largest for MML in the largest pores, MPS-9P. As discussed in Section 3.5.1, most lipases have a lid that reveals the active site upon interfacial activation. Such a conformational change is likely to require considerable space. When comparing native MML free in solution with immobilized MML it was observed that the specific activity was more than twice as large for MML in MPS-9P. This is likely due to interfacial activation of MML bound to silica. Since the prepared support materials are calcined, many of the silanol groups on the silica surface are converted into hydrophobic siloxane bridges (see Section 2.2). Hence, the silica surface will be partly hydrophobic, which may promote lipase activation.

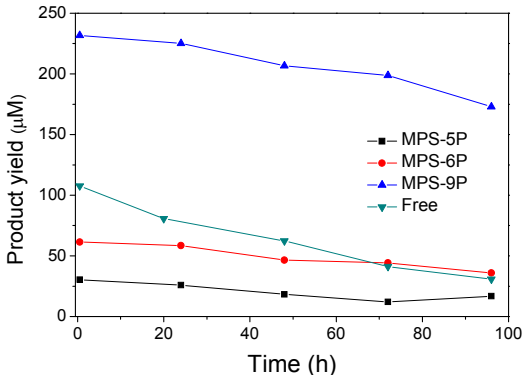

Figure 5.18. Concentration of produced 4-nitrophenol by lipase incorporated in MPS-5P, MPS-6P and MPS 9P and by lipase free in solution. (The amount of free enzyme corresponds to the amount incorporated into MPS-9P at pH 7.6.)

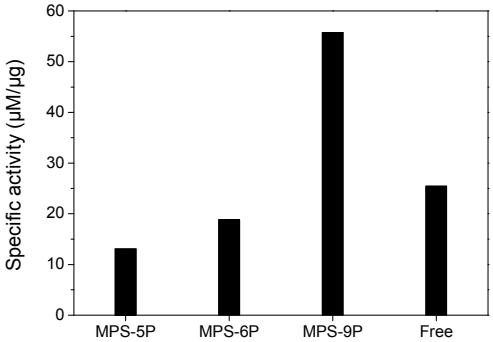

Figure 5.19. Comparison of the initial specific activity (amount of product/mass of enzyme) for MML in SBA-15 and free in solution. The graph is based on data from **Paper I**.

In **Paper II** the catalytic activity of MML and ROL in the three supports with different particle morphology but with similar pore diameter was compared (Figure 5.6 and Figure 5.9). As shown in Figure 5.14, the enzyme loading was approximately the same in the three materials. However, both MML and ROL were considerably more active in MPS-300 compared to the two other materials (Figure 5.20). A probable explanation to the lower lipase activity in the larger MPS-1000 particles is that these particles have longer pores, which means that a smaller relative amount of enzymes are accessible to the substrate. Enzymes far down the longer pores may not be utilized. Along this way of reasoning the smallest particles, MPS-40, would provide the highest lipase activity. This was not the case, however. We believe that the relatively poor performance of MPS-40 in this respect is due to the fact that the pores have a much broader pore size distribution (Figure 5.11) than the two other materials (Figure 5.8). Even if the average pore size of MPS-40 is the same as for MPS-300 and MPS-1000, only a small fraction of the pores in MPS-40 are actually around the optimum size of 9 nm.

When investigating the pH dependence on loading and activity in MPS-300 it was found that both MML and ROL were most active when immobilized at pH 8 (MML-8 and ROL-8) and that the activity decreased with decreasing pH during the immobilization (Figure 5.21). (All activity tests were performed in a phosphate buffer of pH 7.) The specific activity of MML-8 was more than four times as high as of MML free in solution. The difference was much less pronounced for ROL. Surface tension measurements of the two lipases showed that MML is more surface active (47 mN/m) than ROL (60 mN/m). This indicates that MML will interact more strongly with hydrophobic patches on the silica pore walls, which could explain the more pronounced activation.

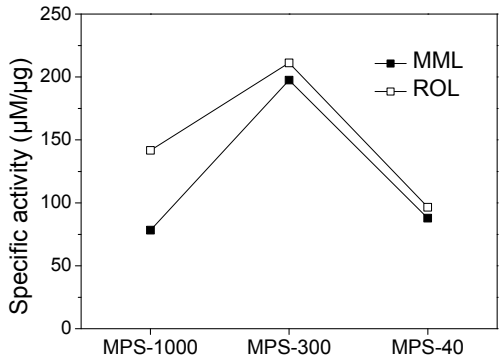

Figure 5.20. Comparison of the specific activity for MML and ROL (amount of product/mass of enzyme) entrapped in MPS-1000, MPS-300 and MPS-40 at pH 6.

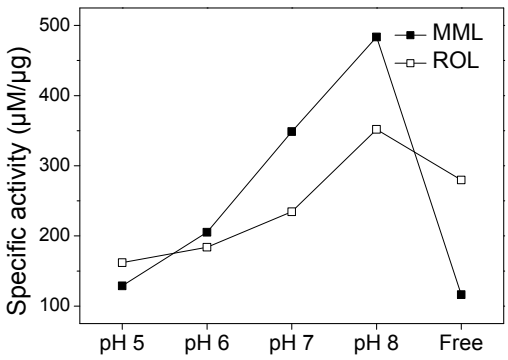

Figure 5.21. Comparison of the specific activity for MML and ROL in MPS-300 (amount of product/mass of enzyme) at pH 5, 6, 7 and 8.

In **Paper III** the transesterification reaction of methyl ferulate (MFA) with 1-butanol into butyl ferulate (BFA) was used as a model reaction for the immobilized enzyme (see Figure 1 in **Paper III**). Figure 5.22 shows that FAE immobilized into MPS-9P resulted in significantly higher transesterification yield compared to MPS-5P. FAE immobilized into MPS-9P was also 3.5 times more active in terms of specific transesterification activity (see Table 2 in **Paper III**). The larger space for the enzyme in MPS-9P may explain the higher activity compared to when the enzyme was immobilized in MPS-5P. A better substrate access in the 9 nm pores may also be a contributing factor. Comparing the initial activity of MPS-9P with that of free enzyme, 40 % of the specific BFA activity was lost. However, a significantly higher overall yield was obtained when the enzyme was immobilized in the MPS-9P material and this enzyme preparation also retained the activity better throughout the reaction.

The hydrolysis of MFA into ferulic acid (FA) was also quantified and the product selectivity, defined by the BFA/FA molar ratio, was compared. Under normal conditions FAE hydrolyses the ester bond to yield FA and an alcohol. However, in this study, it was observed that the immobilized enzyme consistently generated less FA (higher BFA/FA ratio) than was the case for the free enzyme (Figure 5.23). The BFA/FA ratios in the reactions with the enzyme immobilized in MPS-5P and MPS-9P were very similar, thus independent of pore size. It is therefore likely that the higher BFA/FA ratio for the immobilized enzyme compared to the free enzyme is related to the enzyme being adsorbed to the silica surface rather than a confining effect of the pore. This hypothesis was confirmed by immobilizing Depol740L onto non-porous silica particles, which gave a similar BFA yield as with MPS-9P. It remains to be determined whether this phenomenon is due to a conformational change of the enzyme or a favorable arrangement of water and butanol molecules on the silica surface. Important to note is that also other proteins and enzymes in the crude Depol740L preparation may influence the FAE activity.

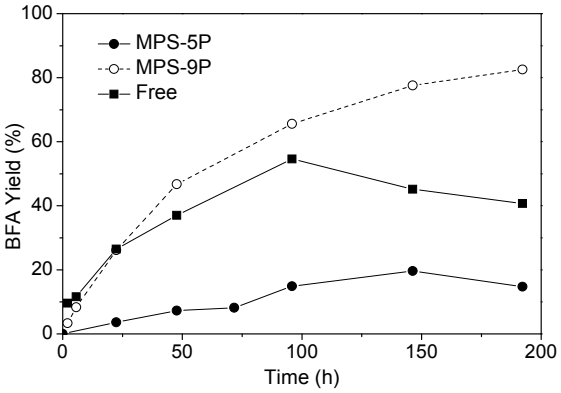

Figure 5.22. Transesterification of MFA (20 mM) into BFA over time, in a 92.5/7.5% mixture of 1-butanol and water, for MPS-5P, MPS 9P, and free enzyme (amount of free enzyme corresponds to the amount immobilized into MPS-5P).

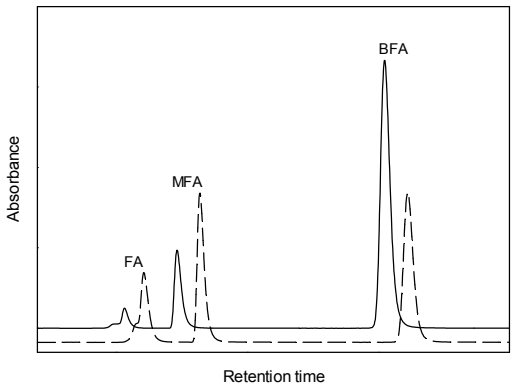

Figure 5.23. Typical HPLC chromatogram illustrating the higher BFA/FA molar ratio of immobilized enzyme (solid line) compared to free enzyme (dashed line).

Immobilized FAE was relatively stable throughout 6 runs, retaining 70% and 96% of the activity compared to the first run for MPS-5P and MPS-9P, respectively. The better reusability of MPS-9P can partly be explained by the large BFA yield (~85%), where a decrease in activity will not be as easily noticeable as for MPS-5P with a significantly lower yield (15–20%). Another explanation can be that the enzymes in MPS-9P are conformationally stabilized inside the pores by protein–silica surface interactions and enzyme confinement, as described previously for other enzymes [132, 133]. No activity could be detected in the supernatant, indicating that the slow decrease in activity of the immobilized enzyme is mainly due to inactivation of the enzyme and not leakage. This suggests that the interaction to the silica surface is strong under the conditions used in the study.

5.2.2 Towards understanding the immobilization process

As shown in Section 5.2.1, the activity of an immobilized enzyme is often different from that of the free enzyme. The confinement of an enzyme inside a pore can affect both the specific activity and the substrate selectivity. Understanding how the microenvironment and the material properties of the mesoporous particles affect the enzyme is an important issue in order to design immobilization conditions that lead to optimal enzyme performance. In this section the results from real-time monitoring of the immobilization process, using quartz crystal microbalance with dissipation monitoring (QCM-D), are presented (**Paper V**). A method to study the microenvironment inside the pores has also been developed (**Paper IV**).

Following the immobilization in real time

The most common method to monitor protein immobilization is to retrieve samples from the external solution at different times during the immobilization process and measure the amount of enzyme remaining in the surrounding solution (method used in **Papers I-III**). This indirect

approach usually requires manual sampling and results in a low time resolution, typically tens of minutes. Since enzyme immobilization may occur within minutes the indirect monitoring may miss a large portion of the process and will not allow for studies of the complete adsorption kinetics.

In **Paper V** QCM-D was used as a direct method to study the immobilization of a lipase (ROL) and a feruloyl esterase (FoFAEC) into mesoporous particles attached to a solid surface (Figure 5.24). The QCM-D technique measures the mass added to the particles with a time resolution in the sub-second range (see Section 4.7). Silica-coated sensors were first grafted with amino groups followed by adsorption of HMM particles, after which the enzyme immobilization into the mesoporous particles could be studied in real time.

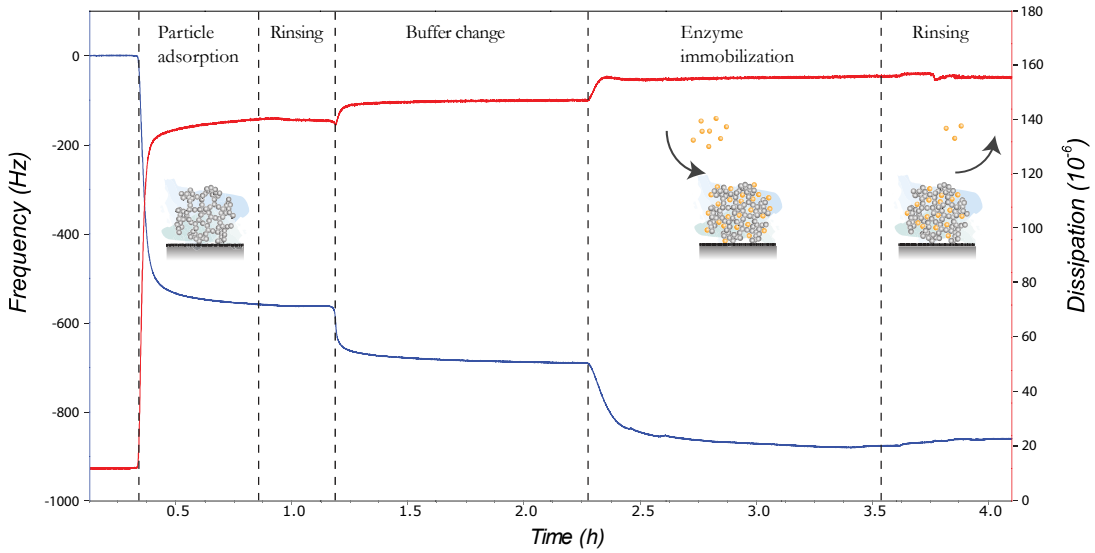

Figure 5.24. Schematic illustration and typical frequency and dissipation curves for immobilization of an enzyme in mesoporous HMM particles. Initially the HMM particles are attached to the APTMS modified sensor followed by a rinsing step and buffer change. The enzyme is then loaded using the same buffer and finally the sensor is washed once again to follow the desorption (leakage) of the enzyme out of the porous particles.

In this case the enzyme immobilization had reached a maximum (the frequency had stopped decreasing) within the first 30 min and the kinetics would not have been possible to study without the enhanced time resolution (Figure 5.25). The amount of immobilized enzyme was much larger for the mesoporous particles than for the non-porous particles. This is a clear indication that the majority of the enzymes are located inside the pores and not on the outer surface of the particles. The flat silica surface, which was included as a reference, resulted in a low amount of immobilized enzyme, as expected.

As discussed in Section 2.2, HMM particles lose a large part of the surface silanol groups during calcination, hence becoming more hydrophobic. In order to evaluate the importance of the surface characteristics of the support experiments with rehydroxylated HMM particles were also performed. A smaller amount of FoFAEC became immobilized into the rehydroxylated particles compared to the non-rehydroxylated particles (Figure 5.25a). For ROL the immobilization pattern was similar for the two supports (Figure 5.25b). The rehydroxylated particles can be regarded as entirely polar with a strong negative surface charge and the non-rehydroxylated

particles can be seen as more of a hybrid material consisting of both negatively charged and more hydrophobic surface patches. The results seem to indicate that for FoFAEC, but not for ROL, hydrophobic interactions play a role in the immobilization to the non-rehydroxylated particles.

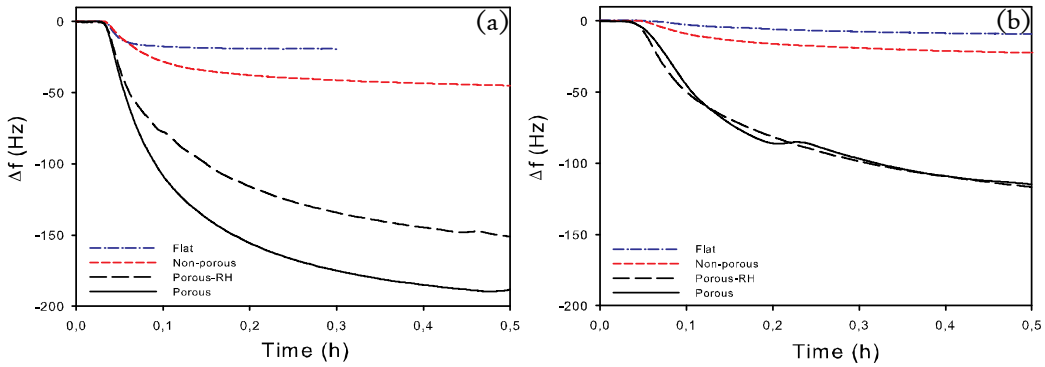

Figure 5.25. QCM-D results, presented as frequency shifts (Δf) as a function of time, during the immobilization of (a) FoFAEC and (b) ROL to different silica particles and to a flat silica surface. Porous-RH stands for porous particles that have been rehydroxylated by boiling in water.

To visualize the viscoelastic effect of the immobilized enzymes the frequency shift was plotted against the corresponding dissipation (Figure 5.26). The curves in these f/D plots can be divided into different regimes, representing variations in the enzyme behavior during the adsorption. For the adsorption of FoFAEC to the porous particles two regimes were observed where the first regime shows a large shift both in frequency and dissipation (Figure 5.26a). In the second regime the dissipation clearly levels off whereas the frequency keeps increasing. We speculate that in the first regime FoFAEC mainly adsorbs to the rough outer particle surface and pore openings contributing to an increase in dissipation. In the second regime the enzyme still adsorbs according to the continuous shift in frequency but here the diffusion into the porous structure is dominating, which leads to a constant dissipation. For non-porous silica particles and a flat silica surface only the first regime was observed, representing adsorption onto a non-porous surface. For ROL a similar behavior was observed (Figure 5.26b). However, the second regime for the rehydroxylated porous particles was not as apparent, which could be explained by the lower amount of adsorbed ROL. The increase in dissipation was not as large as for FoFAEC, indicating a more rigidly adsorbed protein layer.

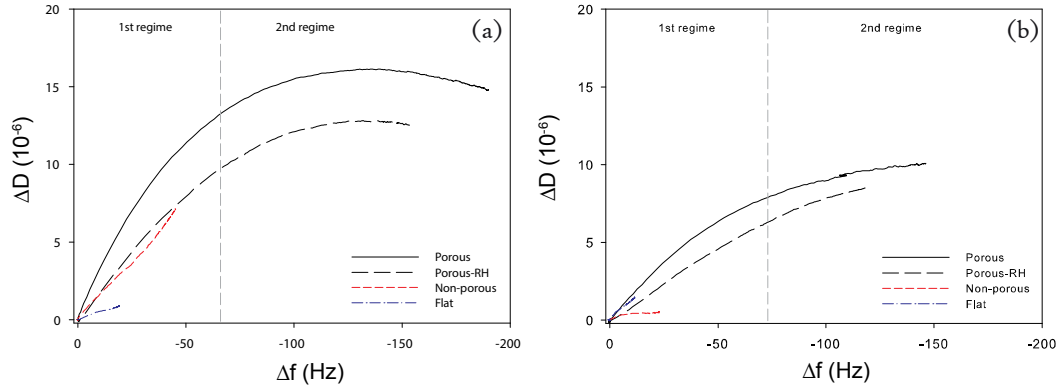

Figure 5.26. QCM-D results, presented as shift in frequency (Δf) plotted against the change in dissipation (ΔD) during immobilization of (a) FoFAEC and (b) ROL to different silica particles and to a flat silica surface.

QCM-D was also used to map the pH dependence of the immobilization process. The immobilized amount of ROL increased with a decrease in pH within the pH interval 5–8 (Figure 5.27b). This is an expected trend because the electrostatic attraction between ROL and silica should increase as the pH decreases. The trend for FoFAEC (pI 6.8) was completely opposite that for ROL. Almost double the amount of FoFAEC was immobilized at pH 8 compared to pH 5 (Figure 5.27a). For the flat silica surface however, the trend was similar to that of ROL with the amount immobilized increasing as the pH decreased (Fig. S5, **Paper V**). We speculate that the larger FoFAEC, which adsorbs readily at lower pH (5–6), as seen for the flat surface, interacts so strongly with the pore walls, by a combination of electrostatic attraction and hydrophobic interaction that the pore entrance becomes blocked, thereby preventing new enzymes from entering. This hypothesis also fits well with the large increase in dissipation for FoFAEC during the course of the immobilization at high pH, which indicates that the enzyme is more loosely bound. For FAEC all four curves can be divided into one regime representing adsorption to the outer surface and pore openings and another regime representing further adsorption inside the pores. This behavior was also observed for ROL at pH 5 and 6. However, at pH 7 and 8 only the first regime is present. This may be explained by the low level of adsorption with the enzyme mainly adsorbing to the outer surface of the particles. Both FoFAEC and ROL were found to be better retained when immobilized in the pores compared to when adsorbed to either the flat silica surface or the non-porous particles. Interestingly, the desorption from the porous particles only showed a small pH dependence. It is remarkable that the enzymes are so well retained even at a pH where there is almost no net charge of the enzyme. It seems that once the enzyme is inside the pore and adsorbed to the pore wall, it is virtually stuck there and not much affected by washing, regardless of the pH of the washing solution.

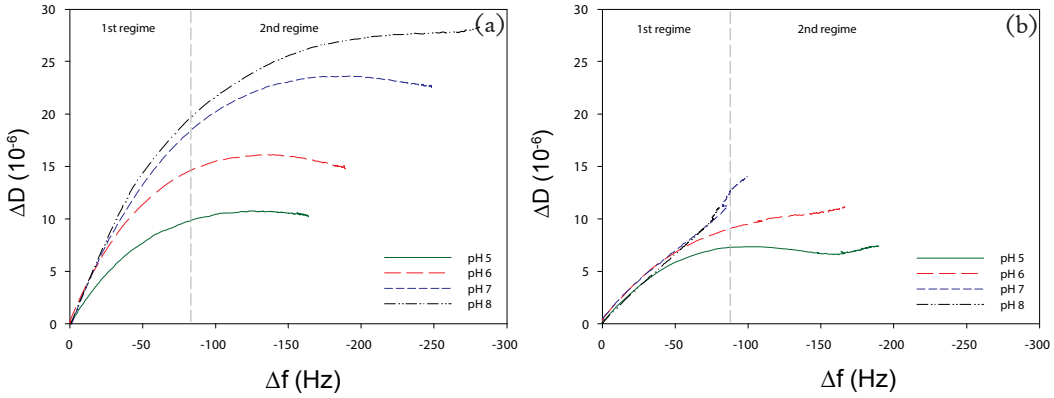

Figure 5.27. QCM-D results, presented as shift in frequency (Δf) plotted against the corresponding shift in dissipation (ΔD) during immobilization of (a) FoFAEC and (b) ROL to the porous particles at varying pH.

Microenvironment

The mechanisms behind the change in enzyme stability, specific activity and product selectivity are likely due to a combination of MPS-protein interactions and an altered microenvironment inside the pores compared to the external bulk solution. Earlier studies have assessed the pH inside MPS by binding pH-sensing molecules directly onto the pore surface [72]. However, using

surface-attached pH probes to monitor acidity inside MPS pores may be misleading regarding immobilized proteins. The mobile proteins are likely to experience a different environment than the attached probe because they are free to access the whole pore volume and may be repelled by the pore wall due to size exclusion and electrostatic repulsion. In **Paper IV**, the proteins themselves have been used as pH-sensors by labeling them with the fluorescent pH probe SNARF1. The method is a spectroscopic assay that measures pH at the actual position of the immobilized proteins. Two proteins were used in this study; bovine serum albumin (BSA) and FoFAEC.

Figure 5.28 shows the emission spectra of the MPS-immobilized SNARF1/protein when the particles were suspended in aqueous solution (solid curves) or in a butanol/water mixture (dashed curves), two common solvents for immobilized proteins. The immobilized proteins both exhibited a pH dependence similar to free SNARF1/protein (**Paper IV**, Figure 1). This demonstrates that protein-bound SNARF1 can be used to probe the pH inside MPS and that it seems to be independent of protein type. In Table 5.3 it is seen that the effective pH inside the pores is closer to neutral than the pH in the surrounding bulk solution, which suggests that the pores possess some kind of buffering capacity. This phenomenon is possibly due to a buffering effect caused by the surface silanol groups.

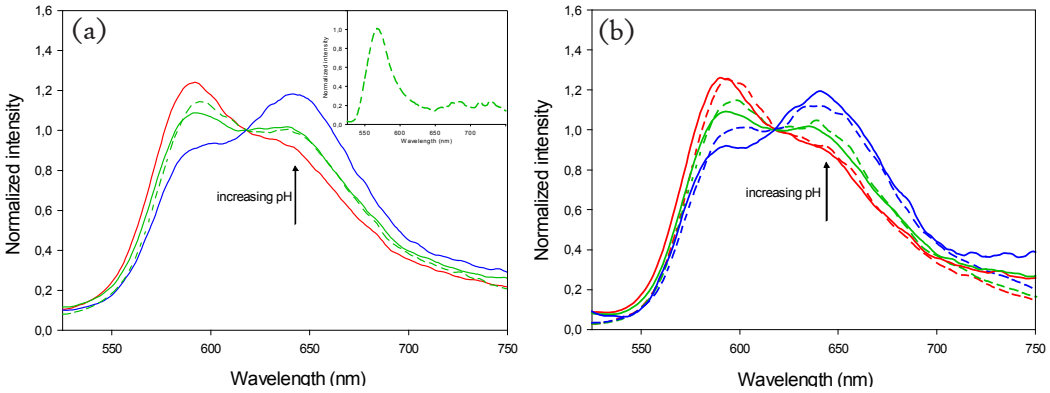

Figure 5.28. Emission spectra of (a) SNARF1-modified BSA and (b) SNARF1-modified FoFAEC immobilized in MPS particles which are suspended either in aqueous buffer solutions (solid lines) or in a 92.5/7.5% mixture of 1-butanol and water (dashed lines). The pH of the bulk solution (or in the water fraction of the solvent mixture) is 6 (red), 7 (green) or 8 (blue). The spectra have been corrected for leaked SNARF1/protein. Inset in (a): Emission spectrum of the supernatant after the MPS particles had been removed from the 1-butanol/aqueous buffer mixture by centrifugation. Excitation at 488 nm, emission spectra were normalized at 618 nm.

The emission spectra of SNARF1/protein immobilized in MPS particles that were suspended in a butanol/water mixture and of SNARF1/protein free in a butanol/water mixture are very different from each other (Figure 5.28a). This demonstrates that the protein experience a different environment inside the pores compared to the butanol/water bulk solution. The emission spectrum of the immobilized protein in the butanol/water mixture is similar to that of the immobilized protein surrounded by only water, indicating that the immobilized protein molecules are in an essentially aqueous environment also in particles suspended in a dominantly organic solvent. However, an aqueous environment inside the pores could not be confirmed with

Karl-Fischer titration on the supernatant. Instead the environment in the pores seemed to have a similar composition as the surrounding bulk. The butanol/water mixture confined in narrow pores may have different physical properties than the same solvent mixture in bulk solution.

Table 5.3. pH monitored by SNARF1/BSA and SNARF1/FoFAEC inside MPS suspended in various solutions.

Bulk composition and pH	pH by SNARF1/BSA[b]	pH by SNARF1/FoFAEC
Water		
8	7.7	7.7
7	7.1	7.0
6	6.5	6.4
Butanol/Water[a]		
8	na	7.5
7	6.5	7.0
6	na	6.4

[a] 92.5% 1-butanol; 7.5 % water; pH refers to the aqueous component before mixing.
[b] Based on the intensity ratio R=I(640)/(590) and interpolation of the calibration data in Figure 1b in **Paper IV**.

5.2.3 Co-immobilization

By creating a cascade reaction through co-immobilization of several types of enzymes it is possible to avoid undesired byproducts and obtain more well-defined end products compared to conventional organic synthesis processes. Immobilized multi-enzyme systems can also be utilized in biosensors for the quantification of molecules of biological interest, like D-glucose. In **Paper VI** a method for co-immobilization of glucose oxidase (GOD) and horseradish peroxidase (HRP) is described by combining immobilization of GOD in mesoporous HMM particles and HRP conjugated with a cationic dendronized polymer (*de*-PG2) (Scheme 4.14, Section 4.7). The layer-by-layer methodology was used and monitored by QCM-D.

In the same way as in Section 5.2.2 the immobilization of enzyme in HMM was first evaluated. The immobilized amount of GOD was more than three times larger for the mesoporous particles than for the non-porous particles (Figure 5.29). Moreover, a lower enzyme desorption was observed for the porous particles (~5 %) compared to the non-porous particles (~20 %). This is a clear indication that the majority of the enzymes immobilized to the porous particles are located in the pore cavities and not just on the external surface. The immobilized amount could be further increased and the desorption decreased by changing the pH of the buffer from 6 to 5.

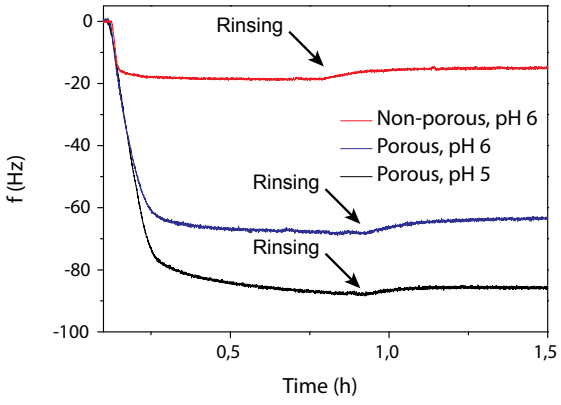

Figure 5.29. QCM-D results, presented as frequency shift (Δf) as a function of time, during the immobilization of GOD into mesoporous silica particles at pH 5 and pH 6 and on non-porous silica particles. The immobilization is followed by a rinsing step.

For the co-immobilization the polycationic dendronized polymer, *de*-PG2, was used as a bottom layer (Figure 5.30a) instead of APTMS (see Section 5.2.2). With the polymer as bottom layer we were able to adsorb a larger amount of HMM particles (Figure S2, **Paper VI** and Figure 5.30b), possibly because the polymer creates a rougher surface with a larger effective surface area. Another possibility is that compared to APTMS the polymer is more efficiently attached to the silica sensor and does not leave any bare spots where the particles are unable to bind. The relative increase in dissipation was lower in this system which could be due to a tighter attachment of the particles to the *de*-PG2-covered silica surface compared to the APTMS-covered surface. The immobilization of GOD was slightly larger than when APTMS was used as the bottom layer but not as large as expected (Figure 5.30c). It is conceivable that the HMM particles are somewhat buried in the polymer layer, which could hinder access to the whole particle. For a successful adsorption of *de*-PG2-HRP to the GOD-loaded HMM particles the pH had to be increased from 5 to 7 (Figure 5.30d). It is likely that the positive effect of the increase in pH is due to an increase in the negative charge of the GOD-loaded particle surface. At pH 5 the overall negative charge of GOD is quite low as its pI is 4.3. The driving force for adsorption of the positively charged *de*-PG2-HRP is likely to increase with increasing negative charge of the substrate surface.

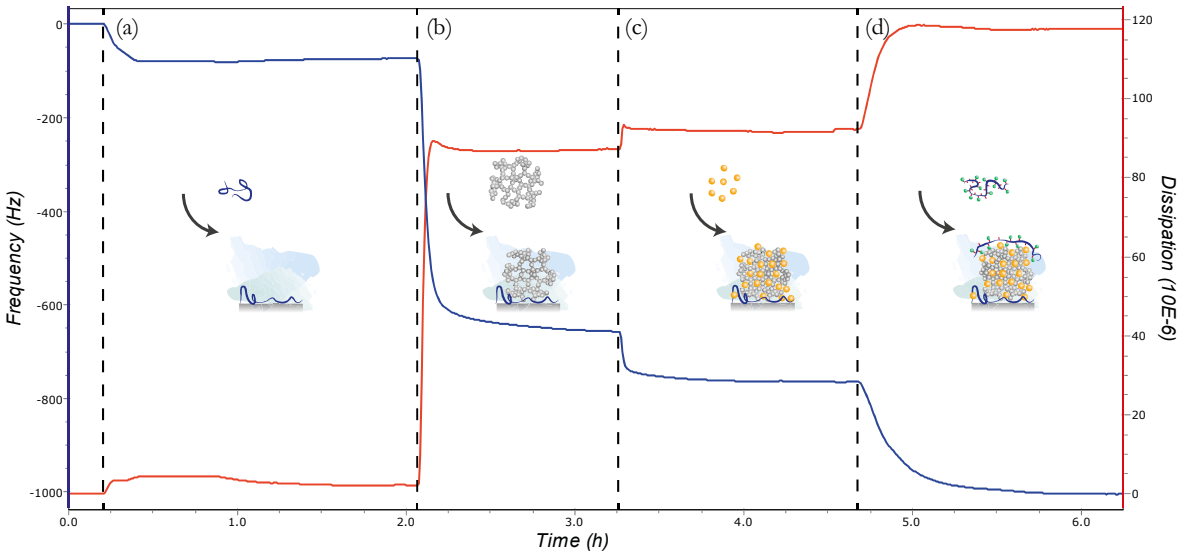

Figure 5.30. Schematic illustration and typical frequency and dissipation curves for the co-immobilization of GOD and HRP through immobilization in mesoporous HMM particles and dendronized polymer (de-PG2) mediated immobilization. Step (a) represents the adsorption of the polycationic *de*-PG2 to a silica-coated sensor, (b) the attachment of silica particles onto the polymer, (c) the GOD immobilization, and (d) the adsorption of HRP covalently linked to the dendronized polymer (*de*-PG2-HRP).

The activity of the enzymes was evaluated by using the same layer by layer methodology as for the QCM-D measurements, but on a glass slide instead of a silica coated sensor. The resulting apparent enzyme concentration corresponds to the amount of substrate-accessible, active enzyme (see the model reaction in Scheme 4.10, Section 4.5.2). For GOD without a covering layer of *de*-PG2-HRP the exhibited activity corresponded to 1 pmol/cm^2 (Figure 5.31a). Within 14 days, the GOD activity decreased to 40 % of the initial value. With a covering layer of *de*-PG2-HRP the GOD activity was reduced to 0.4 pmol/cm^2 but the stability was considerably improved,

retaining 70 % of the activity after more than 2 weeks (Figure 5.31b). Slower diffusion of the substrate to the enzyme and GOD deactivation due to unfavorable interactions with the covering layer are possible explanations for the reduced activity. The HRP activity of the covering *de*-PG2-HRP layer corresponded to 8 pmol/cm^2. As a result of the high HRP loading, the kinetics of the cascade reaction involving both GOD and HRP was dominated by the GOD activity and addition of HRP in the assay solution did not change the rate of product formation.

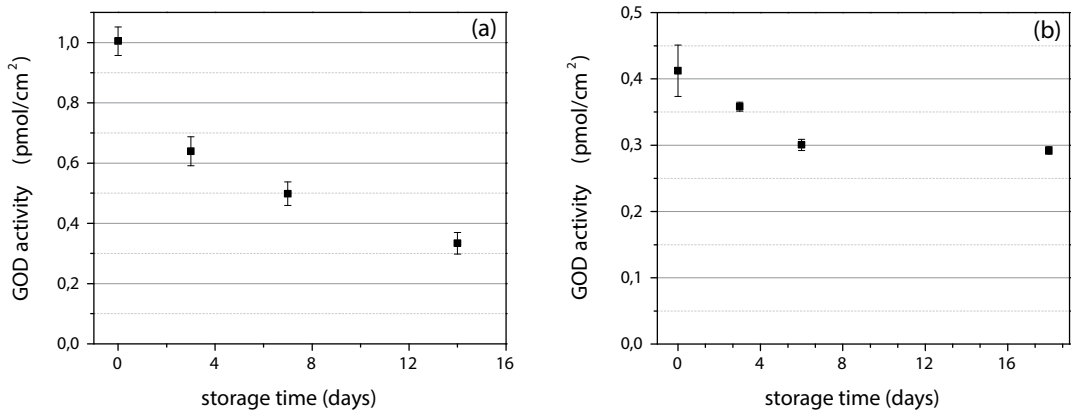

Figure 5.31. Apparent activity and stability of GOD immobilized in HMM particles attached on *de*-PG2-coated glass slides (a), and with an additional layer of *de*-PG2-HRP (b).

To avoid non-specific binding of GOD to the underlying *de*-PG2-HRP layer, HMM particles were preloaded with GOD and the loaded particles were used for build-up of the HMM/GOD layer in a single step. This procedure resulted in a GOD activity corresponding to 0.5 pmol/cm^2 for a surface presenting the GOD/HMM as the top layer (Figure 5.32a), and 0.25 pmol/cm^2 for the *de*-PG2-HRP covered layer (Figure 5.32b). Particles preloaded with GOD seem to be a promising approach to minimize non-specific adsorption of GOD, thereby making a more well-defined cascade reaction possible. This approach will be investigated further.

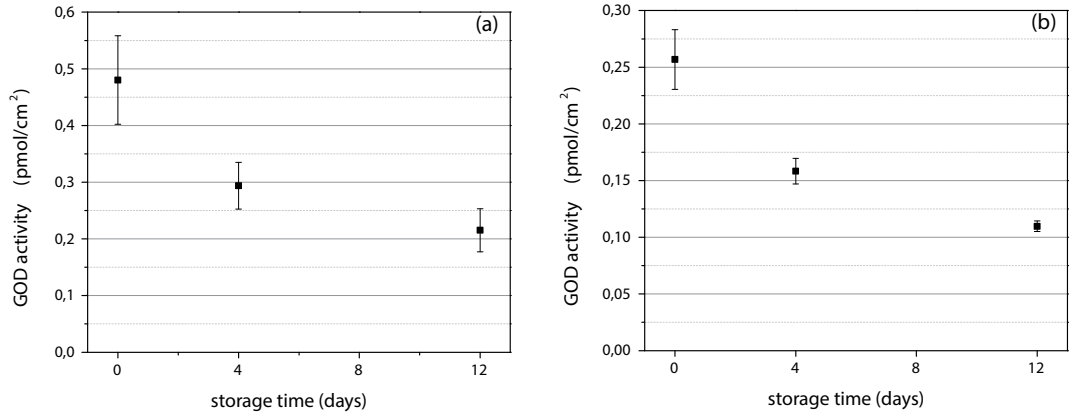

Figure 5.32. Apparent activity and stability of GOD preloaded in HMM particles attached on *de*-PG2-coated glass slides (a), and with an additional layer of *de*-PG2-HRP (b). The latter was measured without additional HRP in the assay mixture, representing the surface localized enzymatic cascade reaction.

With this study we have shown that it is possible to create a functioning cascade reaction by combining the two approaches mentioned above. The next step will be to investigate whether it

is possible to improve the system further. One disadvantage with this approach seems to be that the rather large GOD molecule (153 kDa) [134] is slightly too large for the 9 nm pores in the HMM particles. Turning the system around, i.e. immobilizing the smaller HRP (40 kDa) [135] in the particles and conjugating GOD to the polymer is an option that is now in the process of being evaluated. Preliminary results show that a larger amount of HRP can be loaded in HMM at pH 5 compared to GOD (Figure 5.33). Moreover, the two distinct regimes observed in Figure 5.33b indicate that HRP in the second regime diffuses further into the pores (see explanation in Section 5.2.2). The division into two regimes is not as apparent for GOD (Figure 5.33a).

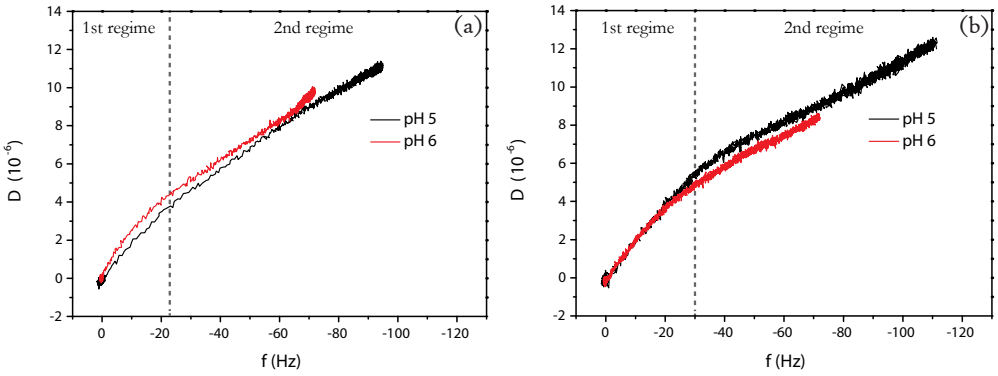

Figure 5.33. QCM-D results, presented as shift in frequency (Δf) plotted against the corresponding dissipation (ΔD) during immobilization of (a) GOD and (b) HRP to the porous particles at varying pH.

Chapter 6

CONCLUDING REMARKS

This thesis was focused on customizing mesoporous silica particles, in terms of surface properties, particle and pore size, as support for immobilized enzymes. The goal was to obtain an optimal biocatalytic performance and long-term operational stability of the enzyme. A more profound knowledge of the immobilization process is a crucial factor for a strategic improvement of biocatalysts. Therefore, developing techniques to obtain useful information about the correlation between enzyme performance and support characteristics was an important aspect of the project.

The findings of this work show that optimal performance of immobilized enzymes, regarding loading, catalytic activity and stability is dependent on both the properties of the mesoporous silica and the enzyme characteristics. Not only the size and the surface properties of the enzyme but also the characteristics of the active site are decisive. The optimal conditions depend on which type of improved performance one is striving for. Is the goal enhanced stability, increased enzymatic activity, altered enzymatic activity or a combination of these? Consequently, the ideal conditions are specific for each type of enzyme and purpose and it is significant to keep in mind that designing an ideal enzyme-support composite is complex and opens for compromises.

By labeling proteins with spectroscopic probes it is possible to characterize the environment inside mesoporous silica particles without perturbing the properties of the material. We have demonstrated that QCM-D is a simple and robust measuring technique for real time study of enzyme immobilization into mesoporous silica particles. The technique is a useful complement to the conventional indirect approach of monitoring entrapment of enzymes that only measures the depletion of the concentration in the surrounding bulk phase. However, there is still room for continued development of physical chemical techniques in order to further improve our understanding of how enzymes function inside silica nanochannels.

Glucose oxidase (GOD) and horseradish peroxidase (HRP) was successfully co-immobilized, which was done by a combination of immobilization of GOD in mesoporous silica particles followed by adsorption of HRP covalently linked to a polycationic dendronized polymer. A cascade reaction was confirmed with enzymatic activity analysis. However, there is potential for improvement of the system. By turning the system around, i.e. immobilizing the smaller HRP in the particles and conjugating GOD to the polymer, a more efficient cascade reaction may be achieved which is in the process of being evaluated.

Furthermore, we consider it important to continue the work on understanding the HMM formation mechanism. By developing a more controlled synthesis of HMM it may be possible to design very small mesoporous silica particles where parameters like pore size and particle diameter can be adapted to specific enzyme characteristics.

ACKNOWLEDGEMENT

Funding from the Swedish research council is acknowledged as a part of the Linnaeus Centre for Bio-inspired Supramolecular Function and Design – SUPRA.

I would also like to express my gratitude to the following people:

First of all, my supervisor, Krister Holmberg, for giving me the opportunity to conduct research at Applied Surface Chemistry and for all your invaluable support and guidance.

My co-supervisor, Lisbeth Olsson, and the other members of the SUPRA enzyme cluster: Christian Thörn, Nils Carlsson and Björn Åkerman for an excellent and productive collaboration and inspirational meetings.

Andreas Küchler and Peter Walde at ETH for a nice joint project and for taking such good care of me in Zürich.

My co-author Emma Björk at Linköping University for contributing to the work and for the great company in Japan.

My project worker (now a fresh PhD student) Simon Isaksson and my former diploma worker Albert Barrabino are acknowledged for contributing to the project.

The people at TYK for creating the nice atmosphere and for being good at making time for fikapauser. Ann Jakobsson for organizing and caring and Kurt Löfgren for all help. Special thanks to all the good friends I have made throughout these years, Alex, Ali, Björn, Emma, Johan, Jonatan, Maria, Markus, Ralph and my former roommate Åsa. I will truly miss having you around almost every day. Also Adriana, even though you left us for physics. And of course, the innebandy crew for the countless laughs and bruises.

Finally, I would like to thank all my wonderful friends and my beloved family for always supporting me and believing in me, no matter what. My darling Mattias, for your endless love and patience.

REFERENCES

[1] Kirk, O., Borchert, T. V. & Fuglsang, C. C. *Curr. Opin. Biotechnol.;* 13, (2002) 345.
[2] Malhotra, B. D. & Chaubey, A. *Sensor Actuat B-Chem;* 91, (2003) 117.
[3] Kim, J., Jia, H. F. & Wang, P. *Biotechnol Adv;* 24, (2006) 296.
[4] Ahuja, S. K., Ferreira, G. M. & Moreira, A. R. *Crit. Rev. Biotechnol.;* 24, (2004) 125.
[5] Koeller, K. M. & Wong, C. H. *Nature;* 409, (2001) 232.
[6] Wang, P., Dai, S., Waezsada, S. D., Tsao, A. Y. & Davison, B. H. *Biotechnol. Bioeng.;* 74, (2001) 249.
[7] Tischer, W. & Kasche, V. *Trends Biotechnol.;* 17, (1999) 326.
[8] Bornscheuer, U. T. *Angew Chem Int Edit;* 42, (2003) 3336.
[9] Beck, J. S., Vartuli, J. C., Roth, W. J., Leonowicz, M. E., Kresge, C. T., Schmitt, K. D., Chu, C. T. W., Olson, D. H. & Sheppard, E. W. *J. Am. Chem. Soc.;* 114, (1992) 10834.
[10] Zhao, D. Y., Feng, J. L., Huo, Q. S., Melosh, N., Fredrickson, G. H., Chmelka, B. F. & Stucky, G. D. *Science;* 279, (1998) 548.
[11] Zhao, D. Y., Huo, Q. S., Feng, J. L., Chmelka, B. F. & Stucky, G. D. *J. Am. Chem. Soc.;* 120, (1998) 6024.
[12] Nelson, D. L. C., Michael M; Lehninger, Albert L. (2008). *Principles of biochemistry*. 5th edit, W. H. Freeman.
[13] Yang, P. D., Zhao, D. Y., Margolese, D. I., Chmelka, B. F. & Stucky, G. D. *Nature;* 396, (1998) 152.
[14] Kartini, I., Meredith, P., da Costa, J. C. D., Riches, J. D. & Lu, G. Q. M. *Curr Appl Phys;* 4, (2004) 160.
[15] Yanagisawa, T., Shimizu, T., Kuroda, K. & Kato, C. *Bull. Chem. Soc. Jpn.;* 63, (1990) 988.
[16] Kresge, C. T., Leonowicz, M. E., Roth, W. J., Vartuli, J. C. & Beck, J. S. *Nature;* 359, (1992) 710.
[17] Slowing, I. I., Trewyn, B. G. & Lin, V. S. Y. *J. Am. Chem. Soc.;* 129, (2007) 8845.
[18] Vallet-Regi, M., Ramila, A., del Real, R. P. & Perez-Pariente, J. *Chem. Mat.;* 13, (2001) 308.
[19] Han, Y. J., Stucky, G. D. & Butler, A. *J. Am. Chem. Soc.;* 121, (1999) 9897.
[20] Sayari, A. *Chem. Mater.;* 8, (1996) 1840.
[21] Hartmann, M. *Chem. Mater.;* 17, (2005) 4577.
[22] Yiu, H. H. P. & Wright, P. A. *J. Mater. Chem.;* 15, (2005) 3690.
[23] Deere, J., Magner, E., Wall, J. G. & Hodnett, B. K. *J. Phys. Chem. B;* 106, (2002) 7340.
[24] Díaz, J. F. & Balkus, K. J. *J. Mol. Cat. B: Enzym.;* 2, (1996) 115.
[25] Holmberg, K., Jönsson, B., Kronberg, B. & Lindman, B. (2003). *Surfactants and Polymers in Aqueous Solution*. 2nd edit, John Wiley & Sons, Ltd.
[26] Gustafsson, H., Isaksson, S. & Holmberg, K. *To be published.*
[27] Hench, L. L. & West, J. K. *Chem. Rev. (Washington, DC, U. S.);* 90, (1990) 33.
[28] Beck, J. S., Vartuli, J. C., Roth, W. J., Leonowicz, M. E., Kresge, C. T., Schmitt, K. D., Chu, C. T. W., Olson, D. H., Sheppard, E. W., Mccullen, S. B., Higgins, J. B. & Schlenker, J. L. *J. Am. Chem. Soc.;* 114, (1992) 10834.
[29] Matsuyama, I., Satoh, S., Katsumoto, M. & Susa, K. *J. Non-Cryst. Solids;* 135, (1991) 22.
[30] Wan, Y. & Zhao, D. Y. *Chem. Rev. (Washington, DC, U. S.);* 107, (2007) 2821.
[31] Berggren, A. & Palmqvist, A. E. C. *J. Phys. Chem. C;* 112, (2008) 732.
[32] Zhao, D. Y., Sun, J. Y., Li, Q. Z. & Stucky, G. D. *Chem. Mater.;* 12, (2000) 275.
[33] Yu, C., Fan, J., Tian, B., Zhao, D. & Stucky, G. D. *Advanced Materials;* 14, (2002) 1742.

[34] Yokoi, T., Sakamoto, Y., Terasaki, O., Kubota, Y., Okubo, T. & Tatsumi, T. *J. Am. Chem. Soc.;* 128, (2006) 13664.
[35] Yu, C., Fan, J., Tian, B. & Zhao, D. *Chem. Mat.;* 16, (2004) 889.
[36] Boissiere, C., Larbot, A., van der Lee, A., Kooyman, P. J. & Prouzet, E. *Chem. Mater.;* 12, (2000) 2902.
[37] Linton, P., Hernandez-Garrido, J.-C., Midgley, P. A., Wennerstrom, H. & Alfredsson, V. *Physical Chemistry Chemical Physics;* 11, (2009) 10973.
[38] Ruggles, J. L., Gilbert, E. P., Holt, S. A., Reynolds, P. A. & White, J. W. *Langmuir;* 19, (2003) 793.
[39] Galarneau, A., Cambon, H., Di Renzo, F. & Fajula, F. *Langmuir;* 17, (2001) 8328.
[40] Kocherbitov, V. & Alfredsson, V. *J. Phys. Chem. C;* 111, (2007) 12906.
[41] Zhao, X. S., Lu, G. Q., Whittaker, A. K., Millar, G. J. & Zhu, H. Y. *J. Phys. Chem. B;* 101, (1997) 6525.
[42] Kleitz, F., Schmidt, W. & Schuth, F. *Micropor. Mesopor. Mater.;* 65, (2003) 1.
[43] Yang, L. M., Wang, Y. J., Luo, G. S. & Dai, Y. Y. *Micropor. Mesopor. Mater.;* 81, (2005) 107.
[44] Johansson, E. M., Cordoba, J. M. & Oden, M. *Mater. Lett.;* 63, (2009) 2129.
[45] Bae, Y. K. & Han, O. H. *Micropor. Mesopor. Mater.;* 106, (2007) 304.
[46] Manet, S., Schmitt, J., Impéror-Clerc, M., Zholobenko, V., Durand, D., Oliveira, C. L. P., Pedersen, J. S., Gervais, C., Baccile, N., Babonneau, F., Grillo, I., Meneau, F. & Rochas, C. *The Journal of Physical Chemistry B;* 115, (2011) 11330.
[47] Zholobenko, V. L., Khodakov, A. Y., Impéror-Clerc, M., Durand, D. & Grillo, I. *Adv. Colloid Interface Sci.;* 142, (2008) 67.
[48] Imperor-Clerc, M., Grillo, I., Khodakov, A. Y., Durand, D. & Zholobenko, V. L. *Chem. Commun.*, (2007) 834.
[49] Flodström, K., Teixeira, C. V., Amenitsch, H., Alfredsson, V. & Lindén, M. *Langmuir;* 20, (2004) 4885.
[50] Flodstrom, K., Wennerstrom, H. & Alfredsson, V. *Langmuir;* 20, (2004) 680.
[51] Malmsten, M., Linse, P. & Cosgrove, T. *Macromolecules;* 25, (1992) 2474.
[52] Gov, N., Borukhov, I. & Goldfarb, D. *Langmuir;* 22, (2006) 605.
[53] Sayari, A., Han, B.-H. & Yang, Y. *J. Am. Chem. Soc.;* 126, (2004) 14348.
[54] Wang, Y. G., Zhang, F. Y., Wang, Y. Q., Ren, J. W., Li, C. L., Liu, X. H., Guo, Y., Guo, Y. L. & Lu, G. Z. *Mater. Chem. Phys.;* 115, (2009) 649.
[55] Johansson, E. M., Córdoba, J. M. & Odén, M. *Mater. Lett.;* 63, (2009) 2129.
[56] Yang, S. M., Yang, H., Coombs, N., Sokolov, I., Kresge, C. T. & Ozin, G. A. *Advanced Materials;* 11, (1999) 52.
[57] Nandiyanto, A. B. D., Kim, S.-G., Iskandar, F. & Okuyama, K. *Micropor. Mesopor. Mater.;* 120, (2009) 447.
[58] Kallenberg, A. I., van Rantwijk, F. & Sheldon, R. A. *Adv. Synth. Catal.;* 347, (2005) 905.
[59] Hudson, S., Cooney, J. & Magner, E. *Angew. Chem.-Int. Edit.;* 47, (2008) 8582.
[60] Lee, C. H., Lin, T. S. & Mou, C. Y. *Nano Today;* 4, (2009) 165.
[61] Jing, H., Li, X. F., Evans, D. G., Duan, X. & Li, C. Y. *J Mol Catal B-Enzym;* 11, (2000) 45.
[62] Grotzky, A., Nauser, T., Erdogan, H., Schluter, A. D. & Walde, P. *J. Am. Chem. Soc.;* 134, (2012) 11392.
[63] Thörn, C., Udatha, D. B. R. K. G., Zhou, H., Christakopoulos, P., Topakas, E. & Olsson, L. *J. Mol. Catal. B: Enzym.;* 93, (2013) 65.
[64] Hudson, S., Magner, E., Cooney, J. & Hodnett, B. K. *J. Phys. Chem. B;* 109, (2005) 19496.
[65] Fan, J., Lei, J., Wang, L., Yu, C., Tu, B. & Zhao, D. *Chem. Commun.*, (2003) 2140.
[66] Liese, A. & Hilterhaus, L. *Chem. Soc. Rev.*, (2013).
[67] Takahashi, H., Li, B., Sasaki, T., Miyazaki, C., Kajino, T. & Inagaki, S. *Micropor. Mesopor. Mater.;* 44, (2001) 755.

[68] Sasaki, T., Kajino, T., Li, B., Sugiyama, H. & Takahashi, H. *Appl. Environ. Microbiol.;* 67, (2001) 2208.
[69] Lee, C. H., Lang, J., Yen, C. W., Shih, P. C., Lin, T. S. & Mou, C. Y. *J. Phys. Chem. B;* 109, (2005) 12277.
[70] Lei, C. H., Shin, Y., Liu, J. & Ackerman, E. J. *Nano Lett.;* 7, (2007) 1050.
[71] Bolivar, J. M., Consolati, T., Mayr, T. & Nidetzky, B. *Trends Biotechnol.;* 31, (2013) 194.
[72] Yamaguchi, A., Namekawa, M., Kamijo, T., Itoh, T. & Teramae, N. *Anal. Chem.;* 83, (2011) 2939.
[73] Han, Y., Lee, S. S. & Ying, J. Y. *Chem. Mater.;* 18, (2006) 643.
[74] Zhang, Y. H. P. *Biotechnol Adv;* 29, (2011) 715.
[75] van de Velde, F., van Rantwijk, F. & Sheldon, R. A. *Trends Biotechnol.;* 19, (2001) 73.
[76] Mayer, S. F., Kroutil, W. & Kurt, F. *Chem. Soc. Rev.;* 30, (2001) 332.
[77] Betancor, L. & Luckarift, H. R. *Biotechnol Genet Eng;* 27, (2010) 95.
[78] Kim, S. H., Lee, S. M., Kim, D. U., Cui, J. Z. & Kang, S. W. *Dyes Pigm.;* 49, (2001) 103.
[79] Sharma, R., Chisti, Y. & Banerjee, U. C. *Biotechnol Adv;* 19, (2001) 627.
[80] Brady, L., Brzozowski, A. M., Derewenda, Z. S., Dodson, E., Dodson, G., Tolley, S., Turkenburg, J. P., Christiansen, L., Huge-Jensen, B., Norskov, L., Thim, L. & Menge, U. *Nature;* 343, (1990) 767.
[81] Wu, X., Jääskeläinen, S. & Linko, W.-Y. *Appl. Biochem. Biotechnol.;* 59, (1996) 145.
[82] Hiol, A., Jonzo, M. D., Rugani, N., Druet, D., Sarda, L. & Comeau, L. C. *Enzyme Microb. Technol.;* 26, (2000) 421.
[83] Brzozowski, A. M., Derewenda, Z. S., Dodson, E. J., Dodson, G. G. & Turkenburg, J. P. *Acta Crystallogr B;* 48, (1992) 307.
[84] Walter, J., Steigemann, W., Singh, T. P., Bartunik, H., Bode, W. & Huber, R. *Acta Crystallogr B;* 38, (1982) 1462.
[85] Gupta, R., Beg, Q. K. & Lorenz, P. *Appl. Microbiol. Biotechnol.;* 59, (2002) 15.
[86] Polgar, L. *Cell. Mol. Life Sci.;* 62, (2005) 2161.
[87] Fazary, A. E. & Ju, Y. H. *Acta Bioch Bioph Sin;* 39, (2007) 811.
[88] Topakas, E., Vafiadi, C. & Christakopoulos, P. *Process Biochem.;* 42, (2007) 497.
[89] Murakami, A., Nakamura, Y., Koshimizu, K., Takahashi, D., Matsumoto, K., Hagihara, K., Taniguchi, H., Nomura, E., Hosoda, A., Tsuno, T., Maruta, Y., Kim, H. W., Kawabata, K. & Ohigashi, H. *Cancer Lett;* 180, (2002) 121.
[90] Kikuzaki, H., Hisamoto, M., Hirose, K., Akiyama, K. & Taniguchi, H. *J. Agric. Food Chem.;* 50, (2002) 2161.
[91] Giuliani, S., Piana, C., Setti, L., Hochkoeppler, A., Pifferi, P. G., Williamson, G. & Faulds, C. B. *Biotechnol. Lett.;* 23, (2001) 325.
[92] Topakas, E., Stamatis, H., Mastihobova, M., Biely, P., Kekos, D., Macris, B. J. & Christakopoulos, P. *Enzyme Microb. Technol.;* 33, (2003) 729.
[93] Krieg, R. & Halbhuber, K. J. *Cell. Mol. Biol.;* 49, (2003) 547.
[94] Veitch, N. C. *Phytochemistry;* 65, (2004) 249.
[95] Welinder, K. G. *FEBS Lett.;* 72, (1976) 19.
[96] Henriksen, A., Smith, A. T. & Gajhede, M. *J. Biol. Chem.;* 274, (1999) 35005.
[97] Wohlfahrt, G., Witt, S., Hendle, J., Schomburg, D., Kalisz, H. M. & Hecht, H. J. *Acta Crystallogr D;* 55, (1999) 969.
[98] Wilson, R. & Turner, A. P. F. *Biosensors and Bioelectronics;* 7, (1992) 165.
[99] Wong, C. M., Wong, K. H. & Chen, X. D. *Appl. Microbiol. Biotechnol.;* 78, (2008) 927.
[100] Bankar, S. B., Bule, M. V., Singhal, R. S. & Ananthanarayan, L. *Biotechnol Adv;* 27, (2009) 489.
[101] Zhu, J. H., Zhu, Z. Q., Lai, Z. S., Wang, R., Guo, X. M., Wu, X. Q., Zhang, G. X., Zhang, Z. R., Zhang, Z. R., Wang, Y. T. & Chen, Z. Y. *Sensors;* 2, (2002) 127.
[102] Ciesla, U. & Schüth, F. *Micropor. Mesopor. Mater.;* 27, (1999) 131.

[103] Brunauer, S., Emmett, P. H. & Teller, E. *J. Am. Chem. Soc.;* 60, (1938) 309.
[104] Barrett, E. P., Joyner, L. G. & Halenda, P. P. *J. Am. Chem. Soc.;* 73, (1951) 373.
[105] Broekhof.Jc & Deboer, J. H. *J. Catal.;* 9, (1967) 8.
[106] Broekhof.Jc & Deboer, J. H. *J. Catal.;* 9, (1967) 15.
[107] Lukens, W. W., Schmidt-Winkel, P., Zhao, D. Y., Feng, J. L. & Stucky, G. D. *Langmuir;* 15, (1999) 5403.
[108] Kruk, M., Jaroniec, M. & Sayari, A. *Langmuir;* 13, (1997) 6267.
[109] Sing, K. S. W., Everett, D. H., Haul, R. A. W., Moscou, L., Pierotti, R. A., Rouquerol, J. & Siemieniewska, T. *Pure Appl. Chem.;* 57, (1985) 603.
[110] Lei, C., Shin, Y., Magnuson, J. K., Fryxell, G., Lasure, L. L., Elliott, D. C., Liu, J. & Ackerman, E. J. *Nanotechnology;* 17, (2006) 5531.
[111] Shannon, L. M., Kay, E. & Lew, J. Y. *J. Biol. Chem.;* 241, (1966) 2166.
[112] Lowry, O. H., Rosebrough, N. J., Farr, A. L. & Randall, R. J. *J. Biol. Chem.;* 193, (1951) 265.
[113] Smith, P. K., Krohn, R. I., Hermanson, G. T., Mallia, A. K., Gartner, F. H., Provenzano, M. D., Fujimoto, E. K., Goeke, N. M., Olson, B. J. & Klenk, D. C. *Anal. Biochem.;* 150, (1985) 76.
[114] Bradford, M. M. *Anal. Biochem.;* 72, (1976) 248.
[115] Wiechelman, K. J., Braun, R. D. & Fitzpatrick, J. D. *Anal. Biochem.;* 175, (1988) 231.
[116] Cooney, J. & et al. *Angewandte Chemie International Edition*, (2008) NA.
[117] Lei, C. & et al. *Nanotechnology;* 19, (2008) 125102.
[118] Childs, R. E. & Bardsley, W. G. *Biochem. J.;* 145, (1975) 93.
[119] Fornera, S., Bauer, T., Schluter, A. D. & Walde, P. *J. Mater. Chem.;* 22, (2012) 502.
[120] Rotenberg, Y., Boruvka, L. & Neumann, A. W. *J. Colloid Interface Sci.;* 93, (1983) 169.
[121] Stalder, A. F., Melchior, T., Muller, M., Sage, D., Blu, T. & Unser, M. *Colloid Surface A;* 364, (2010) 72.
[122] Höök, F., Kasemo, B., Nylander, T., Fant, C., Sott, K. & Elwing, H. *Anal. Chem.;* 73, (2001) 5796.
[123] Voinova, M. V., Rodahl, M., Jonson, M. & Kasemo, B. *Phys. Scr.;* 59, (1999) 391.
[124] McCubbin, G. A., Praporski, S., Piantavigna, S., Knappe, D., Hoffmann, R., Bowie, J. H., Separovic, F. & Martin, L. L. *Eur Biophys J Biophy;* 40, (2011) 437.
[125] Rodahl, M., Hook, F., Krozer, A., Brzezinski, P. & Kasemo, B. *Rev. Sci. Instrum.;* 66, (1995) 3924.
[126] Sauerbrey, G. *Z Phys;* 155, (1959) 206.
[127] Johansson, E. M., Ballem, M. A., Córdoba, J. M. & Odén, M. *Langmuir;* 27, (2011) 4994.
[128] Boissiere, C., Martines, M. A. U., Tokumoto, M., Larbot, A. & Prouzet, E. *Chem. Mater.;* 15, (2003) 509.
[129] Lonnqvist, I., Hakansson, B., Balinov, B. & Soderman, O. *J. Colloid Interface Sci.;* 192, (1997) 66.
[130] Mohlin, K., Lorén, N. & Nydén, M. *Colloids Surf., A;* 297, (2007) 114.
[131] Rosenholm, J. M. & Linden, M. *Chem. Mater.;* 19, (2007) 5023.
[132] Ravindra, R., Shuang, Z., Gies, H. & Winter, R. *J. Am. Chem. Soc.;* 126, (2004) 12224.
[133] Urabe, Y., Shiomi, T., Itoh, T., Kawai, A., Tsunoda, T., Mizukami, F. & Sakaguchi, K. *ChemBioChem;* 8, (2007) 668.
[134] *Toyobo Co. Ltd., Japan*.
[135] Lavery, C. B., MacInnis, M. C., MacDonald, M. J., Williams, J. B., Spencer, C. A., Burke, A. A., Irwin, D. J. G. & D'Cunha, G. B. *J. Agric. Food Chem.;* 58, (2010) 8471.